uOttawa

L'Université canadienne
Canada's university

FACULTÉ DES ÉTUDES SUPÉRIEURES ET POSTOCTORALES

uOttawa

L'Université canadienne
Canada's university

FACULTY OF GRADUATE AND POSDOCTORAL STUDIES

Sumin Jeong

AUTEUR DE LA THÈSE / AUTHOR OF THESIS

M.A.Sc. (Mechanical Engineering)

GRADE / DEGREE

Department of Mechanical Engineering

FACULTÉ, ÉCOLE, DÉPARTEMENT / FACULTY, SCHOOL, DEPARTMENT

A New Approach to Ice-Induced Vibrations through the Conservation of Momentum

TITRE DE LA THÈSE / TITLE OF THESIS

Dr. N. Baddour

DIRECTEUR (DIRECTRICE) DE LA THÈSE / THESIS SUPERVISOR

CO-DIRECTEUR (CO-DIRECTRICE) DE LA THÈSE / THESIS CO-SUPERVISOR

EXAMINATEURS (EXAMINATRICES) DE LA THÈSE / THESIS EXAMINERS

Dr. R. Langlois

Dr. D. Necsulescu

Gary W. Slater

Le Doyen de la Faculté des études supérieures et postdoctorales / Dean of the Faculty of Graduate and Postdoctoral Studies

A New Approach to Ice-Induced Vibrations through the Conservation of Momentum

by

Sumin Jeong

Thesis submitted to the
Faculty of Graduate and Postdoctoral Studies
In partial fulfillment of the requirements
For the M.A.Sc. degree in
Mechanical Engineering

Department of Mechanical Engineering
Faculty of Engineering
University of Ottawa

Your file Votre référence
ISBN: 978-0-494-59901-3
Our file Notre référence
ISBN: 978-0-494-59901-3

Abstract

This thesis proposes a new ice-induced vibration model which is not based on the existing ice-induced vibration (IIV) modeling approaches. The new model is derived from a different perspective so that it is able to respond to the influence of fluid flow and shortcomings in existing ice-induced vibration models. The effect of a flowing fluid on ice-induced vibrations has not been investigated in past research inspite of its significant contributions to the dynamics of both structure and ice. By combining the equation of a one degree-of-freedom oscillator with Morison's equation, the flow effect is added to the structural response and its influence is examined. The deficiencies of the existing IIV models are investigated by reproducing two existing models, and demonstrating the need for a new model. The new model, the impact IIV model, which is developed from the conservation of momentum is completed by the inclusion of the flow effect on the structure.

Acknowledgements

First of all, I would like to thank my supervisor professor Natalie Baddour who has provided me a comfortable research environment, so I was able to concentrate on my thesis in the way I preferred. Without her guidance and help, this thesis would not have been completed.

I would also like to thank Dr. Hong, Hoonbin. His academical and non-academic advices helped me a lot.

Finally, I would like to dedicate this thesis to my family. With their support, I could get this far. I have never spoken out but thank you as always.

Contents

List of Tables

List of Figures

Nomenclature

$\bar{c}$	damping coefficient of a structure per unit length
$\bar{f}(t)$	forcing function per unit length
$\bar{F}_m$	maximum force per unit length
$\bar{F}_m$	maximum force per unit length
$\bar{k}$	stiffness of a structure per unit length
$\bar{m}$	mass of a structure per unit length
$\bar{M}_a$	added mass per unit length
$\ddot{u}$	acceleration of flow
$\ddot{x}$	acceleration of a structure
$\ddot{\tilde{x}}$	normalized structural acceleration
δ	deflection of a ice sheet
$\delta_D(t)$	Dirac delta function
$\dot{u}$	velocity of flow
$\dot{x}$	velocity of a structure
$\dot{z}$	velocity of ice
$\dot{z}_r$	relative velocity between a structure and ice sheet
$\dot{z}_t$	transitional relative ice velocity
$\dot{\tilde{x}}$	normalized structural velocity
$\dot{\tilde{x}}_{0e}$	normalized initial value of velocity in an extrusion phase
$\dot{\tilde{x}}_{0l}$	normalized initial value of velocity in a loading phase
$\dot{\tilde{x}}_{0s}$	normalized initial value of velocity in a separation phase

$\dot{\tilde{z}}$	normalized ice velocity
ℓ	length of a structure
γ_ρ	density ratio
$\hat{F}(\omega)$	Fourier transform of function $f(t)$
ω_d	damped natural frequency
ω_N	Nth forcing frequency
ω_n	natural frequency
$\overline{q}_D$	viscous term of Morison's equation
$\overline{q}$	Morison's equation
$\overline{q}_I$	inviscid term of Morison's equation
ρ_s	density of a structure
ρ	fluid density
σ_c	compressive strength
τ	forcing period
θ_N	phase shift
$\tilde{\sigma}_f$	normalized crushing strength
$\tilde{F}_e$	normalized residual force from the previous crush
$\tilde{k}_c$	normalized effective contact stiffness
$\tilde{p}$	normalized distance between adjacent teeth of Matlock's model
$\tilde{t}$	normalized time
$\tilde{t}_e$	normalized initial value of time in an extrusion phase
$\tilde{t}_l$	normalized initial value of time in a loading phase
$\tilde{t}_s$	normalized initial value of time in a separation phase
$\tilde{x}$	normalized structural displacement
$\tilde{x}_{0e}$	normalized initial value of displacement in an extrusion phase
$\tilde{x}_{0l}$	normalized initial value of displacement in a loading phase
$\tilde{x}_{0s}$	normalized initial value of displacement in a separation phase
ζ	damping ratio

c	damping coefficient of a structure
C'_D	modified drag coefficient
C_A	added mass coefficient
C_D	drag coefficient
C_M	inertia coefficient
D	diameter of a structure
e	coefficient of restitution
$f(t)$	forcing function
F_c	crushing force
F_e	residual force from the previous crush
F_m	maximum force
F_{fmax}	maximum failure ice force
h	ice thickness
k	stiffness of a structure
k_c	effective contact stiffness
M	ice mass
m	mass of a structure
p	distance between adjacent teeth of Matlock's model
T	total period
t	time
t_c	crushing period
t_e	elastic period
t_{total}	one complete period
x	displacement of a structure
M	magnification factor without flow effect
M_f	magnification factor with flow effect

Chapter 1

Introduction

As an introduction to ice-induced vibrations, the definition of ice-induced vibrations is explained in this chapter. The motive and objectives are also presented.

1.1 Ice-induced Vibrations

Offshore structures in cold regions often experience phenomena called ice-induced vibrations (IIVs). IIVs are vibrations which originate from the dynamical interaction between the structure and the ice sheet which surrounds the structure. External forces such as water flow, wind or thermal expansion drive the ice sheet, and the moving ice sheet transfers force to the structure as it pushes against the structure. The structure is elastically displaced by the ice until the elastic restoring force of the structure exceeds the ice strength. Part of the ice sheet then breaks and the structure bounces back in the opposite direction. As a result of IIVs, the structure not only experiences unexpected vibrations but also is exposed to more fatigue damage and sometimes a resonance condition. Analysis of the IIV mechanism on structures, therefore, is very crucial from both structural and design points of view, since IIV can severely threaten the safety of structures.

Modeling is a typical approach to the analysis of IIVs. During the past decades, two main types of IIV modeling approaches have been proposed. The existing IIV models

based on the two types can partially predict the behavior of IIVs but neither of them is able to consistently explain IIVs because each of the two fundamental IIV modeling approaches possesses deficiencies. Therefore, there are several questions which cannot be answered by the existing IIV models developed with either of these approaches. In addition, most IIV models do not consider the influence of fluid flow although most structures subjected to IIVs are offshore structures. Since fluid flow is one of the main driving forces of IIVs, it can contribute to the dynamics of ice forces as well as that of the structures but it has not been considered in past research. This thesis is motivated by these circumstances of IIV research.

A new perspective of the IIV modeling approach is suggested in this thesis to obtain consistency in the IIV modeling approach. A new IIV model proposed derived from two theories: Morison's equation and the conservation of momentum. Morison's equation is adopted to add the influence of fluid flow on the structure. The conservation of momentum is combined with the coefficient of restitution to derive a new type of an IIV model of which the ice force is considered to be a series of impacts driven by the flow. Numerical simulations are conducted with the developed IIV model to obtain insight into the dynamics of IIVs.

1.2 Contents of the Thesis

This thesis consists of the following chapters:

Chapter 2 introduces a history of IIV research and presents a literature review that introduces the current two main IIV modeling approaches.

Chapter 3 starts with explaining Morison's equation and explains how it is implemented into the equations of IIVs.

Chapter 4 reproduces two IIV models which are proposed by Toyama et. al. and Huang and Liu in order to demonstrate the inconsistency of existing models.

Chapter 5 is the core of the thesis which contains details of a proposed new IIV modeling approach.

Chapter 6 concludes the thesis with the summary of the thesis work and future work.

Chapter 2

Literature Review

Research on ice-induced vibrations began in the early 1960's. Among a variety of experimental and theoretical research, two distinctive modeling approaches became dominant, the characteristic failure frequency model and the self-excited model. In this chapter, a history and review of the two modeling approaches of ice-induced vibrations are briefly explained.

2.1 A Brief History of Ice-Induced Vibration Research

Research on Ice-Induced Vibrations (IIVs) became a new area in the study of vibrations around 1962 when the oil companies in Alaska constructed offshore structures in Cook Inlet [Blenkarn, 1970]. Although the structures were exposed to extremely harsh environments such as wind, low temperature and ice, no design information about the environment of Cook Inlet was available, in particular regarding how ice cover surrounding the structure interacts or influences the structural dynamics. Within the context of a lack of information about the IIV mechanism, the first IIV was reported from the Cook Inlet drilling structure. Other early reports of IIVs came from Finland for single

steel pipe foundations of lighthouses and also from the Chinese Bohai Sea from jacket foundations of oil production platforms [Määttänen, 2001].

From the late 1960s to 1980s, research for analyzing ice mechanics was conducted by the National Research Council of Canada, Canadian Coastguard, U.S. Navy, various universities, the offshore industry as well as oil companies [Dempsey, 1999]. In the early stages of IIV research, field and laboratory experiments were launched to investigate the mechanism for IIVs. Payton was one of the earliest IIV researchers who suggested an IIV mechanism based on his experimental results in the 1960s. According to experiments, the velocity of a uniform-thickness ice sheet is related to the generated ice force [Sodhi, 1989] so that the IIV mechanism seemed to depend mainly on velocities of ice sheets. Blenkarn (1970) presented ice force data which he recorded in drilling platforms of Cook Inlet from the winters of 1963 to 1969. His paper became the basis of the negative damping or self-excited model. Toyama et al. (1983) suggested phase division of an ice forcing function based on small scale tests and this approach was also used by other researchers. Ranta and Räty (1983) also proposed the similar idea of phase division at the same year. A recent experimental publication was presented by Barker et al. (2003) from the Canadian Hydraulics Centre of the National Research Council of Canada. They investigated extensive small scale tests of wind turbines in Danish waters. The results of the paper provided information on ice forces which vary in shapes of structures. Recent publications of Sodhi's experiments, Sodhi and Haehnel (2003), Sodhi (2000), and Sodhi et al. (1998), also contributed to extend the understanding of dependency of ice forces on ice velocities.

The development of theoretical models of IIVs has also been made along with experimental studies. Theoretical models of IIVs were proposed by defining the origin of IIVs. The involvement of several uncertain aspects of environment and circumstance makes the analysis of IIVs a difficult field. After Peyton's early publication (1968), Neil (1976) proposed that crushed ice tends to break into a certain size. He proposed that the fracture size and velocity of an ice sheet determine a characteristic failure frequency which

in turn decides the forcing frequency [Sodhi, 1989]. This point of view defines the origin of IIVs as being the characteristic failure mechanism, a point of view which is supported by Matlock et al. (1971). In opposition to the characteristic failure mechanism, Blenkarn (1970) explained IIVs as a self-excited vibration due to negative damping. According to the self-excited model, IIVs originate from the interaction between a flexible structure and decreasing ice crushing forces with increasing stress rate. Määttänen, who is one of the big contributors of the self-excited model, verified the self-excited IIV model through his field and laboratory experiments [Sodhi and Morris, 1986]. Xu and Wang (1988) also suggested the ice force oscillator model based on the self-excited model. The self-excited model, however, has several objections because it cannot be applied to rigid structures although there is no clear definition of rigid or flexible structures [Määttänen, 1989].

Inspite of the relatively short history of IIV research, extensive studies have been conducted but no theoretical model explains the IIV mechanism completely. Some researchers such as Kärnä and Turunen (1989) or Huang and Liu (2006) attempted to include non-linearity of IIVs in their models. Other researchers like Qu et al. (2006) focused on the randomness of ice forces. Instead of using a one degree-of-freedom model, Eranti et al. (1981) and Jin and Hu (1998) approached IIVs in different ways. Eranti et al. developed a multi degree-of-freedom model by using mode shapes. Jin and Hu introduced an IIV model based on the Hamiltonian principle. Likewise, for the past half century, various investigations and experiments were performed in an attempt to answer the origin of IIVs. IIVs, however, are not a single phenomenon, but rather a more complex one involving non-linearity, randomness and ice properties. The question and possibility for a better model of IIVs still remain open.

2.2 Modeling of Ice-Induced Vibration

Given the complexity of IIVs, several different modeling approaches have been proposed in the past decades. According to the origination of IIVs, the modeling of IIVs can

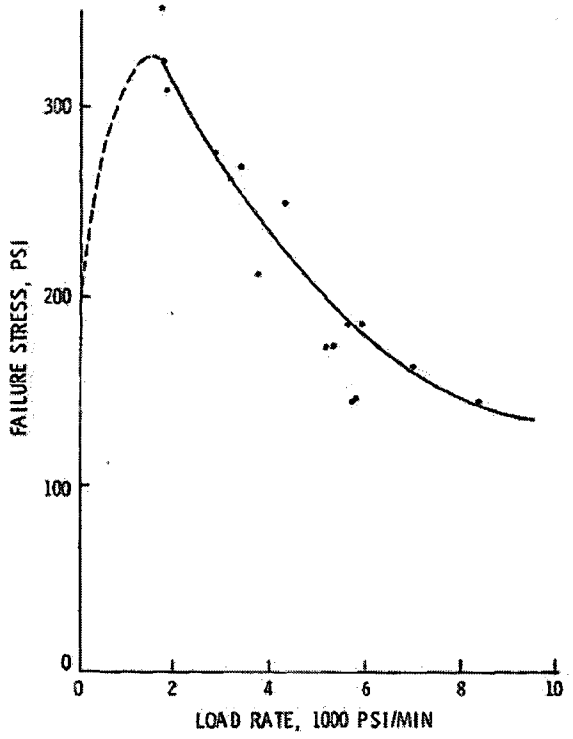

Figure 2.1: Peyton's compressive strength data (from [Blenkarn, 1970])

be categorized into two distinct methods: the first one simulates IIVs as a continuous interaction due to the self-excited effect, while the other explains IIVs as a series of discrete events [Huang and Liu, 2006]. The first theory is often called the self-excited model and the second one is called the characteristic failure frequency model. Both theories, however, have some deficiencies. For instance, the characteristic failure frequency model cannot explain why the fluctuation of the ice force occurs through a constant thickness and velocity of the ice sheet. On the other hand, the self-excited model is only applicable to flexible structures [Määttänen, 1989].

The origin of the self-excited model is tracked back to Blenkarn who discovered that ice forces induced by a uniform ice sheet are not constant [Blenkarn, 1970]. He established the self-excited model based on Payton's experiment showing a decrease in ice strength with increasing loading rate, as shown in Figure 2.1. By considering an ice force as a

function of the relative velocity between the ice sheet and structure, the self-excited model is expressed as [Blenkarn, 1970]

$$m\ddot{x} + c\dot{x} + kx = f(\dot{z} - \dot{x}) \tag{2.1}$$

where m, c, and k are mass, damping coefficient, and stiffness of the structure, respectively. The ice force is a function of the velocities of the ice and structure. For small motions,

$$f(\dot{z} - \dot{x}) = f(\dot{z}) - \dot{x}\frac{\partial f(\dot{z})}{\partial \dot{z}} \tag{2.2}$$

By substitution of equation (2.2) into equation (2.1)

$$m\ddot{x} + \left(c + \frac{\partial f}{\partial \dot{z}}\right)\dot{x} + kx = f(\dot{z}). \tag{2.3}$$

According to Figure 2.1, $\partial f/\partial \dot{z}$ can be negative in a certain range and if the overall damping term is negative, the structure becomes unstable due to the negative damping effect. Since the negative damping effect is not observed in every IIV, Määttänen (1998) discussed the condition of self-excited vibrations. He proposed that the self-excited effect is mainly applicable to flexible structures which interact actively with ice forces. In other words, the dependence of the ice forces on the interaction of the ice and structure determines the self-excited IIV.

The characteristic failure frequency model is more widely accepted than the self-excited model. Contrary to the self-excited model, the structure does not play an active role in the characteristic failure frequency model. The frequencies of IIVs are determined by the ice failure mechanism which is governed by the properties and velocities of the ice contacting with the structure. The relevant properties of the ice include salinity, thickness, temperature, density, and grain structure [Barker et al., 2005]. Along with these properties, other uncertain factors can be involved in the ice failure mechanism, which further complicates the analysis of IIVs. It follows that every ice sheet can fail at different frequencies. By constraining the properties of the ice sheet, researchers have tried to explain the ice failure mechanism which takes place at the contact zone between

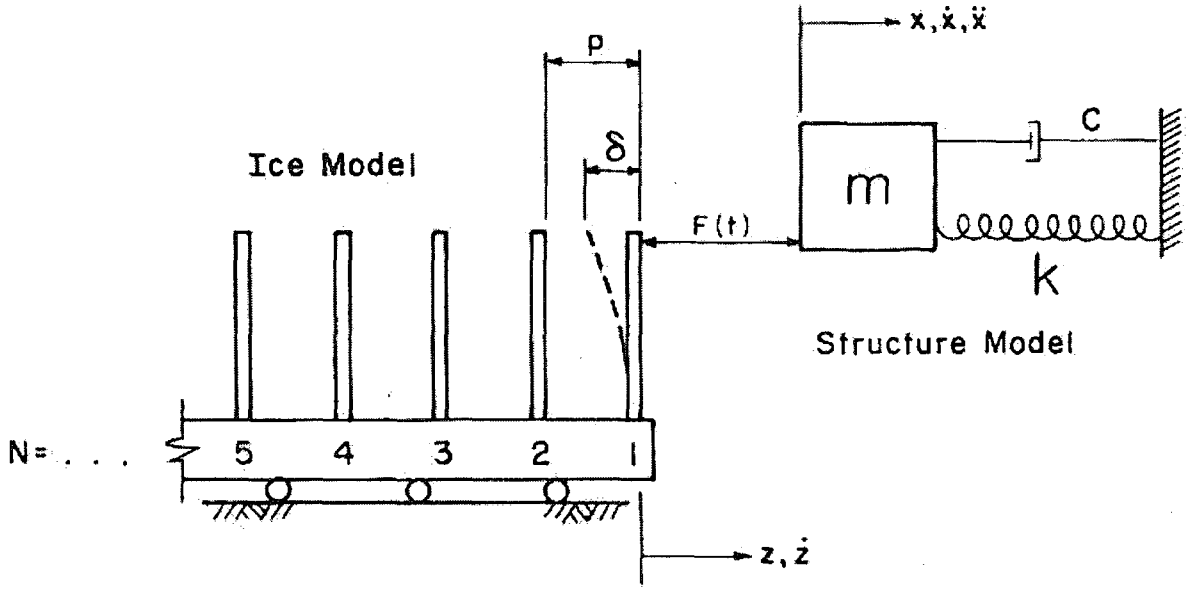

Figure 2.2: Matlock el al. IIV model (from [Sodhi, 1989])

the ice and structure. The details, however, vary from theory to theory due in part to the uncertainty of the ice properties.

Matlock et al. (1971) proposed an intuitive discrete-event IIV model, which is based on the characteristic failure frequency model. Because of its simplicity, Matlock's model has been widely used in IIV research. The model is illustrated in Figure 2.2. The vertical rods on the cart in Figure 2.2 represent discrete ice forces. The first vertical rod comes in contact with the structure which is represented as the mass m, and then deflects up to the loading phase δ. At the end of the loading phase, the first rod breaks and no force is transmitted to the structure until the second phase starts. The first total period p ends with contact of the second rod, and the second loading phase begins. This process keeps repeating so that the ice forces become a periodic function. The structure is represented as a one degree-of-freedom system consisting of the mass m, damping coefficient c, and spring constant k. Despite its simplicity, Matlock's model contains all the essential ideas of the characteristic failure frequency model which are divided phases, periodic saw-tooth forcing functions and dependency on the velocity of the ice.

Chapter 3

Influence of Flow on Ice-induced Vibrations of Structures

Under an ice cover in which ice-induced vibrations take place, there is a moving fluid, typically fresh water or sea water moving due to tides or currents. This moving fluid interacts with the structure so that the characteristics of the ice-induced vibrations may change. The objective of this chapter is to investigate if the fluid flow changes the ensuing IIVs. Morison's equation is used to analyze the effect of flow. By comparing the equations of ice-induced vibrations with flow and without flow, a new non-dimensional parameter is developed to find a range of the flow in which the effect of the fluid flow becomes significant.

3.1 Morison's Equation

Since structures subjected to ice-induced vibrations (IIVs) are located in water, the influence of flow is another important factor to analyze. Most offshore structures such as bridge piles, light houses, and platforms have large portions of submerged parts, therefore the surrounding water strongly contributes to the dynamics of the offshore structures through the parts under water. The flow effect on IIVs, however, has not been fully

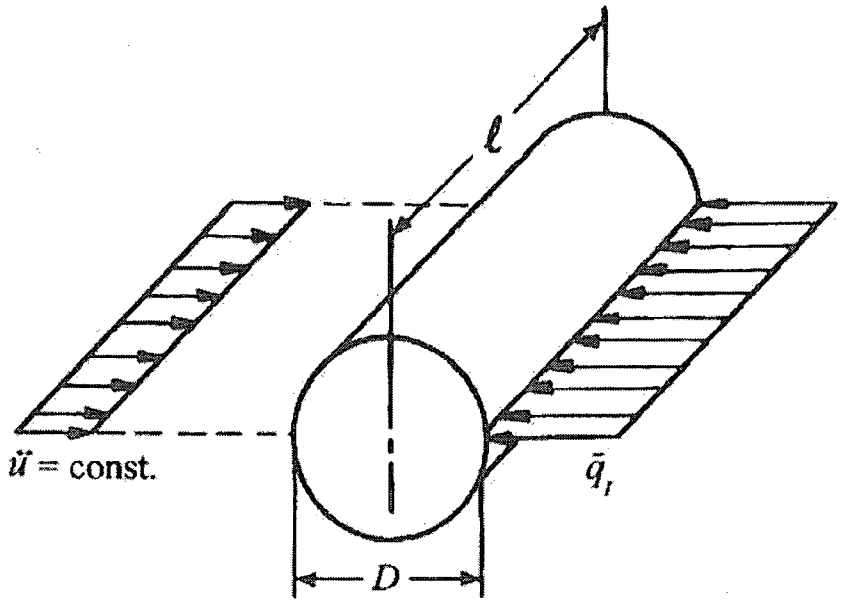

ℓ/D	C_M
1.2	1.62
2.5	1.78
5.0	1.90
9.0	1.96
∞	2

Figure 3.1: Inertia coefficients of a cylinder (from [Wilson et al., 2003])

studied in past research despite its potential significance. Velocity or temperature of the water surrounding the structures were often considered as a factor influencing the properties of the ice but not with regards to structural dynamics. The velocity of the current not only affects the ice forces but also the dynamics of the structures, therefore adding the flow effect to the analysis of IIVs could potentially increase the accuracy of IIV simulations.

The hydraulic forces acting on offshore structures were experimentally proposed by Morison et al. (1950), by an equation referred to as Morison's equation and widely adopted in offshore engineering [Wolfram, 1999]. Morison's equation consists of the drag loading from viscous flow and the inertial loading due to inviscid flow. The inviscid term, $\overline{q}_I$, is expressed [Wilson et al., 2003] as

$$\overline{q}_I = C_M \rho \pi \frac{D^2}{4} \ddot{u} \tag{3.1}$$

where ρ is the fluid density, D is the diameter of the cylinder, and $\ddot{u}$ is the constant free stream acceleration. Further, C_M is a non-dimensional coefficient called the inertia

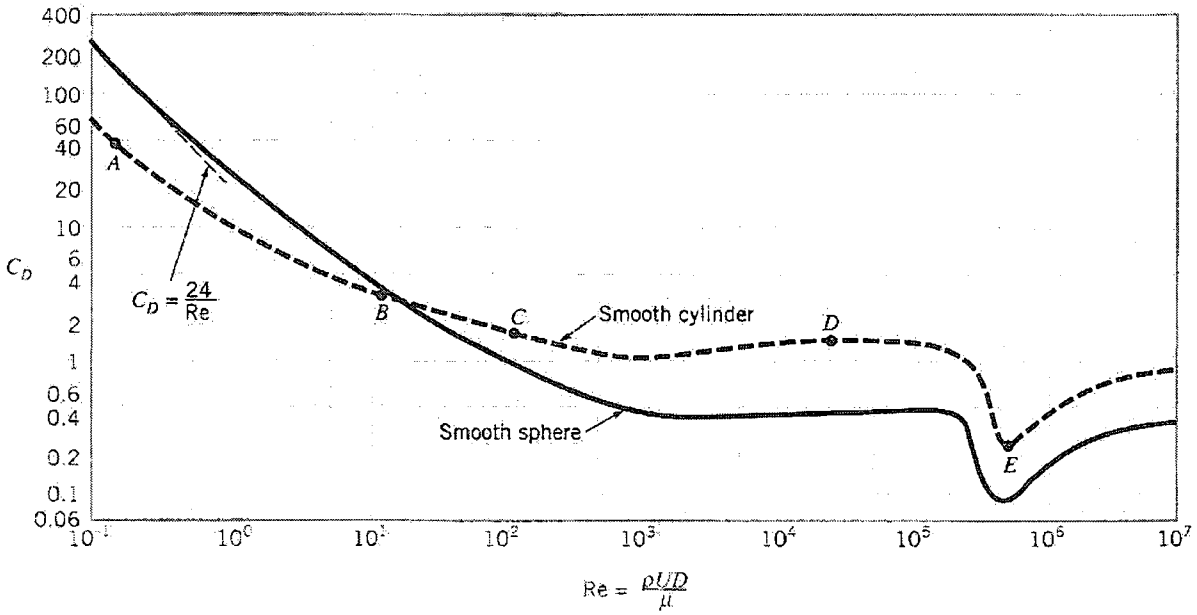

Figure 3.2: Drag coefficient relative to Re (from [Munson et al., 2002])

coefficient and determined by the ratio of length to diameter of a structure. According to Figure 3.1, as the ratio of length to diameter increases, C_M approaches 2. Most offshore structures are relatively slender based on this ratio so that C_M is set equal to 2 in most cases. The other term of Morison's equation is induced by viscous flow. The viscous term, $\bar{q}_D$, is given by [Wilson et al., 2003]

$$\bar{q}_D = C_D \rho \frac{D}{2} |\dot{u}| \dot{u} \tag{3.2}$$

where C_D is the drag coefficient determined by the Reynolds number. As shown Figure 3.2, the drag coefficient of the cylinder approximately remains at 1 for most IIV cases which are in the range of Reynolds number from 1000 to 200,000. Both terms of Morison's equation are formulated in units of force per unit length, and the bars over the letters indicate that the dimensions are given per unit length.

Morison's equation expresses the force required to hold a rigid cylinder in flow as the superposition of the inviscid and viscous loadings. The equation becomes

$$\bar{q} = \bar{q}_I + \bar{q}_D \tag{3.3}$$

or

$$\bar{q} = C_D \rho \frac{D}{2} |\dot{u}| \dot{u} + C_M \rho \pi \frac{D^2}{4} \ddot{u} \tag{3.4}$$

in units of force per unit length [Wilson et al., 2003]. This original Morison's equation contains a non-linearity, hence it needs linearization to be solved in a closed form solution. Berge and Penzien (1974) proposed a linear Morison's equation for small motion [Wilson et al., 2003]. The Berge and Penzien method, however, produces poor results when the drag term becomes dominant relative to the inertia term. Wolfram (1999) suggested alternative approaches to linearization of Morison's equation in wave-induced vibrations by keeping the non-linearity. Later analysis in this chapter will be performed on low flow velocities, therefore the Berge and Penzien method will hold its accuracy in the following.

3.2 Modeling of Ice-induced Vibration with Flow

Among the two types of IIV modeling, the characteristic failure frequency model is more adequate to combine with different expressions of forces than the self-excited model because the characteristic failure frequency model does not need to have a force as a function of ice velocity. Matlock's IIV Model, Figure 2.2, is modified to include the flow effect. The equation of motion of a one degree-of-freedom Matlock's model is

$$m\ddot{x} + c\dot{x} + kx = f(t) \tag{3.5}$$

where $f(t)$ is the forcing function. In Matlock's model, the forcing function is designed to be a periodic function. To add the flow effect, the forcing function of the equation is replaced with the flow force from Morison's equation. For the time being, the equation will state flow-induced vibration. Since Morison's equation is expressed in per unit length units, the equation of motion is also required to be in per unit length units as

$$\bar{m}\ddot{x} + \bar{c}\dot{x} + \bar{k}x = \bar{f}(t) \tag{3.6}$$

where the bars over the top of the letters indicate that the dimensions are given per unit length.

Morison's equation also needs to be slightly rewritten. The drag term of Morison's equation is based on flow passing by a stagnant structure, but the velocity should be the relative velocity between the flow and structure when the structure moves [Wilson et al., 2003]. The inviscid term, however, remains the same because the inertia of the flow is only related to the velocity of the flow. Morison's equation, equation (3.4), thus becomes

$$\bar{q} = C_D \rho \frac{D}{2} |\dot{u} - \dot{x}| (\dot{u} - \dot{x}) + C_M \rho \pi \frac{D^2}{4} \ddot{u} \tag{3.7}$$

According to the Berge and Penzien method, $|\dot{u} - \dot{x}|$ is relatively small in low flow velocity, and Morison's equation can be linearized as

$$C'_D = C_D |\dot{u} - \dot{x}| \approx \text{constant} \tag{3.8}$$

Substituting equation (3.8) into equation (3.7), the linearized Morison's equation is expressed as

$$\bar{q} = C'_D \rho \frac{D}{2} (\dot{u} - \dot{x}) + C_M \rho \pi \frac{D^2}{4} \ddot{u} \tag{3.9}$$

The forcing function of equation (3.6) can be now replaced with equation (3.9).

$$\bar{m}\ddot{x} + \bar{c}\dot{x} + \bar{k}x = C'_D \rho \frac{D}{2} (\dot{u} - \dot{x}) + C_M \rho \pi \frac{D^2}{4} \ddot{u}. \tag{3.10}$$

By adding the flow effect to the equation of motion, another force needs to be considered, which is the added or virtual mass. A structure immersed in a fluid must overcome resistance from the fluid to move through it. This additional resistance is not related to the viscousness of the fluid, but to the volume of the structure. Since the structure needs to replace the same volume of fluid in order to move through the fluid, the moving structure requires more force, as if it had additional mass. The added mass, therefore, is expressed [Wilson et al., 2003] as

$$\bar{M}_a = \left(\bar{m} + C_A \rho \pi \frac{D^2}{4} \right) \tag{3.11}$$

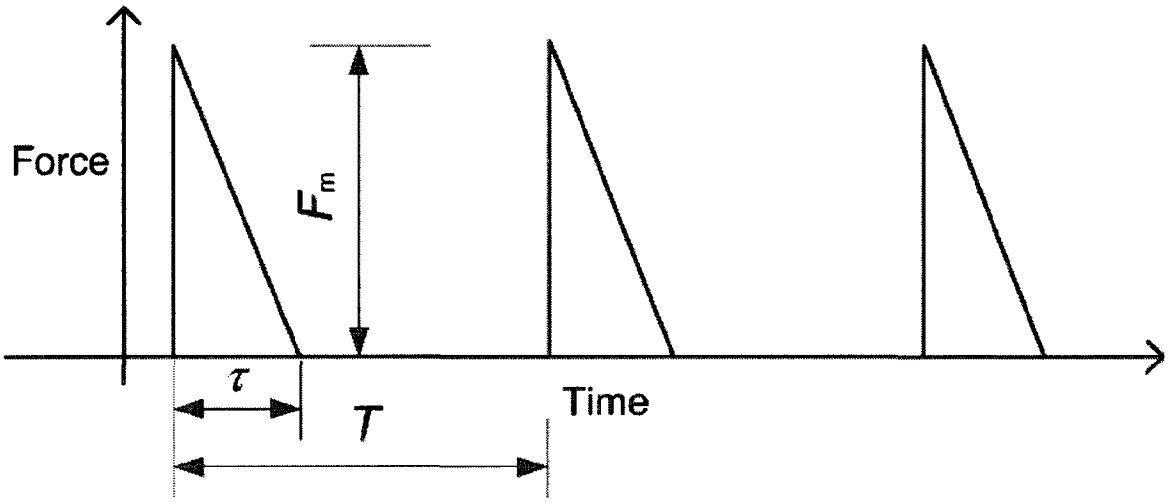

Figure 3.3: Ice forcing function (from [Qu et al., 2006])

where C_A is the added mass coefficient and defined by

$$C_A = C_M - 1 \tag{3.12}$$

As mentioned before, C_M is equal to 2 in most IIV cases, therefore C_A is calculated as 1. By replacing the mass of equation (3.10) with the added mass term, the equation including the flow effect is fully developed as

$$\left(\bar{m} + C_A \rho \pi \frac{D^2}{4}\right) \ddot{x} + \bar{c}\dot{x} + \bar{k}x = C'_D \rho \frac{D}{2} (\dot{u} - \dot{x}) + C_M \rho \pi \frac{D^2}{4} \ddot{u} \tag{3.13}$$

or

$$\bar{M}_a \ddot{x} + \left(\bar{c} + C'_D \rho \frac{D}{2}\right) \dot{x} + \bar{k}x = C'_D \rho \frac{D}{2} \dot{u} + C_M \rho \pi \frac{D^2}{4} \ddot{u} \tag{3.14}$$

The equation shows that the flow influences the structural dynamics through the added mass, change in damping term, as well as additional flow-induced force.

Defining an ice forcing function is the key factor to analyzing IIVs, but the difficulty of IIV analysis is that the actual ice forcing mechanism is a complex non-linear process. In the literature, various linear or non-linear ice forcing functions have been proposed by either field or laboratory experiments. Although mathematical expressions vary from

model to model, ice forcing functions can be globally defined as periodic saw-tooth functions. Yue and Bi (1998, 2000) suggested a simple but effective ice forcing function given by

$$\bar{f}(t) = \begin{cases} \bar{F}_m(1 - t/\tau) & (0 \leq t < \tau) \\ 0 & (\tau \leq t < T) \end{cases} \tag{3.15}$$

where $\bar{F}_m$ is the maximum force. τ and T are the forcing and total periods as shown in Figure 3.3 and correspond to δ and p of Figure 2.2, respectively. To obtain a closed form solution, equation (3.15) is transformed to a harmonic function by using a Fourier series. The forcing function can now be written as

$$\bar{f}(t) = A_0 + \sum_{N=1}^{\infty} \left[A_N \cos\left(\frac{2N\pi}{T}t\right) + B_N \sin\left(\frac{2N\pi}{T}t\right) \right] \tag{3.16}$$

where

$$A_0 = \frac{\bar{F}_m \tau}{2T} \tag{3.17}$$

$$A_N = \frac{\bar{F}_m T}{2N^2\pi^2\tau} \left[1 - \cos\left(\frac{2N\pi\tau}{T}\right) \right] \tag{3.18}$$

and

$$B_N = \frac{\bar{F}_m}{N\pi} - \frac{\bar{F}_m T}{2N^2\pi^2\tau} \sin\left(\frac{2N\pi\tau}{T}\right) \tag{3.19}$$

The right side of equation (3.14) describes the flow-induced force. In addition, C'_D is assumed to be small for linearization, the velocity and acceleration of the flow are assumed small so that the flow-induced force is negligible compared to the ice-induced force. The flow thus affects the structural response only via the flow-induced effect on the structural mass and damping parameters and not through an additional flow-induced force. The expression, therefore, of an IIV including the flow effect is finally developed by replacing the forcing part of equation (3.13) with equation (3.16) as

$$\bar{M}_a\ddot{x} + \left(\bar{c} + C'_D\rho\frac{D}{2}\right)\dot{x} + \bar{k}x = A_0 + \sum_{N=1}^{\infty} \left[A_N \cos\left(\frac{2N\pi}{T}t\right) + B_N \sin\left(\frac{2N\pi}{T}t\right) \right] \tag{3.20}$$

Equation (3.20) can be solved in closed form and easily implemented through numerical simulation.

3.3 Numerical Simulations of Ice-induced Vibrations with Flow

The numerical simulation of equation (3.20) is performed to analyze the effect of flow. Considering a one degree-of-freedom system with a simple harmonic force given by

$$m\ddot{x} + c\dot{x} + kx = F_m \sin(\omega t)$$

the steady-state response of the given system can be calculated by using the magnification factor, M, as

$$x(t) = F_m \mathrm{M} \sin(\omega t + \theta)$$

where θ is the phase difference [Thomson, 1998]. The flow effect, therefore, can be compared by calculating the magnification factors of the structural responses with flow and without flow. Assuming $x(t) = Xe^{i\omega_N t}$ and $\bar{f}(t) = Fe^{i\omega_N t}$, Equation (3.6) becomes

$$X\left(-\omega_N^2 \bar{m} + \bar{c}\omega_N i + \bar{k}\right) e^{i\omega_N t} = Fe^{i\omega_N t} \tag{3.21}$$

or

$$\frac{X}{F} = \frac{1}{\bar{k} - \omega_N^2 \bar{m} + \bar{c}\omega_N i} \tag{3.22}$$

therefore the magnification factor without the flow effect is

$$\mathrm{M} = \left|\frac{X}{F}\right| = \frac{1}{\sqrt{\left(\bar{k} - \omega_N^2 \bar{m}\right)^2 + \left(\bar{c}\omega_N\right)^2}} \tag{3.23}$$

where the Nth forcing frequency is

$$\omega_N = \frac{2N\pi}{T} \tag{3.24}$$

so that the forcing frequency is a function of N. In the same manner, the magnification factor with the flow effect can be obtained from equation (3.14) as

$$\mathrm{M}_f = \frac{1}{\sqrt{\left(\bar{k} - \omega_N^2 \bar{M}_a\right)^2 + \left\{\omega_N \left(\bar{c} + C'_D \rho \frac{D}{2}\right)\right\}^2}} \tag{3.25}$$

Parameter	Model Structure
h (mm)	41
D (mm)	76
m (kg)	1600
c (kNs/m)	0.2
k (MN/m)	1
ℓ (m)	44.93
σ_c (MPa)	1.4
x_{max} (mm)	20

Table 3.1: Parameters for simulations

where the subscript f indicates that the equation is developed under the flow effect. The displacement of the structure with the flow effect can be derived from equation (3.25) by

$$x(t) = \frac{A_0}{\bar{k}} + \sum_{N=1}^{100} \left[\mathrm{M}_f \left\{ A_N \cos\left(\frac{2N\pi}{T} t + \theta_N \right) + B_N \sin\left(\frac{2N\pi}{T} t + \theta_N \right) \right\} \right] \tag{3.26}$$

where

$$\theta_N = \tan^{-1} \left\{ \frac{\omega_N \left(\bar{c} + C'_D \rho \frac{D}{2} \right)}{\bar{k} - \omega_N^2 \bar{M}_a} \right\} \tag{3.27}$$

The number in the summation is arbitrarily picked and confirmed by graphing the original and approximated forcing functions. Figure 3.4 (a) and (b) prove that one hundred summation terms are enough to approximate 96 percent of the peak values of the original forcing function.

The data to perform the numerical simulations are obtained from Kärnä and Turunen (1989). The IIV data of the channel marker in the Baltic were measured by Nordlund et al. during the winter of 1987 to 1988, and the structural properties were specified. Some structural properties not specified on Kärnä and Turunen (1989) are derived from the density of steel, $\rho_{steel} = 7859\,{}^{\mathrm{kg}}/_{\mathrm{m}^3}$, which is assumed to be the material of the channel marker. In Table 3.1, h is the thickness of the ice sheet, and σ_c is the compressive strength

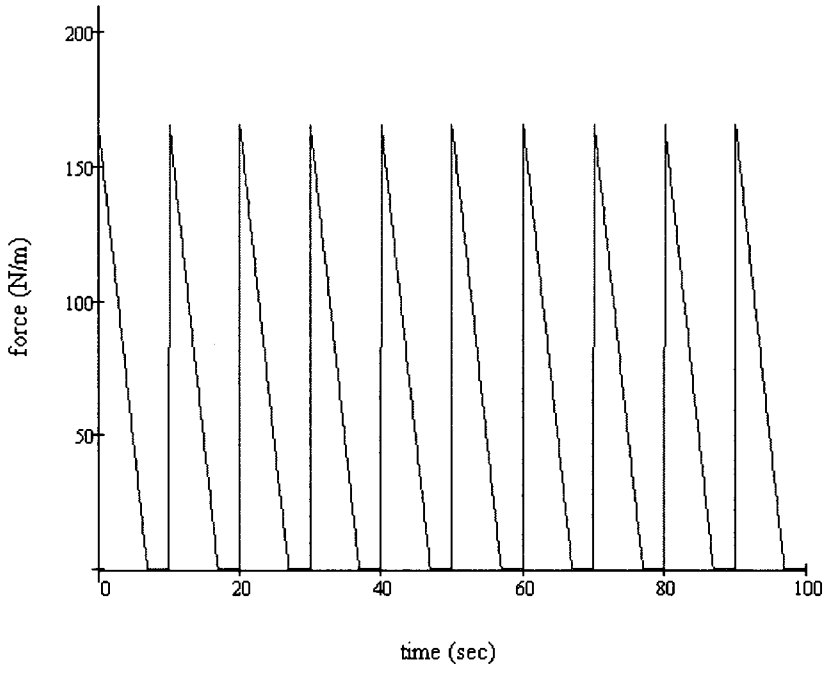

(a) Original forcing function

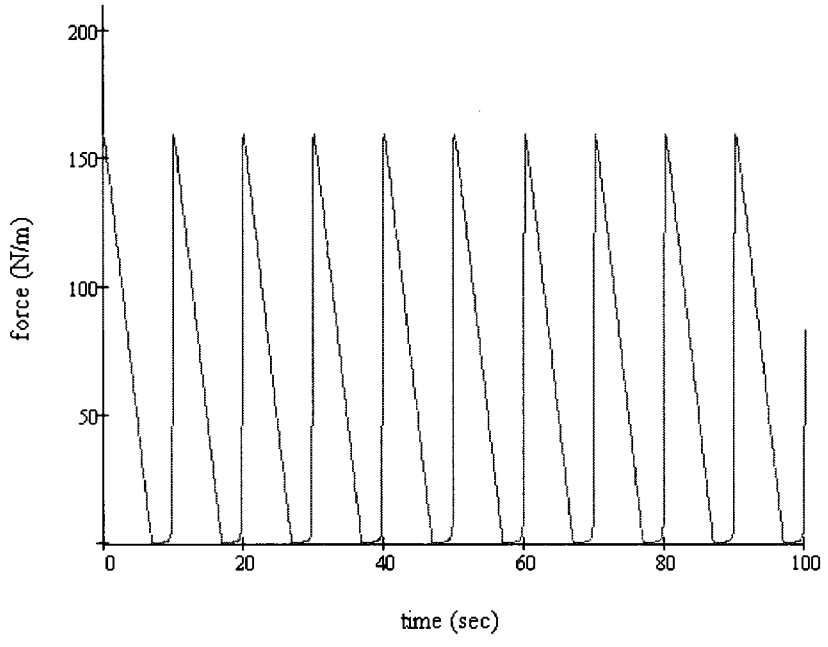

(b) Approximated forcing function

Figure 3.4: Original and approximated forcing functions

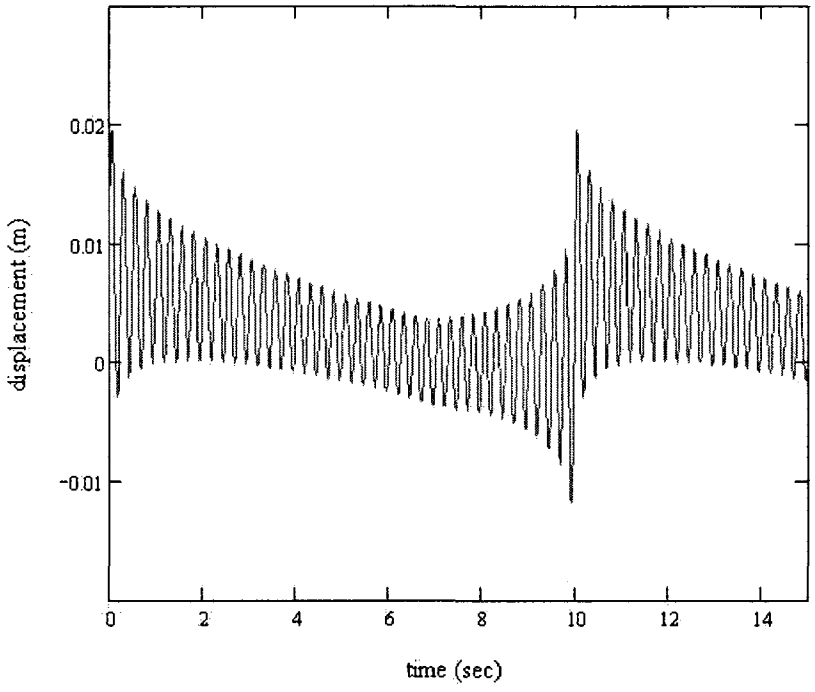

Figure 3.5: Displacement of the structure

of the ice. The initial or maximum ice force is calculated by Korzhavin's approach

$$\bar{F}_m = 0.9\frac{\sigma_c D h}{\ell}\sqrt{1+5\frac{h}{D}} = 168.03\,(^N/_m) \tag{3.28}$$

where ℓ is the length of the structure [Kärnä and Turunen, 1989]. The maximum displacement of the structure x_{max} is used to find τ and T of the ice forcing function. By plotting equation (3.26) τ and T are found as 7 and 10 seconds from Figure 3.5, respectively.

Figure 3.6 is drawn from equation (3.23) and (3.25), which shows that the flow effect lowers the resonance frequency as well as the amplitude. Since the magnification factors of Figure 3.6 have the same forcing function, the flow effect is only related to the structure. According to equation (3.25), the flow effect influences the IIV through $\bar{M}_a$ and C'_D. The frictional drag coefficient C_D is 1 for Reynolds number 1,000 to 200,000 in most IIV cases. C'_D, therefore, takes little part in determining the flow effect as long as the equation remains in the linear region. Once the geometry of the structure is fixed, the

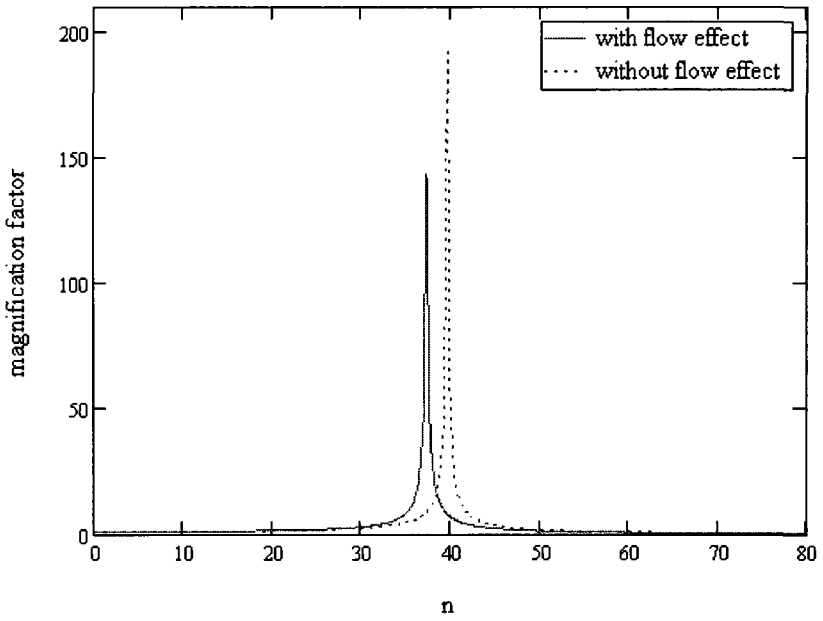

Figure 3.6: Magnitudes of the structure

mass of the structure is the only independent factor influencing the added mass term since C_A and D are determined by the geometry of the structure. Based on the mass of the structure, a non-dimensional parameter called the density ratio γ_ρ can be introduced from equation (3.11) as

$$\bar{M}_a = \left(\bar{m} + C_A \rho \pi \frac{D^2}{4}\right) = \left(\rho_s \frac{\pi D^2}{4} + C_A \rho \pi \frac{D^2}{4}\right) = \frac{\pi D^2}{4}\left(\rho_s + C_A \rho\right)$$

$$= \frac{\pi D^2}{4} \rho \left(\gamma_\rho + C_A\right) \tag{3.29}$$

where

$$\gamma_\rho = \frac{\rho_s}{\rho} \tag{3.30}$$

and ρ_s is the density of the structure and ρ is the density of the fluid in which the structure is located. From equation (3.12), C_A is calculated as 1.

Using equation (3.30) and (3.25), the relation between the density ratio and the magnification factor is obtained. Equation (3.23) and (3.25) are plotted by changing the density ratio to show the flow effect. In Figure 3.7 and 3.8, the black contour peaks on

the left represent the response with the flow effect and the grey contour peaks on the right represent the response without the flow effect. The flow effect lowers the magnitude factor for all the ranges of the density ratio. Figure 3.8, the top view of Figure 3.7, clearly shows that the resonance frequency shifting is significant for low density ratio because the added mass effect in $\bar{M}_a$ becomes relatively larger when the density of the structure is small compared to the density of water. When the density ratio is larger than 8, however, the flow effect has little influence on the frequency change.

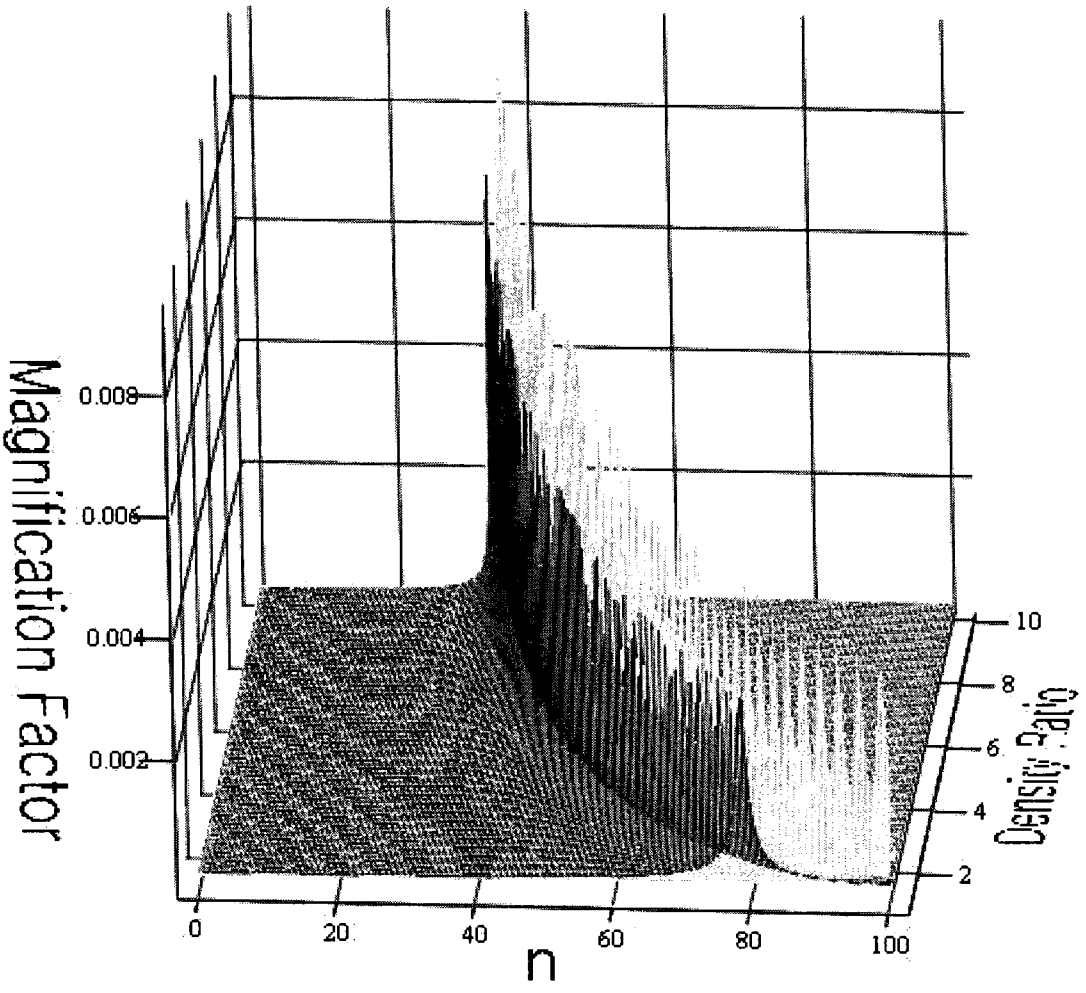

Figure 3.7: Density ratio vs. magnification factor

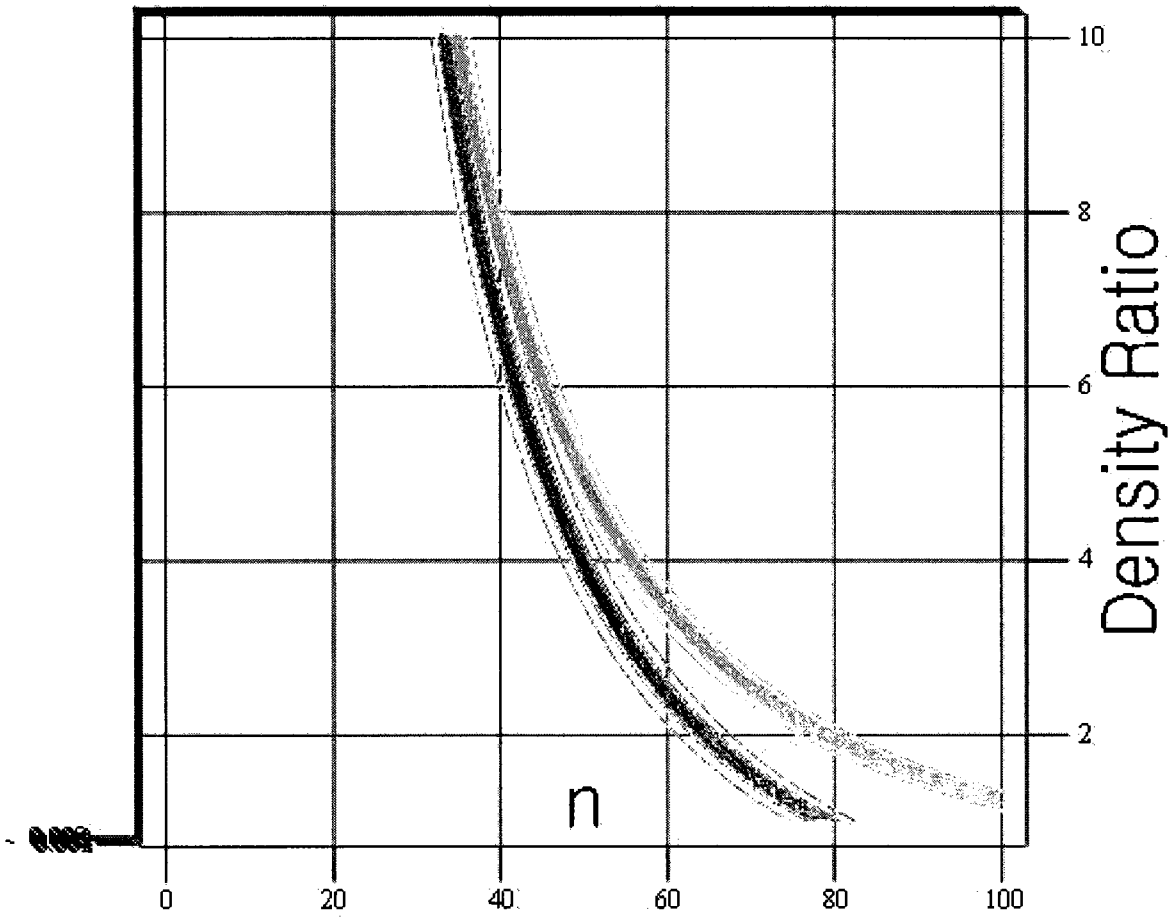

Figure 3.8: Density ratio vs. frequency shift

Chapter 4

Comparison of Selected Modeling Approaches

Since research into ice-induced vibrations began, numerous modeling approaches have been proposed. In this chapter, some models are analyzed and reviewed in depth including simulation results. The proposed modeling approaches can be categorized into two types. The models suggested by Toyama et al. and Huang and Liu are not only classified as the same modeling type, the characteristic failure frequency model, but also have many similar features. These two modeling approaches are thoroughly reviewed and reproduced in this chapter. At the end of the chapter, the two models and the model developed in Chapter 3 are compared to investigate differences and similarities of models based on the same theory.

4.1 Toyama et al. (1983)

The paper written by Toyama et al., Model Tests on Ice-induced Self-excited Vibration of Cylindrical Structure, is a remarkable achievement in the field of ice-induced vibration (IIV) research. The paper proposed dividing the ice forcing into two stages: elastic and crushing phases. The phase division of the ice forcing function was suggested by past

research such as in Matlock et al., however Toyama et al. actually developed equations of motion according to the phase division. Ranta, M. and Räty R. (1983) published the paper titled 'On the Analytic Solution of Ice-induced Vibrations in a Marine Pile Structure' containing the same idea in the same year, but their paper was more focused on the continuity and stability of IIVs. The method of Toyama et al., therefore, is more frequently adopted by other IIV researchers. However, inspite of its pioneering work, the Toyama et al. paper has several parts requiring improvements.

The Toyama et al. paper derives equations for a one degree-of-freedom system, thus the equation of motion is the same as equation (3.5), $m\ddot{x} + c\dot{x} + kx = f(t)$. Toyama et al. refer to their model as the self-excited model, but equation (3.5) is not an equation of motion reflecting the essential idea of the self-excited model. The idea behind the self-excited model is that negative damping must occur in a certain range depending on the forcing function, which in turn induces instability. Toyama et al. define the ice force as two separate phases. An elastic phase is the period for which the structure and ice move at the same velocity due to negligibly small deformations of the ice. Thus $\dot{x} = \dot{z}$ and $\ddot{x} = 0$, and the elastic ice force from equation (3.5) can be written as

$$f(t) = kx + c\dot{z} \tag{4.1}$$

where $\dot{z}$ is the velocity of the ice. The second phase, a crushing phase, starts at the maximum value, F_m, of $f(t)$. The crushing force, F_c, is defined to be constant and smaller than F_m. From equation 3.5, the equation of motion in the crushing phase is given by

$$m\ddot{x} + c\dot{x} + kx = F_c \tag{4.2}$$

Both equations (4.1) and (4.2) present an ice force that is independent of loading rate, therefore the Toyama et al. model is more appropriately considered to be a characteristic failure frequency model. Other researchers who cited Toyama et al. also used it as a characteristic failure frequency model.

The equation of motion for the elastic phase can be obtained by substituting equa-

tion (4.1) into (3.5) as

$$m\ddot{x} + c\dot{x} + kx = kx + c\dot{z} \tag{4.3}$$

Since $\ddot{x} = 0$ during the elastic phase,

$$\dot{x} = \dot{z}$$

Taking integrals on both sides to obtain the displacement of the system,

$$\int \frac{dx}{dt} = \int \frac{dz}{dt}$$

which is

$$x(t) = z(t) + C_1 \tag{4.4}$$

where C_1 is the initial displacement. The displacements of the structure and ice are the same during the elastic phase. When $f(t)$ reaches F_m, the crushing phase starts. Toyama et al. assume that their model has zero or very small damping, so that the system is an under-damped system. For the crushing phase, equation (4.2) has the following homogeneous solution,

$$x_h(t) = e^{-\zeta\omega_n t}\left(A_1 \cos\omega_d t + A_2 \sin\omega_d t\right) \tag{4.5}$$

where ζ, ω_n, and ω_d are the damping ratio, natural frequency, and damped natural frequency which are defined as

$$\zeta = \frac{c}{2m\omega_n}$$

$$\omega_n = \sqrt{\frac{k}{m}}$$

and

$$\omega_d = \omega_n\sqrt{1-\zeta^2}$$

respectively. Since F_c is constant, the particular solution is

$$x_p(t) = C_2 \tag{4.6}$$

and

$$\dot{x}_p = \ddot{x}_p = 0 \tag{4.7}$$

Substituting equation (4.6) and (4.7) into equation (4.2)

$$kx_p = F_c$$

or

$$x_p = C_2 = \frac{F_c}{k} \tag{4.8}$$

Therefore, the total solution is expressed as

$$x(t) = x_h(t) + x_p(t) = e^{-\zeta\omega_n t}\left(A_1 \cos\omega_d t + A_2 \sin\omega_d t\right) + \frac{F_c}{k} \tag{4.9}$$

With the following initial conditions [Toyama et al., 1983],

$$x_0 = \frac{(F_m - c\dot{z})}{k} \text{ and } \dot{x}_0 = \dot{z},$$

the A_1 can be calculated from equation (4.9) as

$$x(0) = A_1 + \frac{F_c}{k} = \frac{F_m - c\dot{z}}{k} \tag{4.10}$$

or

$$A_1 = \frac{1}{k}\left(F_m - F_c - c\dot{z}\right). \tag{4.11}$$

The velocity can be obtained by taking the derivative of equation (4.9)

$$\dot{x}(t) = -\zeta\omega_n e^{-\zeta\omega_n t}\left(A_1 \cos\omega_d t + A_2 \sin\omega_d t\right) + \omega_d e^{-\zeta\omega_n t}\left(-A_1 \sin\omega_d t + A_2 \cos\omega_d t\right) \tag{4.12}$$

and substituting the initial condition

$$\dot{x}(0) = -\zeta\omega_n A_1 + \omega_d A_2 = -\frac{1}{k}\zeta\omega_n\left(f_m - f_c - c\dot{z}\right) + \omega_d A_2 = \dot{z} \tag{4.13}$$

or

$$A_2 = \frac{\zeta\omega_n}{k\omega_d}\left(F_m - F_c - c\dot{z}\right) + \frac{\dot{z}}{\omega_d} \tag{4.14}$$

The solutions of the elastic and crushing phases are thus completely derived. Toyama et al. insisted that IIVs can be described as alternatively repeating solutions of the elastic and crushing phases, corresponding to equations (4.4) and (4.9).

The unique work done by Toyama et al. is of calculating the duration of each phase. One complete period consists of the elastic period, t_e, followed by the crushing period, t_c.

$$t_{total} = t_e + t_c \tag{4.15}$$

Based on experimental data, Toyama et al. calculated the elastic and crushing periods [Toyama et al., 1983] as

$$\frac{t_e}{t_n} = \frac{1-\beta}{\pi\alpha} \tag{4.16}$$

and

$$\frac{t_c}{t_n} = 1 \text{ to } \frac{1}{\pi}\tan^{-1}\left(\frac{1-\beta}{\alpha}\right) \tag{4.17}$$

where

$$\alpha = \frac{k\dot{z}}{f_m\omega_n} \tag{4.18}$$

$$\beta = \frac{F_c}{F_m} \tag{4.19}$$

and

$$t_n = \frac{2\pi}{\omega_n}. \tag{4.20}$$

Now that the complete solutions and periods of each phase have been obtained, numerical simulations can be performed.

4.1.1 Numerical Simulations

The numerical simulations of the Toyama et al. model were performed, based on the parameters which presented in Table 3.1 of Chapter 3. Additionally, two more parameters, F_c and $\dot{z}$, need to be introduced. Equation (4.18) and (4.19) can only be used when β is larger than 0.5, therefore F_c is arbitrarily chosen as 5700 N so that β becomes 0.755 [Toyama et al., 1983]. Since the velocity of ice is not specified or limited by Toyama et al.,

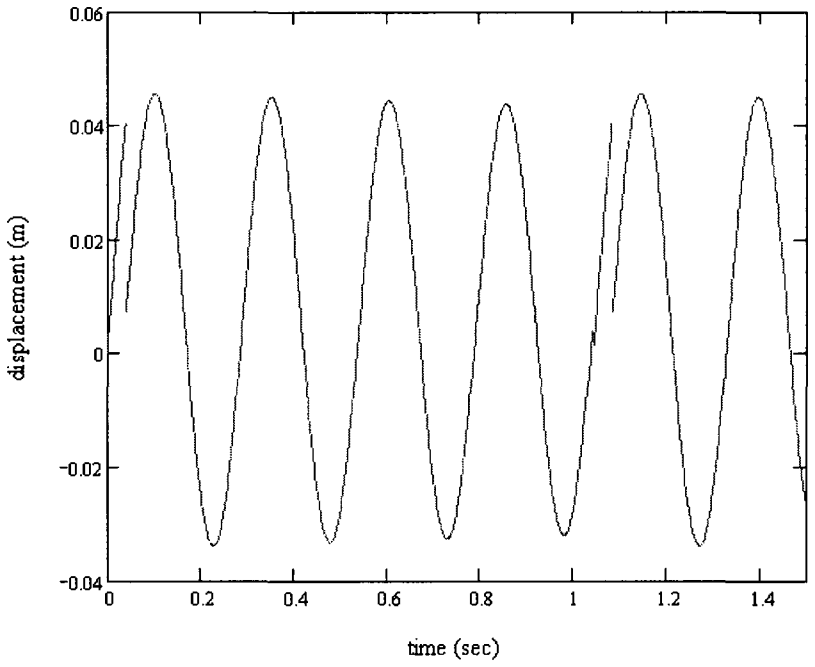

Figure 4.1: Calculated IIV based on Toyama et al. (1983)

the velocity of ice is also randomly chosen from 0.001 to 1 $^{m}/_{s}$. Applying the parameters to equation (4.18), α is calculated as 5.229. By substituting α and β into equation (4.16) and (4.17), the elastic and crushing periods are obtained as $t_e = 0.042$ and $t_c = 1.002$ seconds. Equation (4.5) and (4.9) can be evaluated over the periods of t_e and t_c.

Figure 4.1 shows the result calculated rigorously based on the Toyama et al. model. Although β, which determines the applicability of the theory, is larger than 0.5, discontinuities appear between the elastic and crushing phases, as well as between total periods. The discontinuities continue to exist for all ranges of ice velocities even at the very low ice velocity of 0.001 $^{m}/_{s}$. This indicates that the Toyama et al. method cannot model all cases of IIVs. The Toyama et al. model requires improvement to be applicable to more general cases of IIVs.

The discontinuities between the phases are closely related to the initial conditions. The amount of displacement at the end of the elastic phase should be equal to the initial

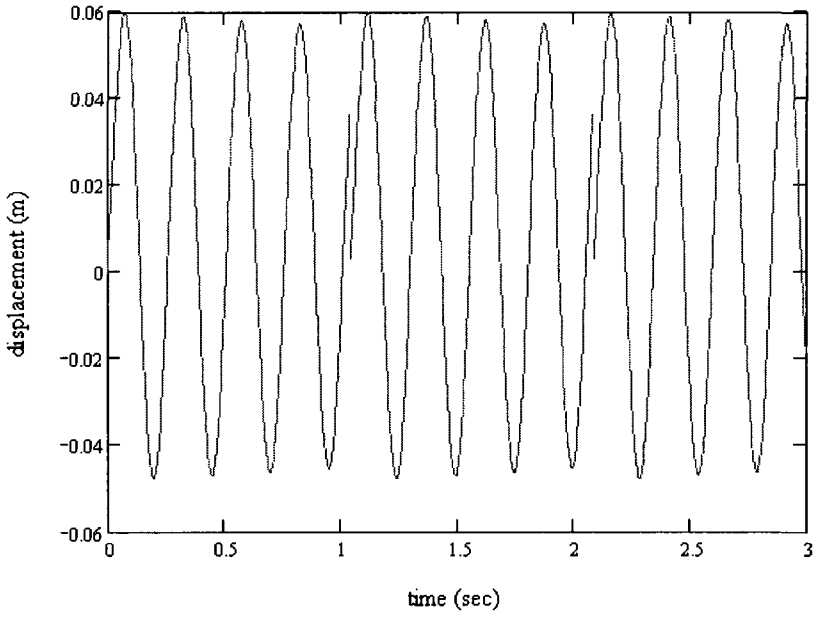

Figure 4.2: IIV based on the modified Toyama et al. method

displacement of the crushing phase. Thus equation (4.1) can be written at $t = t_e$ as

$$f(t_e) = kx_e + c\dot{z} = k\left(\dot{x} \cdot t_e\right) + c\dot{z} = k\left(\dot{z} \cdot t_e\right) + c\dot{z} = F_m \tag{4.21}$$

which follows since $\dot{x} = \dot{z}$ for the elastic phase. However, equation (4.21) does not hold for all cases, especially for the given parameters. Therefore, the initial condition for displacement at the beginning of the crushing phase needs to be changed so that it is the same as the displacement at the end of the elastic phase. According to the definition of the elastic phase by Toyama et al., the velocities of the ice and structure are the same during the elastic phase. In other words, the ice travels the same displacement as the structure does. From the definition, a new initial condition for the displacement is presented as

$$x_0 = \dot{z} \cdot t_e + C_3 \tag{4.22}$$

where C_3 is a constant to compensate the initial displacement of the elastic phase.

Figure 4.2 is the IIV with the modified initial conditions when C_3 is set to be zero. The discontinuities between the phases are eliminated but after one complete period,

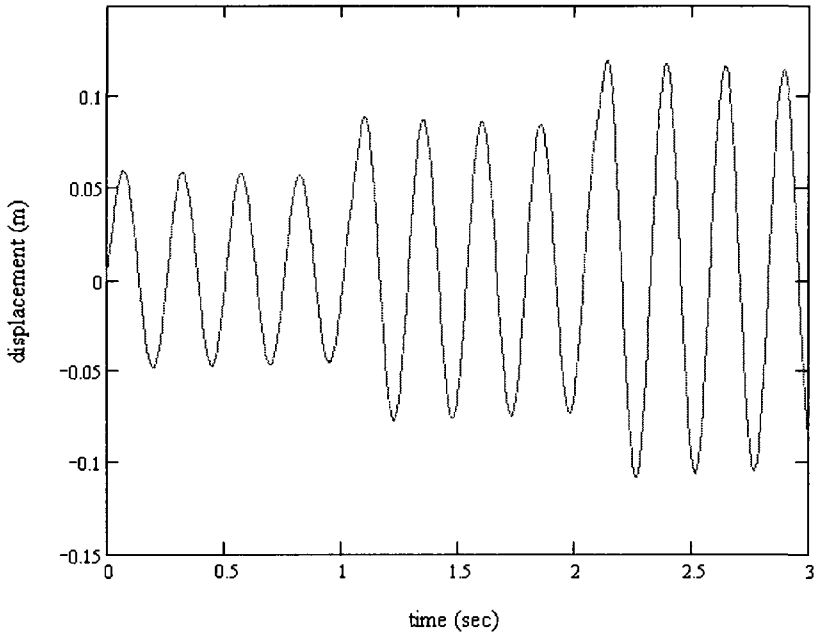

Figure 4.3: IIV based on the fully modified Toyama et al. method

which consists of one elastic phase and one crushing phase, discontinuities still exist. The end of the crushing phase does not match the beginning of the second elastic phase. If the ice velocity decreases to lower than 0.01 $^{m}/_{s}$, those discontinuities disappear. This means that the Toyama et al. method is only applicable at very low ice velocities.

C_3 of equation (4.22) can be used to fix the gap between the complete periods. After each complete period, the end displacement is compensated by $C_3 = x(t_{total})$, and the compensated initial condition becomes

$$x_0 = \dot{z} \cdot t_e + C_3 = \dot{z} \cdot t_e + x\left(t_{total}\right) \tag{4.23}$$

With the compensated initial conditions, equation (4.9) is solved every complete period. Figure 4.3 presents three complete periods plotted by the fully modified Toyama et al. model. When the ice velocity is larger than 0.01 $^{m}/_{s}$, the vibrations grow as time increases. As long as the ice velocity or the ice force remain the same, the vibration will keep increasing or decreasing because the duration of the elastic and crushing phases are fixed by the ice velocity and the ice force.

4.2 Huang and Liu (2006)

There are several reasons why Huang and Liu (2006) is chosen for an in-depth review after reviewing Toyama et al. (1983). First, Huang and Liu (2006) is one of the most recent IIV papers and thus should contain state-of-the-art theories and research. Secondly, both Huang and Liu (2006) and Toyama et al. (1983) are based on the characteristic failure frequency model. Although Toyama et al. considered their model as the self-excited model, it was shown in the previous section to be more appropriate as a characteristic failure frequency model. In addition, the model proposed by Huang and Liu is a more advanced model along the lines of the Toyama et al. model. Huang and Liu divide IIVs into three phases according to the velocity and deflection of a contacting ice sheet while Toyama et al. separate the phases of IIVs into two phases, based on the ice forcing function. Contrary to the Toyama et al. model, which uses fixed phases, each phase of the Huang and Liu model is instantaneously determined as the evolution of IIV is calculated. Finally, Huang and Liu (2006) provide detailed parameters of their simulations so that other researchers can easily reproduce their results.

Huang and Liu define ice forces as loading, extrusion, and separation phases. The definitions of the loading and extrusion phases are similar to those of the elastic and crushing phases of Toyama et al. with the exception of the conditions of each phase. Huang and Liu disagree with the idea of Toyama et al. that the structural and ice velocities are the same during the elastic phase. Instead, they suggest that both loading and extrusion phases occur when the structural velocity is less than that of the ice. The phase division between the loading and extrusion phases depends on whether the deflection of the ice exceeds the failure deflection, δ_f, or not. If the amount of ice deflection is less than the failure deflection, the structure is under the loading phase. The extrusion phase starts once the ice deflection is greater than the failure deflection. The ice deflection is derived directly from Figure 2.2 [Huang and Liu, 2006] as

$$\delta = x_0 + \dot{z}t - x(t) - p(n-1) \tag{4.24}$$

where x_0 is the initial displacement of the ice sheet and n is the number of the tooth in contact. The ice force at the loading phase is expressed as $f(t) = k_c\delta(t) + F_e$ where F_e is the residual force from the previous crush and k_c is the effective contact stiffness. During the extrusion phase, the ice force remains at F_e, which corresponds to the crushing phase of Toyama et al. (1983). The separation phase begins when the structural velocity is greater than the ice velocity, therefore no force is transmitted during the separation phase.

Combining the ice forces of each phase with a one degree-of-freedom system, the equation of motion is given by [Huang and Liu, 2006]

$$m\ddot{x} + c\dot{x} + kx = \begin{cases} k_c\left[x_0 + \dot{z}t - x - p\left(n-1\right)\right] + F_e & 0 \leq \delta < \delta_f \quad \text{and} \quad \dot{x} \leq \dot{z} \\ F_e & \delta_f \leq \delta < p \quad \text{and} \quad \dot{x} \leq \dot{z} \\ 0 & \dot{x} > \dot{z} \end{cases} \tag{4.25}$$

Huang and Liu normalize equation (4.25) by using

$$\Delta = \frac{F_{fmax}}{k} \tag{4.26}$$

where F_{fmax} is the maximum failure ice force [Huang and Liu, 2006]. x, x_0, p, and δ can be normalized by dividing by Δ. Other terms are normalized as

$$\tilde{k}_c = {}^{k_c}/_{k}$$

$$\tilde{F}_e = {}^{F_e}/_{F_{fmax}}$$

and

$$\dot{\tilde{z}} = {}^{\dot{z}}/_{\omega_n \Delta}$$

in which the tildes over the letters indicates that the terms are normalized. Finally, normalized time is introduced as

$$\tilde{t} = \omega_n t.$$

Using the normalized factors, equation (4.25) becomes the non-dimensional equation given by

$$\ddot{\tilde{x}} + 2\zeta\dot{\tilde{x}} + \tilde{x} = \begin{cases} \tilde{k}_c\left[\tilde{x}_0 + \dot{\tilde{z}}\tilde{t} - \tilde{x} - \tilde{p}\,(n-1)\right] + \tilde{F}_e & 0 \le \tilde{\delta} < \tilde{\delta}_f \quad \text{and} \quad \dot{\tilde{x}} \le \dot{\tilde{z}} \\ \tilde{F}_e & \tilde{\delta}_f \le \tilde{\delta} < \tilde{p} \quad \text{and} \quad \dot{\tilde{x}} \le \dot{\tilde{z}} \\ 0 & \dot{\tilde{x}} > \dot{\tilde{z}} \end{cases} \tag{4.27}$$

where $\ddot{\tilde{x}}$ and $\dot{\tilde{x}}$ are second and first derivatives of the normalized displacement, $\ddot{\tilde{x}} = {}^{d^2\tilde{x}}/_{d\tilde{t}^2}$ and $\dot{\tilde{x}} = {}^{d\tilde{x}}/_{d\tilde{t}}$ [Huang and Liu, 2006]. The failure deflection, $\tilde{\delta}_f$, is defined as

$$\tilde{\delta}_f\left({}^{\dot{z}_r}/_{\dot{z}_t}\right) = \frac{\tilde{\sigma}_f\left({}^{\dot{z}_r}/_{\dot{z}_t}\right) - \tilde{F}_e}{\tilde{k}_c} \tag{4.28}$$

where $\dot{z}_r$ is the relative velocity between the structure and ice sheet, and $\dot{z}_t$ is the transitional relative ice velocity corresponding to $\dot{\varepsilon}_t$ of Figure 4.4 which is the transitional strain rate. In addition, the normalized crushing strength, $\tilde{\sigma}_f$, is expressed as

$$\tilde{\sigma}_f\left({}^{\dot{z}_r}/_{\dot{z}_t}\right) = \begin{cases} (1-\tilde{\sigma}_{fd})\left({}^{\dot{z}_r}/_{\dot{z}_t}\right)^{\mu} + \tilde{\sigma}_{fd} & {}^{\dot{z}_r}/_{\dot{z}_t} \le 1 \\ (1-\tilde{\sigma}_{fd})\left({}^{\dot{z}_r}/_{\dot{z}_t}\right)^{\nu} + \tilde{\sigma}_{fd} & 1 < {}^{\dot{z}_r}/_{\dot{z}_t} \end{cases} \tag{4.29}$$

in which $\tilde{\sigma}_{fd}$ and $\tilde{\sigma}_{fb}$ again correspond to Figure 4.4 and are normalized by dividing by $\tilde{\sigma}_{fmax}$.

The closed form solutions of equation (4.27) are given by Huang and Liu. For the loading phase,

$$\begin{aligned} \tilde{x}\left(\tilde{t}_l\right) = e^{-\zeta\tilde{t}_l}\left\{\left[\tilde{x}_{0l}\left(1-k_r\right) - \tfrac{\tilde{F}_e - 2\zeta\dot{\tilde{z}}}{k_q^2}\right]\cos\omega_l\tilde{t}_l + \tfrac{1}{\omega_l}\left[\dot{\tilde{x}}_{0l} + \zeta\tilde{x}_{0l}\left(1-k_r\right)\right.\right. \\ \left.\left. - \tfrac{\zeta\tilde{F}_e}{k_q^2} - k_r\dot{\tilde{z}}\left(1 - \tfrac{2\zeta^2}{k_q^2}\right)\right]\sin\omega_l\tilde{t}_l\right\} + \tfrac{\tilde{F}_e}{k_q^2} + k_r\left(\tilde{x}_{0l} + \dot{\tilde{z}}\tilde{t}_l - \tfrac{2\zeta\dot{\tilde{z}}}{k_q^2}\right) \end{aligned} \tag{4.30}$$

where the subscripts $0l$ mean the initial values of the loading phase and $\tilde{t}_l = \tilde{t} - \tilde{t}_{0l}$; $\omega_l^2 = k_q^2 - \zeta^2$; $k_q^2 = 1 + \tilde{k}$; and $k_r = {}^{\tilde{k}}/_{1+\tilde{k}}$. The solution of the extrusion phase is given by

$$\tilde{x}\left(\tilde{t}_e\right) = e^{-\zeta\tilde{t}_e}\left\{\left(\tilde{x}_{0e} - \tilde{F}_e\right)\cos\omega_e\tilde{t}_e + \frac{1}{\omega_e}\left[\dot{\tilde{x}}_{0e} + \zeta\left(\tilde{x}_{0e} - \tilde{F}_e\right)\right]\sin\omega_e\tilde{t}_e\right\} + \tilde{F}_e \tag{4.31}$$

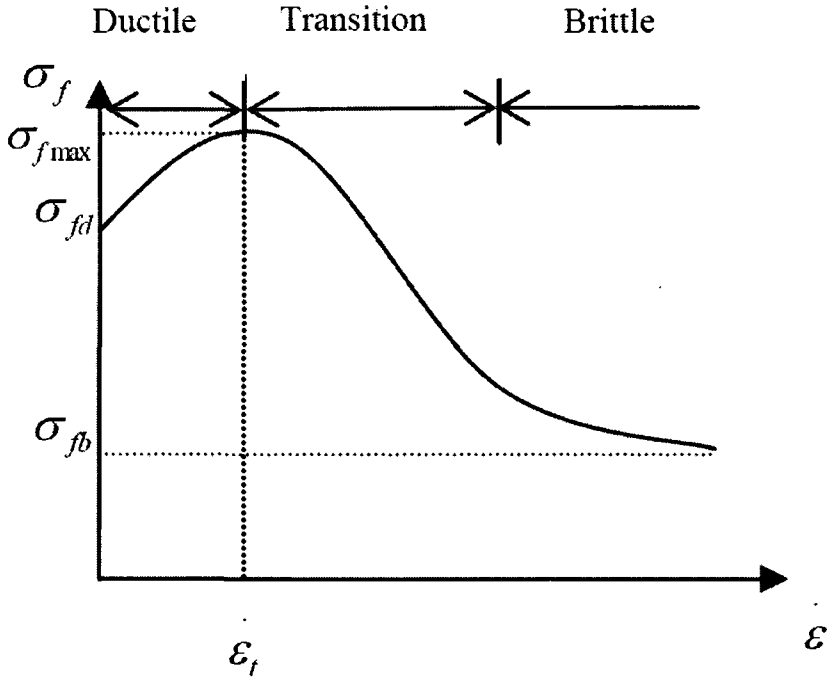

Figure 4.4: Ice Crushing Strength vs. Strain Rate (from [Huang and Liu, 2006])

in which the terms with the subscripts $0e$ are again the initial values of the extrusion phase, $\omega_e^2 = 1-\zeta^2$, and $\tilde{t}_e = \tilde{t}-\tilde{t}_{0e}$. In Huang and Liu (2006), the sine term of the extrusion phase is misprinted as $\left[\dot{\tilde{x}}_{0e} + \zeta\left(\tilde{x}_{0e} - \tilde{F}_e\right)\sin\omega_e\tilde{t}_e\right]$, and is corrected in equation (4.31). Finally, the separation phase is expressed as

$$\tilde{x}\left(\tilde{t}_s\right) = e^{-\zeta\tilde{t}_s}\left[\tilde{x}_{0s}\cos\omega_e\tilde{t}_s + \frac{1}{\omega_e}\left(\dot{\tilde{x}}_{0s} + \zeta\tilde{x}_{0s}\right)\sin\omega_e\tilde{t}_s\right] \tag{4.32}$$

where the subscripts $0s$ indicate the initial values of the separation phase, and $\tilde{t}_s = \tilde{t}-\tilde{t}_{0s}$.

4.2.1 Numerical Simulations

Since equation (4.27) is a nonlinear equation, the numerical simulation is performed with a small time step. Beginning with the initial displacement and velocity, the deflection of the ice, δ, and the relative velocity, $\dot{\tilde{z}}$, are calculated at every time step to determine which phase the system is in. To know the deflection of the ice and the relative velocity, however,

parameter	value
$\tilde{k}$	0.1
ζ	0.04
$\tilde{\sigma}_{fd}$	0.7
$\tilde{\sigma}_{fb}$	0.5
μ	0.5
ν	-2
$\tilde{p}$	10
$\tilde{F}_e$	0.2
$\dot{\tilde{z}}_t$	1

Table 4.1: Normalized parameters for simulations

the solutions, equation (4.30), (4.31), and (4.32), must be solved previously. Therefore, the phase conditions and solutions should technically be evaluated simultaneously, but the actual algorithm calculates the phase conditions based on the values from the previous time step because of the nonlinearity and mutual dependency. Once the phase is selected, the initial values of the phase are determined from the end values of the previous phase. The initial values of the phase remain the same until a phase change occurs. With this algorithm, the parameters given in Table 4.1 are applied to obtain the non-dimensional response of the system and ice force.

Figure 4.5 is plotted with the initial conditions $\tilde{x}_0 = 0$ and $\dot{\tilde{x}}_0 = 0$, and the ice velocity $\dot{\tilde{z}} = 2.2\dot{\tilde{z}}_t$ where $\dot{\tilde{z}}_t$ is again the normalized transitional relative ice velocity. The response of the Huang and Liu model does not display the discontinuity which was observed in the Toyama et al. model. It is evident that all initial values of each phase are properly determined so that the ends of each phase correspond to the beginning of the next phase. The calculated response, however, is notably different from the response presented in Huang and Liu (2006), Figure 4.6. Although the ice forces of Figure 4.5 and 4.6 illustrate similar behavior, the magnitudes and frequencies of the responses are

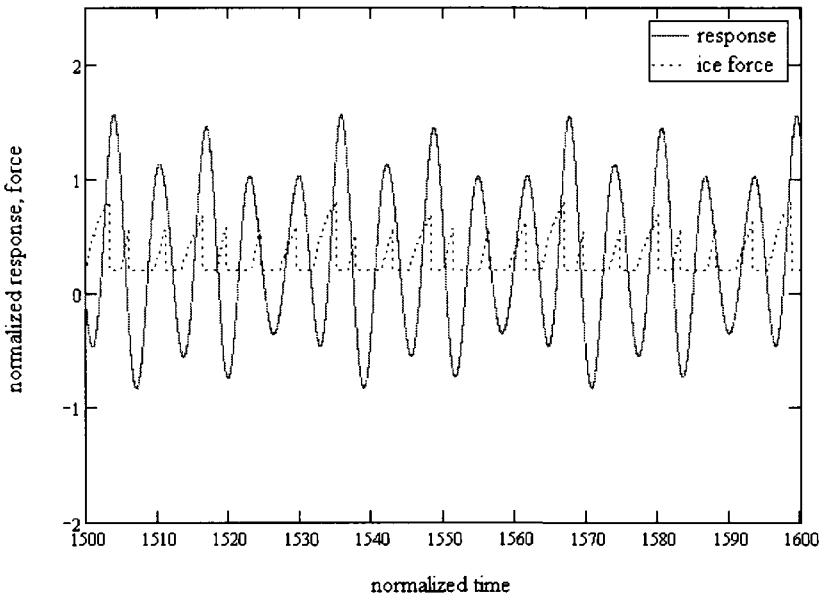

Figure 4.5: Response and ice force of the Huang and Liu model

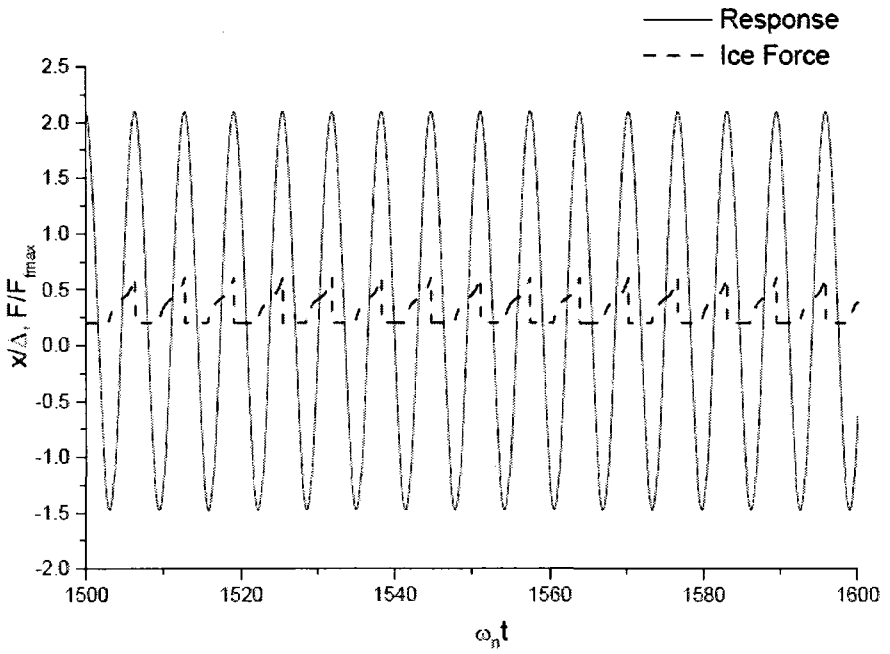

Figure 4.6: Response and ice force (from [Huang and Liu, 2006])

not identical. There are several possible reasons for this disagreement. The algorithm used to reproduce the Huang and Liu model is very sensitive to changes in parameters. The precision of simulation programs, therefore, can significantly influence the calculation results. In addition, the algorithm itself may be different from the one used by Huang and Liu, of which no details are given. Since the Huang and Liu model includes nonlinearity, there is the possibility that a small difference in the beginning can lead to a considerable difference in the final stage.

4.3 Comparison of the Three Models

So far, three different modeling approaches of IIVs have been investigated in Chapters 3 and 4. These three modeling approaches have one common feature which is the characteristic failure frequency model. Although expressions vary from model to model, the foundation of the three models is a one degree-of-freedom system based on the characteristic failure frequency model. Therefore, if the same parameters are applied, the predictions of the three models can be compared. Two sets of the parameters have been used to run the numerical simulations, Table 3.1 and 4.1. Since the Huang and Liu model uses normalized parameters, Table 4.1, it should be reversible to the original equation to be applicable the parameters given in Table 3.1. Huang and Liu, however, do not provide enough information for the original equation, therefore the other two models, the Toyama et al. model and model proposed in Chapter 3, are normalized to utilize Table 4.1.

From now on, the model proposed in Chapter 3 will be addressed as the Yue and Bi model because the model is developed from the forcing function suggested by Yue and Bi [Qu et al., 2006]. Equation (3.15) is rewritten in the following form as

$$f(t) = \begin{cases} F_m(t/\tau) & (0 \leq t < \tau) \\ 0 & (\tau \leq t < T) \end{cases} \tag{4.33}$$

Combining equation (4.33) with (3.5),

$$m\ddot{x} + c\dot{x} + kx = \begin{cases} F_m(t/\tau) & (0 \leq t < \tau) \\ 0 & (\tau \leq t < T) \end{cases} \tag{4.34}$$

Normalization can be done by using the same normalized quantities given in the previous section. The first line of equation (4.34) is divided by m and $\Delta = F_{fmax}/k$,

$$\frac{\ddot{x}}{\Delta} + \frac{c}{m\Delta}\dot{x} + \frac{k}{m\Delta}x = \frac{F_m}{m\Delta}\left(\frac{t}{\tau}\right) \tag{4.35}$$

Since $\tilde{x} = x/\Delta$ and $\tilde{t} = \omega_n t$,

$$\frac{d}{dt} = \frac{d}{d\tilde{t}}\frac{d\tilde{t}}{dt} = \omega_n \frac{d}{d\tilde{t}} \tag{4.36}$$

Substituting equation (4.36) into (4.35),

$$\omega_n^2 \frac{d^2\tilde{x}}{d\tilde{t}} + \omega_n \frac{c}{m}\frac{d\tilde{x}}{d\tilde{t}} + \omega_n^2 \tilde{x} = \frac{F_m}{m\Delta}\left(\frac{t}{\tau}\right) \tag{4.37}$$

Dividing equation (4.35) by ω_n^2,

$$\ddot{\tilde{x}} + 2\zeta\dot{\tilde{x}} + \tilde{x} = \frac{F_m}{k\Delta}\left(\frac{\omega_n t}{\omega_n \tau}\right) = \tilde{F}_m\left(\frac{\tilde{t}}{\tilde{\tau}}\right) \tag{4.38}$$

where $\tilde{F}_m = F_m/F_{fmax}$. In Chapter 3, the ice force is 0 for $\tau \leq t < T$. Since this phase is theoretically much closer to the extrusion phase of the Huang and Liu model than the separation phase, 0 is replaced with $\tilde{F}_e$ from the Huang and Liu model for normalized time, and $\tilde{F}_e$ is also added to $\tilde{F}_m\left(\tilde{t}/\tilde{\tau}\right)$ as a residual force. Therefore, the non-dimensional Yue and Bi model becomes

$$\ddot{\tilde{x}} + 2\zeta\dot{\tilde{x}} + \tilde{x} = \begin{cases} \tilde{F}_m\left(\tilde{t}/\tilde{\tau}\right) + \tilde{F}_e & 0 \leq \tilde{t} < \tilde{\tau} \\ \tilde{F}_e & \tilde{\tau} \leq \tilde{t} < \tilde{T} \end{cases} \tag{4.39}$$

where $\tilde{\tau} = \omega_n \tau$ and $\tilde{T} = \omega_n T$.

The forcing function of equation (4.39) can be transformed to a harmonic function by using a Fourier series. The forcing function is given by

$$\tilde{f}(t) = a_0 + \sum_{N=1}^{\infty}\left[a_N \cos\left(\frac{2N\pi}{\tilde{T}}\tilde{t}\right) + b_N \sin\left(\frac{2N\pi}{\tilde{T}}\tilde{t}\right)\right] \tag{4.40}$$

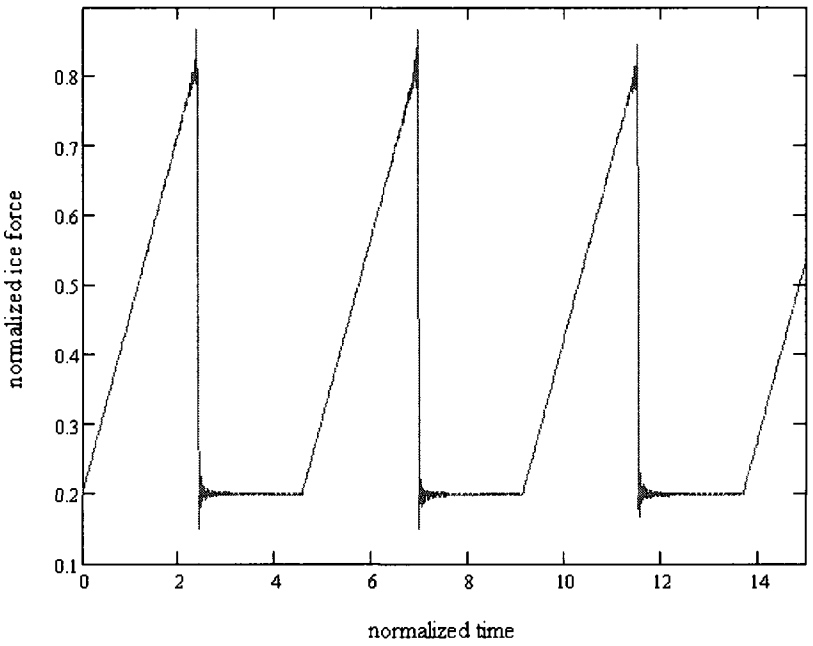

Figure 4.7: Approximated ice force

where

$$a_0 = \frac{\tilde{F}_m \tilde{\tau}}{2\tilde{T}} + \tilde{F}_e$$

$$a_N = \frac{\tilde{F}_m \tilde{T}}{2N^2\pi^2\tilde{\tau}} \left(\cos \frac{2N\pi\tilde{\tau}}{\tilde{T}} - 1 \right) + \frac{\tilde{F}_m}{N\pi} \sin \frac{2N\pi\tilde{\tau}}{\tilde{T}}$$

and

$$b_N = \frac{\tilde{F}_m \tilde{T}}{2N^2\pi^2\tilde{\tau}} \sin \frac{2N\pi\tilde{\tau}}{\tilde{T}} - \frac{\tilde{F}_m}{N\pi} \cos \frac{2N\pi\tilde{\tau}}{\tilde{T}}$$

$\tilde{\tau}$ and $\tilde{T}$ are obtained directly from Figure 4.5, $\tilde{\tau} = 2.41$ and $\tilde{T} = 4.57$. $\tilde{F}_m$ is also measured from Figure 4.5 as 0.806. Figure 4.7 is plotted with a hundred summation terms and shows close approximation of the ice force of Figure 4.5. The response of the system can be calculated in the same manner as equation (3.26) in Chapter 3 as

$$\tilde{x}\left(\tilde{t}\right) = a_0 + \sum_{N=1}^{100} \left[\mathrm{M} \left\{ a_N \cos\left(\frac{2N\pi}{\tilde{T}} \tilde{\tau} + \theta_N \right) + b_N \sin\left(\frac{2N\pi}{\tilde{T}} \tilde{\tau} + \theta_N \right) \right\} \right] \tag{4.41}$$

where

$$\mathrm{M} = \frac{1}{\sqrt{\left(1 - \omega_N^2\right)^2 + \left(2\zeta\omega_N\right)^2}} \tag{4.42}$$

and

$$\theta_N = \tan^{-1} \frac{2\zeta\omega_N}{1-\omega_N^2} \tag{4.43}$$

Equation (4.41) is developed without the flow effect.

The Toyama et al. model can also be normalized by using Δ. From the equation of motion of the Toyama et al. model [Toyama et al., 1983],

$$m\ddot{x} + c\dot{x} + kx = \begin{cases} kx + c\dot{z} & 0 \le t < t_e \\ F_c & t_e \le t < t_c \end{cases} \tag{4.44}$$

Equation (4.44) is divided by Δ and m. F_e is added to the elastic force and t_e, t_c, and F_c are replaced with τ, T and F_e, respectively in order to synchronize the ice force with the ice forces of the other two models. Normalization is performed through the same procedure as the Yue and Bi model and expressed as

$$\ddot{\tilde{x}} + 2\zeta\dot{\tilde{x}} + \tilde{x} = \begin{cases} \tilde{k}\tilde{x} + 2\zeta\dot{\tilde{z}} + \tilde{F}_e & 0 \le \tilde{t} < \tilde{\tau} \\ \tilde{F}_e & \tilde{\tau} \le \tilde{t} < \tilde{T} \end{cases} \tag{4.45}$$

Responses of the non-dimensional Toyama et al. model are obtained from the modified approach which is proposed in the first section of Chapter 4 to remove discontinuities. For the elastic phase, the response is calculated as

$$\tilde{x}\left(\tilde{t}\right) = \dot{\tilde{z}}\tilde{t} + C_3 \tag{4.46}$$

The response for the crushing phase is expressed as

$$\tilde{x}\left(\tilde{t}\right) = e^{-\zeta\tilde{t}}\left[A_3 \cos\sqrt{1-\zeta^2}\tilde{t} + A_4 \sin\sqrt{1-\zeta^2}\tilde{t}\right] + \tilde{F}_e \tag{4.47}$$

C_3, A_3, and A_4 can be calculated from the initial values of each phase.

The responses of the Toyama et al. model and Yue and Bi model corresponding to the same ice force are plotted in Figure 4.8 and 4.9. Including the Huang and Liu model, all three models are developed based on a saw-tooth ice forcing function. By using the same τ, T, F_e, and F_m, the ice forcing functions of the three models have identical frequency and magnitude. The responses of the three models, however, shown in Figure 4.5, 4.8,

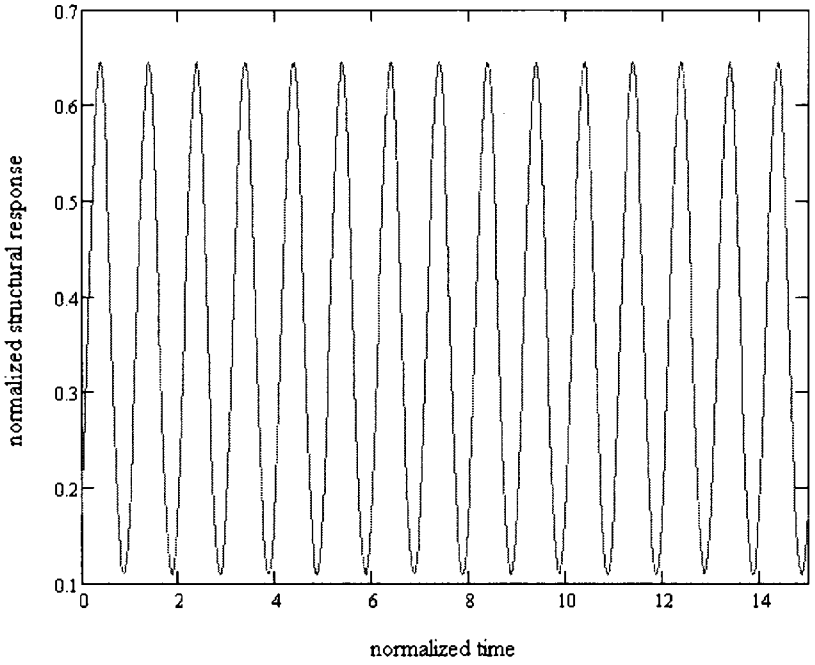

Figure 4.8: Response of the Yue and Bi model

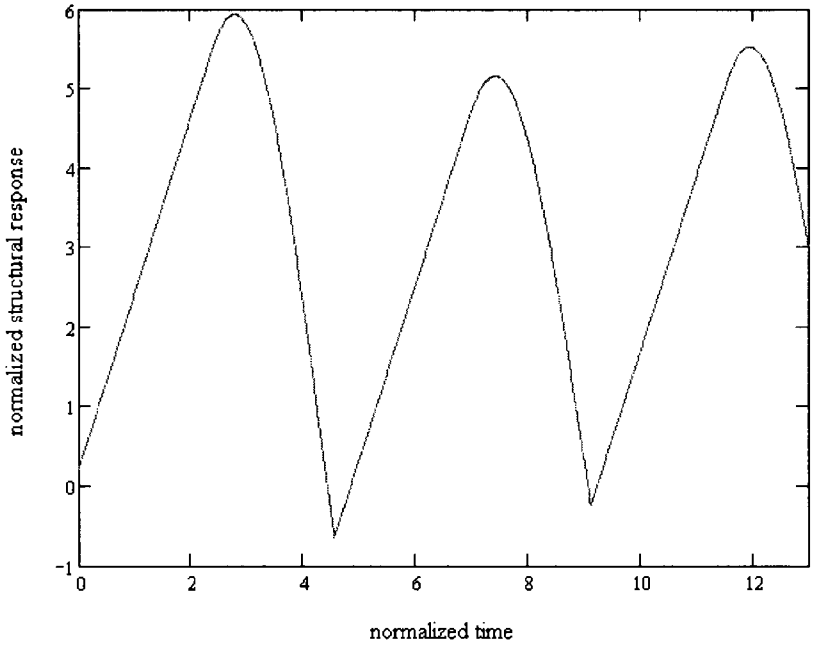

Figure 4.9: Response of the Toyama et al. model

and 4.9 completely differ from each other even though the same structural properties are applied. The Toyama et al. model calculates the magnitude of the response to be much larger than the other two models, and the Yue and Bi model vibrates at higher frequencies than the others. In other words, none of the models or at least two of them can be assured that they predict the response of the given ice force. This means that the models do not reflect the real physics of the phenomena. Since the derivations of each model were conducted without logical flaws, the root of this problem could be the basic model, the characteristic failure frequency model, itself. Therefore, another perspective of IIVs is required to solve the problem.

Chapter 5

A New Modeling Approach through the Conservation of Momentum

Ice-induced vibrations possess several characteristics. Among them, a moving fluid and periodic ice forces give the motivation for a new perspective on ice-induced vibrations. Based on these two characteristics, a new ice-induced vibration model is proposed in this chapter in order to address the problems of the existing models. The new model is developed based on both linearized and quadratic drag forces, which are compared via numerical simulations. A resonance condition of the new model is analyzed through a Fourier transform. Finally, the complete new model including the flow effect is suggested at the end of the chapter.

5.1 Motivation

The lack of consistency in the characteristic failure frequency model was brought to light in the previous chapter. The only difference between the three models which have been investigated in the previous chapter is the modeling approach. The solutions are intended to simulate vibrations which all come from the same source of vibration, therefore any discrepancy in the resulting solutions must come from the modeling approach. Since the

two ice-induced vibration (IIV) modelling approaches were first proposed in the early stages of IIV research, no major advance in the modeling approach has been achieved. In the literature review of Chapter 2, the deficiencies of the two IIV modeling approaches were addressed. The characteristic failure frequency model considers the velocities of a contacting ice sheet to be the same over the entire ice sheet. In the area where the ice sheet fails and deforms, however, the ice moves with different velocities compared to the area where the deformation of the ice does not start. In other words, the characteristic failure model nearly ignores the time dependency of ice velocities due to the deformation of the ice. The self-excited model is developed to include time-varying ice velocities. Since the ice strength varies depending on the loading rate, the model reflects time-varying ice velocities in the area of deformation. The self-excited model, however, cannot be established on highly damped or rigid structures. These inadequacies of each IIV model catalyze the need for a new IIV modeling approach which can eliminate the flaws of the two existing approaches.

Both existing modeling approaches analyze the process of IIVs from a microscopic point of view. Researchers have measured and investigated the detailed cracking propagation of ice failures and have tried to analyze and classify the shapes of ice failures. Barker et al. (2005) is a typical microscopic approach to IIVs. They conducted numerous small scale tests and distinguished ice failures into four different modes by the sizes of failed ice pieces and the structural responses [Barker et al., 2005]. The procedure of defining the ice failure modes is a painstaking and obscure task. Sometimes a macroscopic point of view can give more thorough insight into a physical phenomena. For instance, a detailed analysis of all vibrations and deformations is not generally considered when a collision of two cars is analyzed. In that case, the whole collision process can be efficiently analyzed with a single parameter, the coefficient of restitution. If the collision of the cars occurs repetitively, the behaviors of the two cars resemble those of IIVs.

This simple concept provides the inspiration for the new modeling approach to the IIV analysis. The vibration characteristics of IIVs can be summarized as being the result

of a periodic forcing function. If all the microscopic ice failure processes can be condensed into the coefficient of restitution, the remaining vibration characteristics are similar to those of the repetitive collisions of the two cars. The ice is modeled as one of the cars in the collision and the structure corresponds to the other. IIVs can now be modeled and simulated by using the conservation of momentum along with the coefficient of restitution, which is a totally different perspective from the existing IIV models.

5.2 Modeling of Ice-induced Vibration with the Conservation of Momentum

In an IIV model, the force which drives an ice sheet needs to be considered so that collisions occur repetitively. The ice sheet causing IIVs is driven by various external forces such as wind and thermal expansion, but one of the main driving forces is fluid flow. Depending on the initial displacement and velocity of the flow, the velocity of the ice sheet is determined just prior to the time of impact, and the maximum velocity of the ice sheet is the velocity of the flow. The ice sheet moves until the ice sheet collides with the structure. After the impact, part of the ice sheet stops or bounces back in the opposite direction of the flow depending on the coefficient of restitution. Since the ice and flow now have a relative velocity with respect to each other, the ice is forced to move in the same direction by the flow until the ice reaches once again the velocity of the flow. The ice moving toward the structure transfers its momentum to the structure again when the relative displacement between the ice and structure becomes 0 (i.e. when a collision occurs). In some cases, the structure can transfer momentum to the ice when the momentum of the structure is larger than that of the ice, which is a similar condition of the separation phase of the Huang and Liu model or the self-excited model. This whole process keeps repeating, but due to the structural damping and fluid drag the momenta which are transferred to each other gradually decrease.

Figure 5.1 is a schematic diagram of two masses which collide repetitively. Mass M

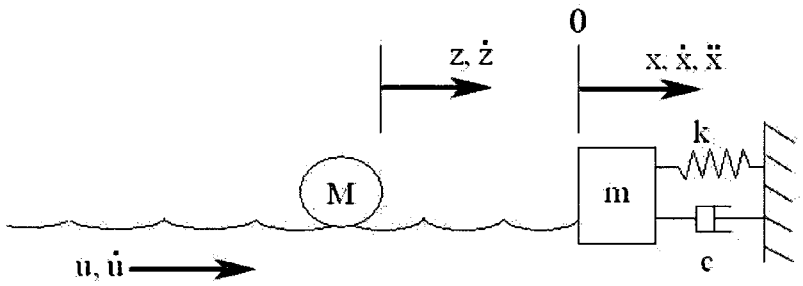

Figure 5.1: The impact IIV model

represents the ice and mass m represents the structure as a lumped parameter. Mass M does not mean the mass of the entire ice sheet, rather part of it. The definition of mass M is that of the mass directly related to the impact and is called the ice mass. Since mass M is floating on the flow, it is free to move. The flow, however, moves with its own velocity $\dot{u}$, which in this case is always assumed to be positive (to the right in the figure). The displacement of the ice is given by the variable z and that of the structure is given by the variable x. The ice mass is driven by the drag force, f_D, which is present when there is a relative velocity between the flow and the ice. There are four conditions depending on the relative velocities.

- When $\dot{z} \geq 0$ and $|\dot{z}| \geq |\dot{u}|$, $f_D \leq 0$.
- When $\dot{z} \geq 0$ and $|\dot{z}| < |\dot{u}|$, $f_D > 0$.
- When $\dot{z} < 0$ and $|\dot{z}| \geq |\dot{u}|$, $f_D \geq 0$.
- When $\dot{z} < 0$ and $|\dot{z}| < |\dot{u}|$, $f_D > 0$.

No force is transmitted to the ice except the drag force. The drag force by fluid dynamics is defined as

$$f_D = -\frac{1}{2}\rho C_D A \left(\dot{z} - \dot{u}\right)^2 \tag{5.1}$$

where ρ, C_D, and A are the density of the fluid, drag coefficient, and area related to the drag coefficient, respectively [Munson et al., 2002]. Area A again is not the area of the entire ice sheet, but rather is the area that influences the drag force. However, the drag force which influences the system of Figure 5.1 changes the forcing direction according to the relative velocities as explained above. The drag force for the ice of Figure 5.1, therefore, is expressed as

$$f_D = -\frac{1}{2}\rho C_D A \left|\dot{z} - \dot{u}\right| (\dot{z} - \dot{u}) \tag{5.2}$$

The equation of motion of the ice can be obtained from equation (5.2) since no other forces are involved. The equation of motion of the ice is thus given as

$$M\ddot{z} = f_D$$

or

$$M\ddot{z} = -\frac{1}{2}\rho C_D A \left|\dot{z} - \dot{u}\right| (\dot{z} - \dot{u}) \tag{5.3}$$

Since equation (5.3) is a non-linear equation, it needs linearization or a numerical approach to be solved. The linearized version of equation (5.3) is developed in the same manner as the linearized Morison's equation in Chapter 3. By assuming the relative velocity is small, equation (5.3) is linearized as

$$M\ddot{z} = -b(\dot{z} - \dot{u}) \tag{5.4}$$

where

$$b = \frac{1}{2}\rho C_D A \left|\dot{z} - \dot{u}\right| \tag{5.5}$$

$|\dot{z} - \dot{u}|$ is assumed to be small and constant. Equation (5.4) can be rewritten as

$$M\ddot{z} + b\dot{z} = b\dot{u} \tag{5.6}$$

The solution of equation (5.6) consists of a homogeneous and particular solutions. By assuming $z = e^{\lambda t}$, the homogeneous solution can be obtained as

$$M\lambda^2 e^{\lambda t} + b\lambda e^{\lambda t} = \lambda (M\lambda + b) e^{\lambda t} = 0 \tag{5.7}$$

Since $\lambda = 0$ and $\lambda = -b/M$,

$$z_h(t) = c_1 + c_2 e^{-\frac{b}{M}t} \tag{5.8}$$

where c_1 and c_2 are constants. The particular solution of equation (5.6) can be calculated by following the method of undetermined coefficients [Kreyszig, 1999]

$$z_p(t) = c_1' t + c_2' \tag{5.9}$$

By substituting equation (5.9) into equation (5.6),

$$b(c_1') = b\dot{u} \tag{5.10}$$

or

$$c_1' = \dot{u} \tag{5.11}$$

From equation (5.9) and (5.11), the particular solution is expressed as

$$z_p(t) = \dot{u}t + c_2' \tag{5.12}$$

Combining equation (5.8) and (5.12), the total solution of the ice can be obtained as

$$z(t) = c_1 + \dot{u}t + c_2 e^{-\frac{b}{M}t} \tag{5.13}$$

The velocity of the ice can be calculated by taking first derivative of equation (5.13) with respect to time.

$$\dot{z}(t) = \dot{u} - c_2 \frac{b}{M} e^{-\frac{b}{M}t} \tag{5.14}$$

Equation (5.13) is a closed form solution of linearized equation (5.3). The solution of non-linear equation (5.3) will be developed later in the chapter since it requires a numerical approach.

The structure is modeled as a one degree-of-freedom system consisting of a mass, damper, and spring without external forces as in Figure 5.1. Since the source of structural vibrations originates from the transfer of momenta during collisions, outside the

collision times the structure vibrates as a free simple harmonic oscillator. The equation of structural motion is expressed as

$$m\ddot{x} + c\dot{x} + kx = 0 \tag{5.15}$$

For an under-damped case, equation (5.15) has the following solution.

$$x(t) = c_3 e^{-\zeta\omega_n t}\cos\omega_d t + c_4 e^{-\zeta\omega_n t}\sin\omega_d t \tag{5.16}$$

with ζ, ω_d and ω_n having the usual interpretation and definition as damping coefficient, damped frequency and natural frequency. By taking the first derivative with respect to time, the velocity of the structure at time t can be calculated as

$$\dot{x}(t) = -\omega_d c_3 e^{-\zeta\omega_n t}\sin\omega_d t - \zeta\omega_n c_3 e^{-\zeta\omega_n t}\cos\omega_d t + \omega_d c_4 e^{-\zeta\omega_n t}\cos\omega_d t - \zeta\omega_n c_4 e^{-\zeta\omega_n t}\sin\omega_d t \tag{5.17}$$

From equation (5.13), (5.14), (5.16), and (5.17), the displacements and velocities of the ice and structure at any given time can be found. Substituting these expressions for displacement and velocity into the equations for the conservation of total system momentum and the equation for the coefficient of restitution, the displacements and velocities of the ice and structure immediately after impact can be evaluated. Each of the ice and structure, however, has two unknowns after impact. Thus the unknowns after impact are the displacement and velocity of the ice, and displacement and velocity of the structure. Since only two equations can be developed from the conservation of momentum and the coefficient of restitution equation, the number of unknowns exceeds the number of equations by two. Salapaka et al. (1998), in Complex Dynamics in Repeated Impact Oscillators, also investigated a similar modeling approach. They developed the equation of a mass-spring system driven by a vibrating table which impacts the mass at a certain position repetitively. Salapaka et al. faced the same problem of excessive unknowns and introduced an assumption to eliminate the extra two unknowns, the displacements of the ice and structure after the impact [Salapaka et al., 1998]. They assumed that the displacements of the ice and structure before and after impact remain the same, and by making this assumption the number of unknowns after impact is reduced to 2.

The instants just before and just after impact will be denoted t_k and t_f. Since the impact occurs when the displacements of the ice and structure are the same, the displacements at time t_k are given as

$$x(t_k) = z(t_k) = x_k \tag{5.18}$$

Using the same notation, the velocities at impact can be expressed as

$$\dot{x}(t_k) = \dot{x}_k$$

$$\dot{x}(t_f) = \dot{x}_f$$

$$\dot{z}(t_k) = \dot{z}_k$$

and

$$\dot{z}(t_f) = \dot{z}_f$$

From the conservation of momentum, the total momentum of the two masses, m and M, is conserved so that

$$m\dot{x}_f + M\dot{z}_f = m\dot{x}_k + M\dot{z}_k \tag{5.19}$$

The second relevant impact equation is obtained from the coefficient of restitution [Bedford and Fowler, 1999] as

$$\dot{x}_f - \dot{z}_f = e(\dot{z}_k - \dot{x}_k) \tag{5.20}$$

Equation (5.19) and (5.20) can be rewritten in matrix form as

$$\begin{bmatrix} m & M \\ 1 & -1 \end{bmatrix} \begin{bmatrix} \dot{x}_f \\ \dot{z}_f \end{bmatrix} = \begin{bmatrix} m\dot{x}_k + M\dot{z}_k \\ e\dot{z}_k - e\dot{x}_k \end{bmatrix} \tag{5.21}$$

or

$$\begin{bmatrix} \dot{x}_f \\ \dot{z}_f \end{bmatrix} = \frac{-1}{m+M} \begin{bmatrix} -1 & -M \\ -1 & m \end{bmatrix} \begin{bmatrix} m\dot{x}_k + M\dot{z}_k \\ e\dot{z}_k - e\dot{x}_k \end{bmatrix} \tag{5.22}$$

From equation (5.22), the velocities of the ice and structure after the impact, $\dot{x}_f$ and $\dot{z}_f$, are calculated as

$$\dot{x}_f = \frac{1}{m+M}(m\dot{x}_k + M\dot{z}_k + eM\dot{z}_k - eM\dot{x}_k) \tag{5.23}$$

and

$$\dot{z}_f = \frac{1}{m+M}\left(m\dot{x}_k + M\dot{z}_k - em\dot{z}_k + em\dot{x}_k\right) \tag{5.24}$$

After impact, the displacements of the ice and structure are assumed to be the same as before impact. From equation (5.18)

$$x\left(t_f\right) = x\left(t_k\right) = x_k$$

and

$$z\left(t_f\right) = z\left(t_k\right) = x_k$$

Once the impact occurs, the momentum of the ice is transmitted to the structure or vice versa. c_1, c_2, c_3, and c_4 of equation (5.13), (5.14), (5.16), and (5.17) need to be repeatedly calculated after each impact in order to obtain the new responses of the ice and structure. Since the characteristics of the system responses are reset after each impact, the time right after the impact, t_f, is also reset to 0 to calculate c_1, c_2, c_3, and c_4. Substituting $t_f = 0$ into equation (5.13), (5.14),

$$z\left(t_f\right) = z\left(0\right) = c_1 + c_2 \tag{5.25}$$

and

$$\dot{z}\left(t_f\right) = \dot{z}\left(0\right) = \dot{u} - \frac{b}{M}c_2 \tag{5.26}$$

The displacements before and after impact are assumed to be the same, and the velocity of the ice after the impact is calculated from equation (5.24). Equation (5.25) and (5.26) are equal to x_k, and $\dot{z}_f$, respectively.

$$z\left(0\right) = c_1 + c_2 = x_k \tag{5.27}$$

and

$$\dot{z}\left(0\right) = \dot{u} - \frac{b}{M}c_2 = \dot{z}_f \tag{5.28}$$

From equation (5.27) and (5.28), c_1 and c_2 are calculated as

$$c_1 = x_k - \frac{M}{b}\left(\dot{u} - \dot{z}_f\right) \tag{5.29}$$

and

$$c_2 = \frac{M}{b}(\dot{u} - \dot{z}_f) \tag{5.30}$$

Applying the same assumption and equation (5.23) to equation (5.16) and (5.17),

$$x(t_f) = x(0) = c_3 = x_k \tag{5.31}$$

and

$$\dot{x}(t_f) = \dot{x}(0) = -\zeta\omega_n c_3 + \omega_d c_4 = \dot{x}_f \tag{5.32}$$

It then follows that c_3 and c_4 are obtained from equation (5.31) and (5.32) as

$$c_3 = x_k \tag{5.33}$$

and

$$c_4 = \frac{1}{\omega_d}(\dot{x}_f + \zeta\omega_n x_k) \tag{5.34}$$

Substituting the calculated c_1, c_2, c_3, and c_4 into equation (5.13) and (5.16), the responses of the ice and structure after the impact are expressed as

$$z(t) = \left[x_k - \frac{M}{b}(\dot{u} - \dot{z}_f)\right] + \dot{u}t + \frac{M}{b}(\dot{u} - \dot{z}_f)\, e^{-\frac{b}{M}t} \tag{5.35}$$

and

$$x(t) = x_k e^{-\zeta\omega_n t}\cos\omega_d t + \frac{1}{\omega_d}(\dot{x}_f + \zeta\omega_n x_k)\, e^{-\zeta\omega_n t}\sin\omega_d t \tag{5.36}$$

All the equations are developed based on the linearized drag force. Equation (5.35) and (5.36) hold until the next impact. After the next impact c_1, c_2, c_3, and c_4 should be recalculated according to new values of x_k, $\dot{x}_k$, z_k, and $\dot{z}_k$ obtained from the impact equations.

5.3 Numerical Simulations

5.3.1 Linearized Drag Force

For the numerical simulations, there were two main concerns; how to identify the instant of an impact, and how to define the impact condition. Since the basis of the impact

IIV model is exchange of momenta through impacts, the time and condition of the impact which are the backbone of the impact IIV model need to be defined as precisely as possible. The solution to this question taken in this work was to use a time stepping algorithm as used in the simulation of the Huang and Liu model. In the beginning, c_1, c_2, c_3, and c_4 are calculated with the initial conditions. By substituting c_1, c_2, c_3, and c_4 into equation (5.35) and (5.36), the responses of the ice and structure are obtained. Based on the calculated responses, the relative displacement between the ice and structure is compared to the impact condition at every time step. The impact condition is theoretically given by

$$|x(t) - z(t)| = 0$$

The actual numerical simulation, however, cannot achieve enough precision to capture the exact impact condition. Therefore, a tolerance for the impact condition is required to allow for numerical roundoff errors of the numerical simulation.

The tolerance should be considered carefully because too small a tolerance has no meaning and a large tolerance makes impacts occur more often than it should. In the algorithm, the tolerance for the impact condition is set flexibly by the following equation.

$$\Delta = \frac{1}{10} \min\left(|\delta x|, |\delta z|\right)$$

where Δ is the impact condition such that $|x(t) - z(t)| \leq \Delta$ and $\delta x = \dot{x}(t)\,\Delta t$, and $\delta z = \dot{z}(t)\,\Delta t$. Furthermore, Δt is the time step. The flexible impact condition has merit over a fixed one. When the responses of the ice and structure are very small, the fixed impact condition cannot capture some impacts. The flexible impact condition, however, is determined according to the size of the responses, therefore the impact condition is able to capture impacts whether the responses are slow or fast.

After the comparison of the relative displacement and the impact condition, if the relative displacement is larger than the impact condition, the same values of c_1, c_2, c_3, and c_4 will be forwarded to the next time step. Otherwise, the relative displacement is equal to or less than the impact condition and thus an impact takes place. Once the

algorithm catches the impact, c_1, c_2, c_3, and c_4 are calculated based on the values from the previous time step and new conditions corresponding to the impact as explained in the previous section. In addition, the algorithm is performed on two different time scales, one is global time and the other is local time. The global time is the overall time starting with the beginning of the algorithm and the local time counts time duration between impacts, thus after each impact the local time is reset to 0 while the global time increases continuously. With 0 local time, new responses of the system based on the new c_1, c_2, c_3, and c_4 begin and evolve until next impact. This process keeps repeating until the system reaches a steady-state condition.

The steady-state condition is also implemented in the algorithm to avoid infinitesimal impacts which occur at the end of the responses. The steady-state condition involves displacements, velocities, and accelerations. The algorithm verifies at every step whether or not both responses of the ice and structure satisfy the steady-state conditions. The steady-state conditions are given as

- $\max\left(\left|z\left(t\right)\right|, \left|x\left(t\right)\right|\right) < 0.0001$ m
- $\max\left(\left|\dot{z}\left(t\right)\right|, \left|\dot{x}\left(t\right)\right|\right) < 0.0001$ $^{\mathrm{m}}/_{\mathrm{s}}$
- $\max\left(\left|\ddot{z}\left(t\right)\right|, \left|\ddot{x}\left(t\right)\right|\right) < 0.0001$ $^{\mathrm{m}}/_{\mathrm{s}^2}$

The value of 0.0001 was chosen through trial and error. When the system reaches the steady state, the structure is constantly forced by the ice and the equation of motion in the steady state is expressed as

$$m\ddot{x} + c\dot{x} + kx = -b\left(\dot{z} - \dot{u}\right) \tag{5.37}$$

Since the system is in the steady state,

$$kx = b\dot{u} \tag{5.38}$$

In the steady state condition, the ice and structure collide and move together, therefore the responses of the ice and structure are given by

$$x\left(t\right) = z\left(t\right) = \frac{b}{k}\dot{u}, \tag{5.39}$$

which is a constant (steady state) displacement since $\dot{u}$ is the (assumed) constant velocity of the flow. The algorithm replaces equation (5.35) and (5.36) with equation (5.39) when the steady-state condition is satisfied.

Figure 5.2 is plotted using the same structural properties in Table 3.1 of Chapter 3. The ice properties for the impact IIV model, however, cannot be found from the literature. The two ice properties, the mass, M, and area, A, of the ice, are arbitrarily chosen as 1600 kg which is the same as the structural mass and 1 m^2, respectively. The linearization factor, $|\dot{z} - \dot{u}|$, is set as 0.1 $^{m}/_{s}$ because it is the maximum difference between the ice velocity and flow velocity which is set as 0.1 $^{m}/_{s}$. Therefore, the value of b is

$$b = \frac{1}{2}\rho C_D A\,|\dot{z} - \dot{u}| = 49.95\ {}^{kg}/_{s}$$

where ρ is the density of water and C_D, the drag coefficient, is 1. The coefficient of restitution, another important parameter, is assumed to be 1 which implies no energy dissipation through impact. In addition, the initial displacement and velocity of the ice are -0.01 m and 0.01 $^{m}/_{s}$, respectively and 0 m and 0 $^{m}/_{s}$ for the structure. Figure 5.2 shows the responses of the ice and structure based on these parameters.

There is very little IIV data in the literature, especially for displacement measurements. Only laboratory measurements are available from Eranti et al. (1981) and Shih (1991) for displacement measurements. Since the structural data for their tests are not presented, it is inadequate to compare their experimental data to Figure 5.2 directly, but vibration characteristics can be compared. Structural vibrations of IIVs become quasi-static vibrations at low ice velocities and steady-state vibrations at medium ice velocities [Kärnä, 1994] although there is no quantitative definition of low and high ice velocities. The quasi-static vibration is defined by Kärnä (1994) as a transient response which is followed by its maximum response at the peak ice force and is not amplified by the dynamics of the structure. Figure 5.3 (b) represents typical quasi-static vibrations at ice velocity 7.6 $^{mm}/_{s}$ and Figure 5.3 (c) shows the characteristic of a steady-state vibration at ice velocity 39.5 $^{m}/_{s}$. Figure 5.3 (a), however, presents the characteristics of a steady-state vibration although it is plotted at a lower ice velocity than Figure 5.3 (b). This

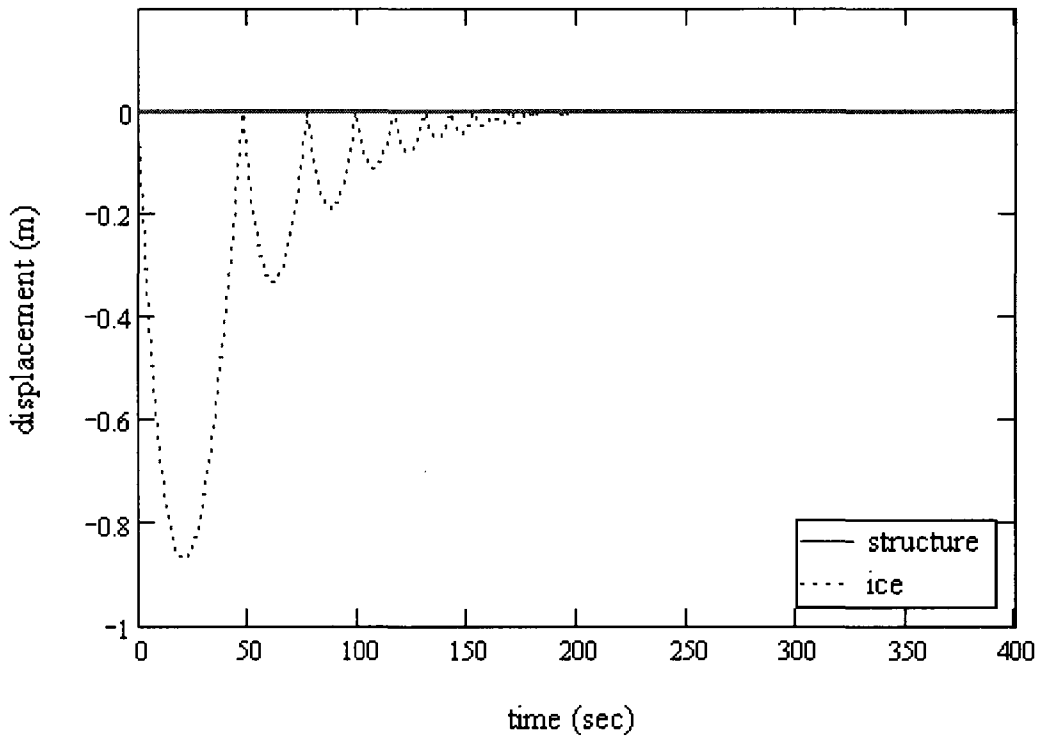

(a) Overall responses

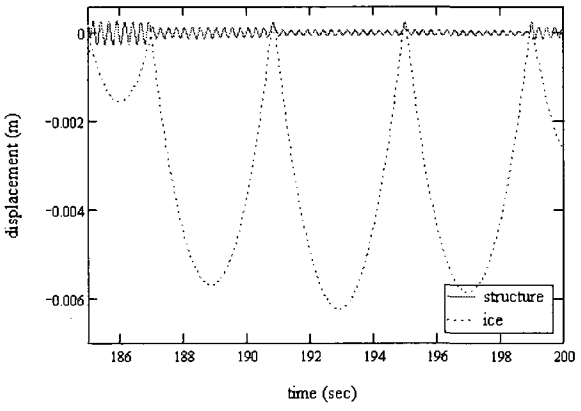

(b) Responses from 185 to 200 seconds

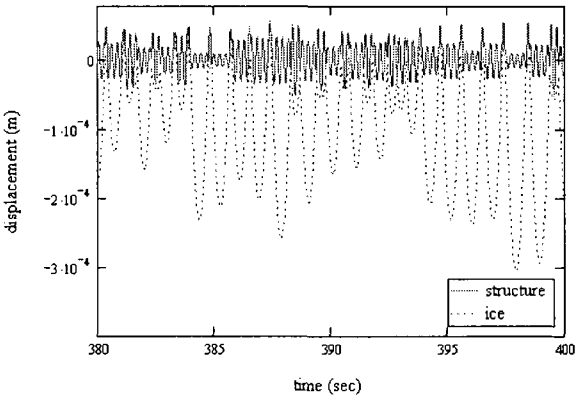

(c) Responses from 380 to 400 seconds

Figure 5.2: Responses of the ice and structure

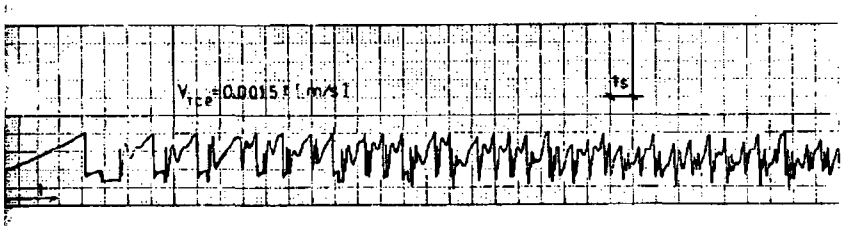

(a) [Eranti et al., 1981]

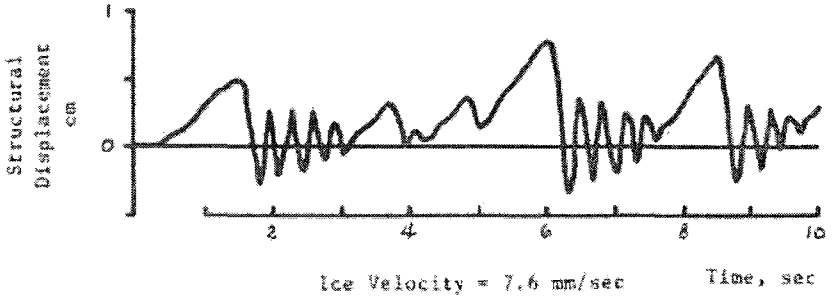

(b) [Shih, 1991]

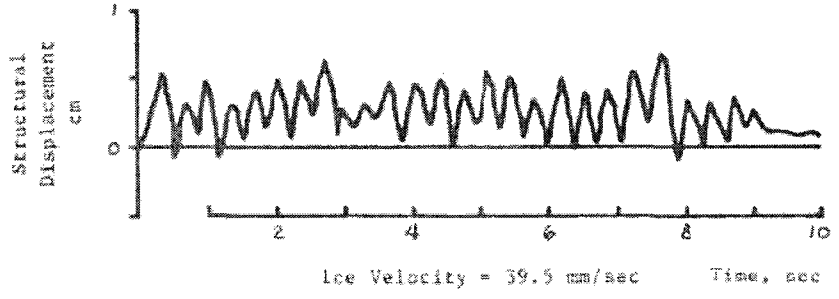

(c) [Shih, 1991]

Figure 5.3: Measured structural responses from the literature

proves that the vibration characteristics of IIVs are not determined by the velocity of the ice alone but by involving all parameters.

As shown in Figure 5.3 (a), actual IIVs display multiple vibration characteristics from quasi-static to steady-state vibrations even at the same ice velocity contrary to the characteristic failure frequency model which predicts one type of characteristic vibration at one ice velocity. In this respect, the impact IIV model possesses an advantage over the characteristic failure frequency model. In the impact IIV model, the velocity of the ice varies from time to time, which is more realistic because part of the ice contacting the structure is deformed as IIVs proceed. Figure 5.2 clearly shows multiple vibration characteristics. Figure 5.2 (b) displays quasi-static vibrations similar to Figure 5.3 (b). From 380 to 400 seconds, the vibrations become stable and steady state shown in Figure 5.2 (c) which is close to the vibration characteristic of Figure 5.3 (c). The vibration characteristics of the impact IIV model, however, cannot be clearly distinguished for the entire duration rather they present a mixture of the characteristics. Therefore, it is reasonable to conclude that the vibration characteristics of the impact IIV model is governed by the momenta of the ice and structure at the time of impact.

The weakness of the impact IIV model is how to define or model the properties of the ice. The definitions of the ice mass and area in the impact IIV model imply that the mass and area directly affect the impact or interaction with the structure. Among the two ice properties, the influence of the ice area A is directly related to the velocity of the flow because of the relation with b given by $b = \frac{1}{2}\rho C_D A\,|\dot{z} - \dot{u}|$. It is inappropriate to simulate the linearized model with large flow velocities since then the linearized model would not be applicable hence varying the ice velocity will not be considered in this section. Therefore, in this section the effect of only a mass change will be investigated in the ice properties.

The mass of the ice plays an important role in the impact IIV model. Defining the ice mass quantitatively through numerical simulations, however, is a difficult task, extensive laboratory experiments would be required. In order to understand the role of the ice

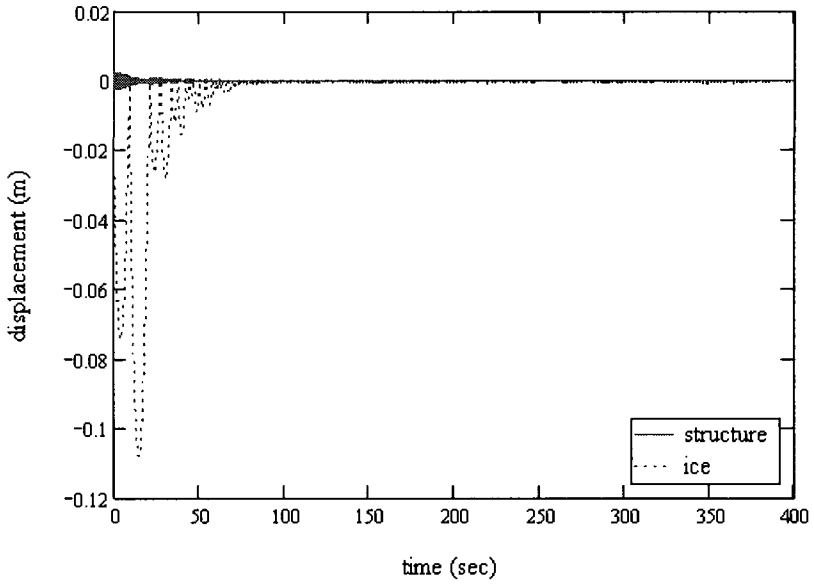

(a) Overall responses with $M = 800$ kg

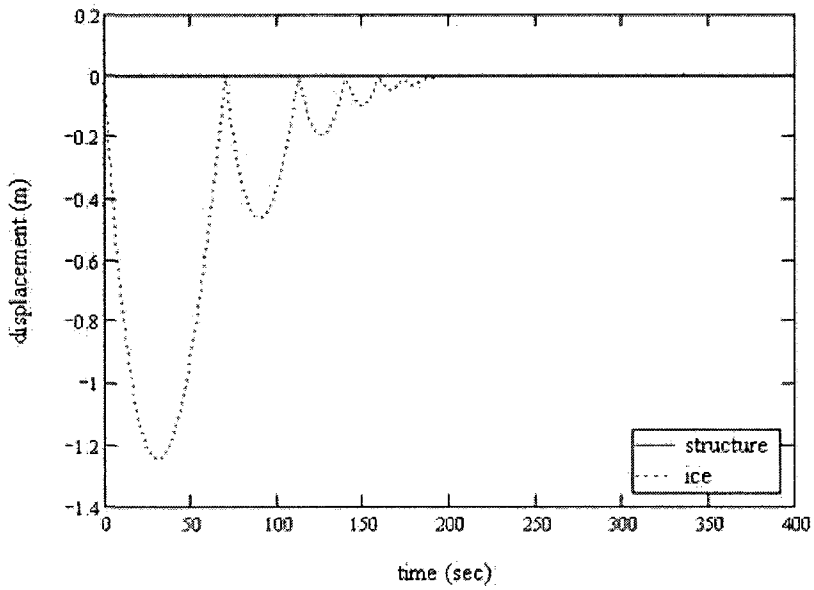

(b) Overall responses with $M = 2400$ kg

Figure 5.4: Responses with different ice masses 1

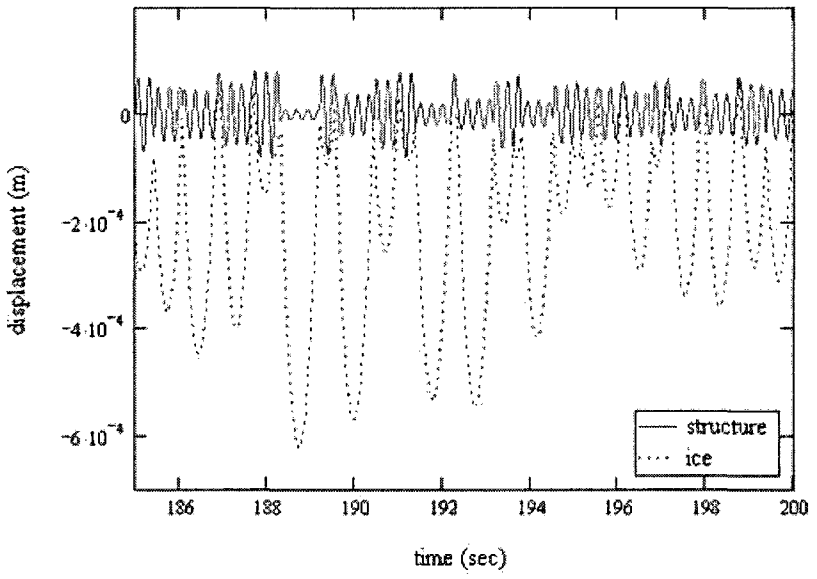

(a) Responses with $M = 800$ kg from 185 to 200 seconds

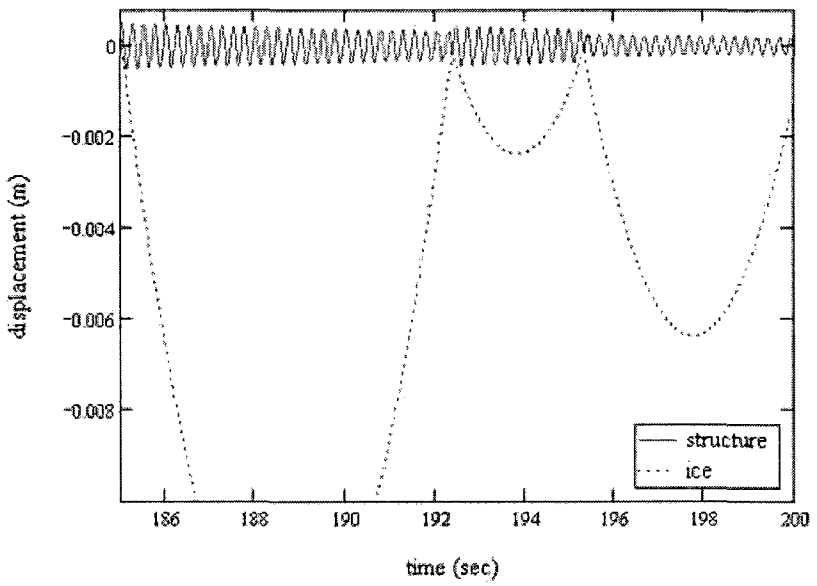

(b) Responses with $M = 2400$ kg from 185 to 200 seconds

Figure 5.5: Responses with different ice masses 2

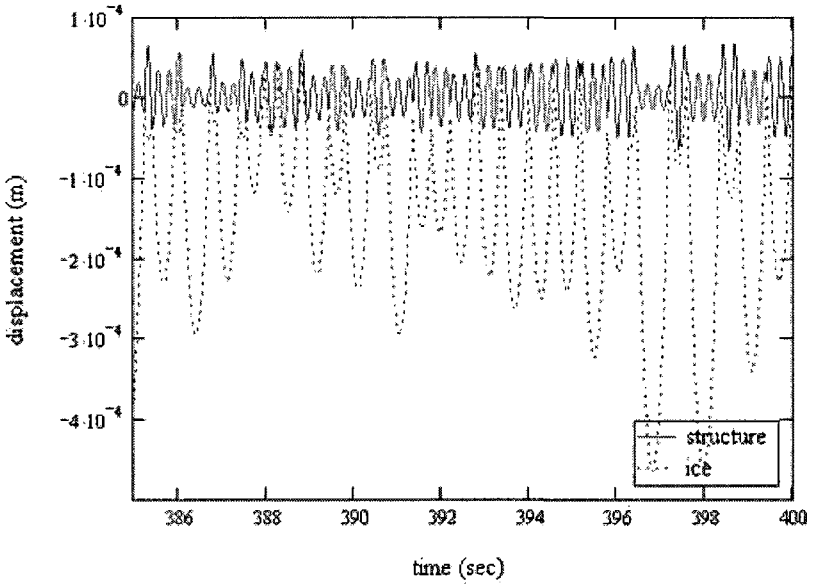

(a) Responses with $M = 800$ kg from 385 to 400 seconds

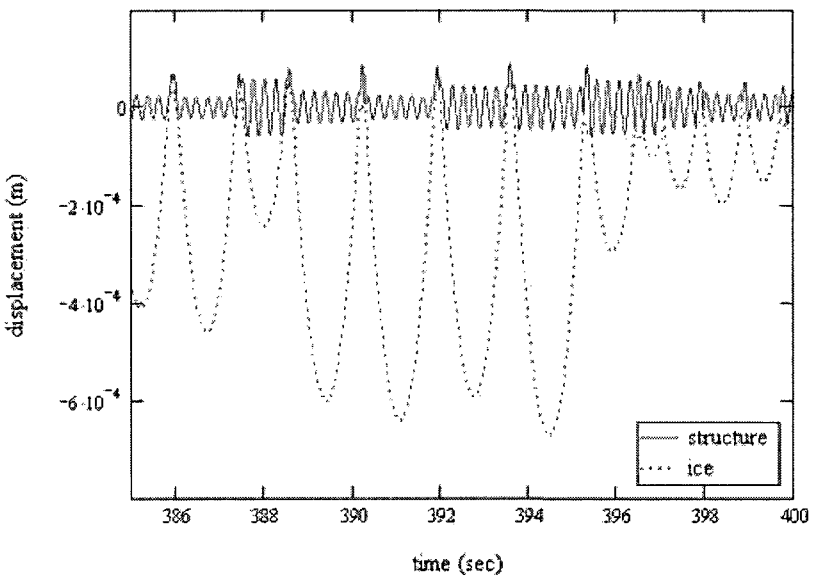

(b) Responses with $M = 2400$ kg from 385 to 400 seconds

Figure 5.6: Responses with different ice masses 3

mass in the impact IIV model, it will be investigated by conducting several numerical simulations with changes in ice mass. Figure 5.4, 5.5, and 5.6 are plotted with the same parameters of Figure 5.2 except with different ice masses which are proportional to the structural mass, 50 and 150 percent of 1600 kg, so that the structural mass can be used as a benchmark. Including Figure 5.2, which is plotted with the ice mass of 100 percent of the structural mass, the responses with three different ice masses are compared. At the beginning of the responses, the heavier ice transfers higher momentum, thus impacts happen less frequently but with larger magnitudes. On the contrary, the lighter ice allows the structure to approach the steady-state vibration in relatively short time. In figure 5.6 the magnitudes of the structural responses are not far different but the heavier ice induces more quasi-static vibrations for longer time. Therefore, it can be concluded that the ice mass has a greater effect on determining the vibration characteristics rather than on the magnitude of the structural response.

Another important factor in the impact IIV model is the coefficient of restitution which essentially abbreviates all the ice properties of the characteristic failure frequency model. The coefficient of restitution also requires experimental research to be defined quantitatively. The conducted numerical simulations can only show how the coefficient of restitution influences the responses of the system. Figure 5.2 is plotted with the coefficient of restitution $e = 1$ which is an unrealistic case. Figure 5.7, 5.8, and 5.9 are simulated based on the same parameters of Figure 5.2 but with different values of e. It becomes obvious that the factor that most influences the magnitudes of the vibrations is the coefficient of restitution rather than the velocities of the ice. The system with $e = 0.1$ approaches the steady state after the first impact. The system with $e = 0.5$ not only approaches the steady-state vibration faster but also shows lower structural magnitudes than the system with $e = 1$, Figure 5.2. Figure 5.8 indicates that the system with $e = 0.5$ loses the majority of its momentum after approximately 54 seconds. This suggests that IIVs can be controlled by manipulating the coefficient of restitution via the properties of the contacting area of the ice. For instance, the magnitudes of IIVs could be significantly

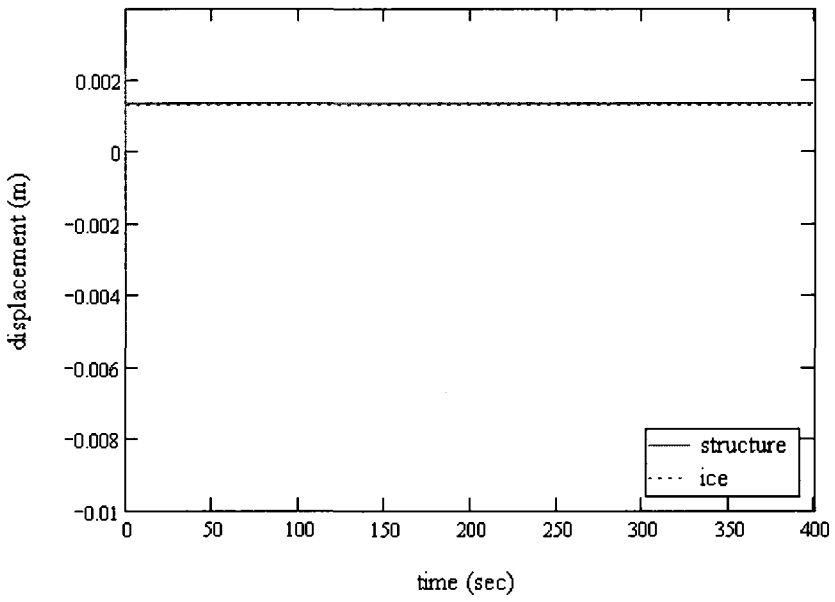

(a) Overall responses with $e = 0.1$

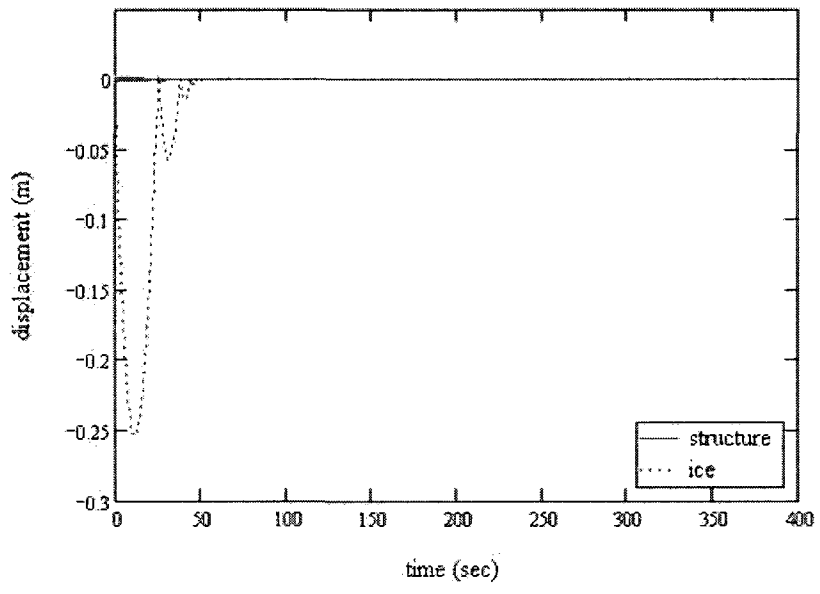

(b) Overall responses with $e = 0.5$

Figure 5.7: Responses with different coefficients of restitution 1

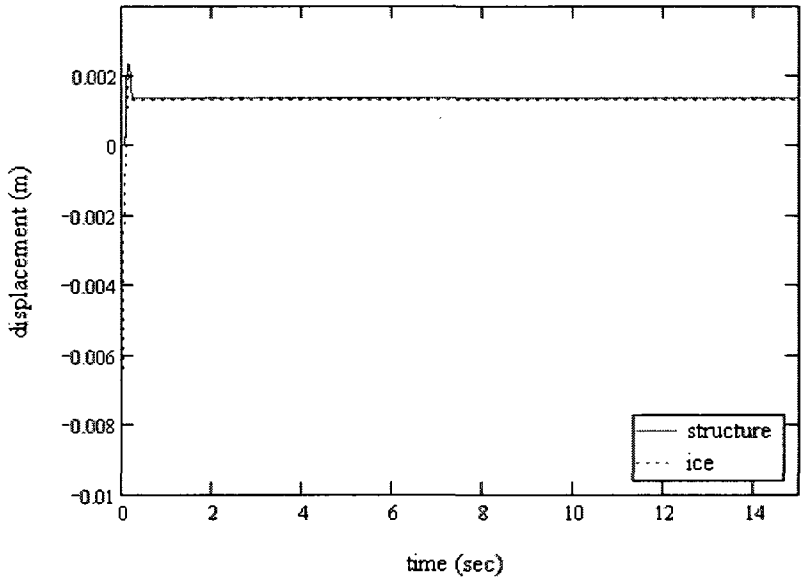

(a) Responses with $e = 0.1$ from 0 to 15 seconds

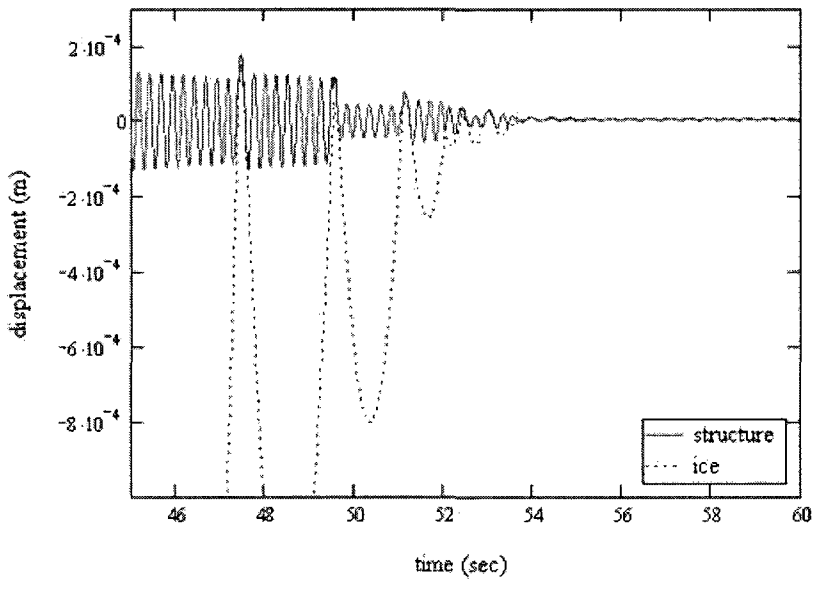

(b) Responses with $e = 0.5$ from 45 to 60 seconds

Figure 5.8: Responses with different coefficients of restitution 2

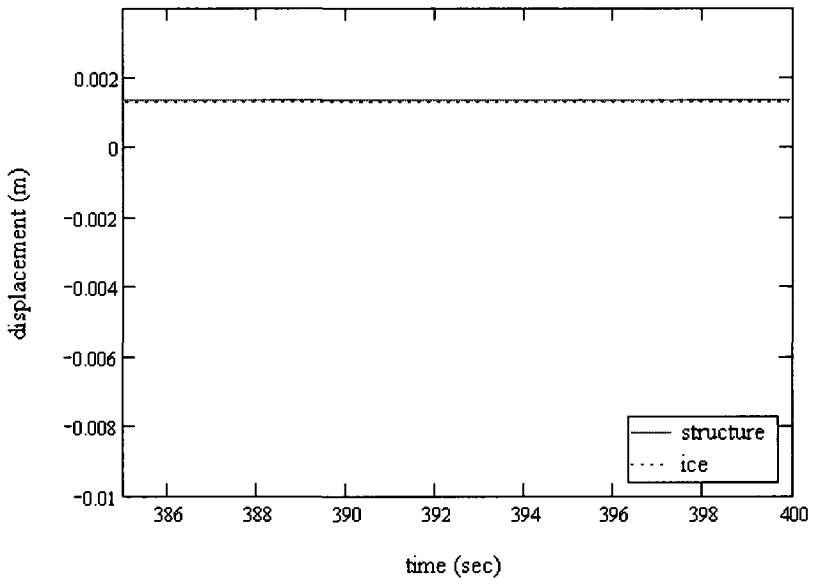

(a) Responses with $e = 0.1$ from 385 to 400 seconds

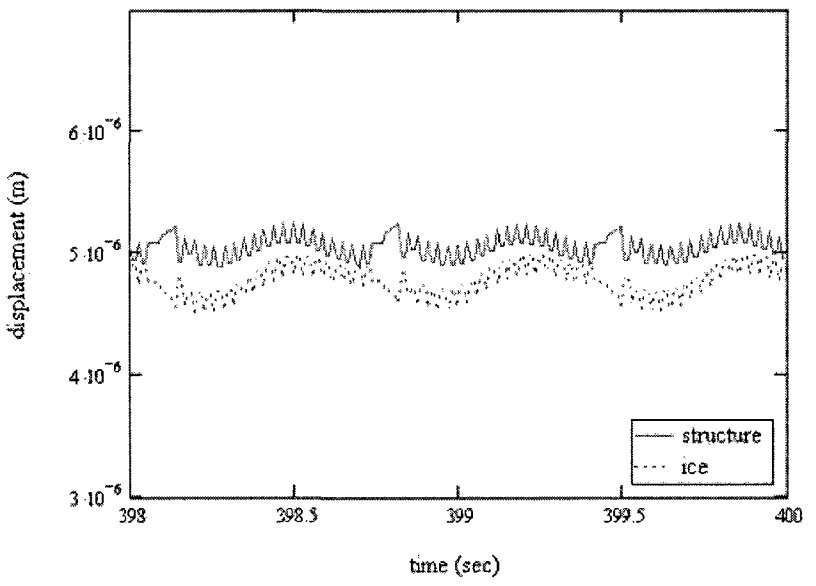

(b) Responses with $e = 0.5$ from 398 to 400 seconds

Figure 5.9: Responses with different coefficients of restitution 3

reduced by increasing the surface roughness of the structure.

5.3.2 Quadratic Drag Force

In the previous section, the impact IIV model was developed based on the linearized drag force which assumes small relative velocity between the velocities of the ice and structure. The linearized impact IIV model, however, is definitely vulnerable to two factors namely when the intervals between impacts exceed several seconds, and when the velocity of the flow is no longer small. Figure 5.10 clearly shows the error between the models based on the linearized drag and quadratic drag as time passes. The displacement of linearized equation (5.3), equation (5.13), is compared with numerically solved equation (5.3) by using the built-in ordinary differential equation solver of MathCad. The difference grows as time goes by, but at high flow velocity the difference decreases in figure 5.10 (b). This is because of the linearization factor, $|\dot{z} - \dot{u}|$, which calibrates the difference between the linear and quadratic models. The solution, however, to the quadratic drag force needs to be developed for a more precise simulation.

Equation (5.3) is not a linear ordinary differential equation and cannot be solved in closed form. A numerical solution is needed to solve equation (5.3) but instead of using the built-in ordinary differential equation solver of MathCad, a simple numerical solution is developed for a faster algorithm. From equation (5.3),

$$M\ddot{z} = -\frac{1}{2}\rho C_D A\,(\dot{z} - \dot{u})\,|\dot{z} - \dot{u}| = -B\,(\dot{z} - \dot{u})\,|\dot{z} - \dot{u}| \tag{5.40}$$

or

$$\ddot{z} = \frac{d\dot{z}}{dt} = -\frac{B}{M}\,(\dot{z} - \dot{u})\,|\dot{z} - \dot{u}| \tag{5.41}$$

where

$$B = \frac{1}{2}\rho C_D A$$

Using i as a counter for the a number of time steps, the displacement of equation (5.41) can be expressed as

$$z_i = z_{i-1} + \frac{dz_{i-1}}{dt}\Delta t = z_{i-1} + \dot{z}_{i-1}\Delta t \tag{5.42}$$

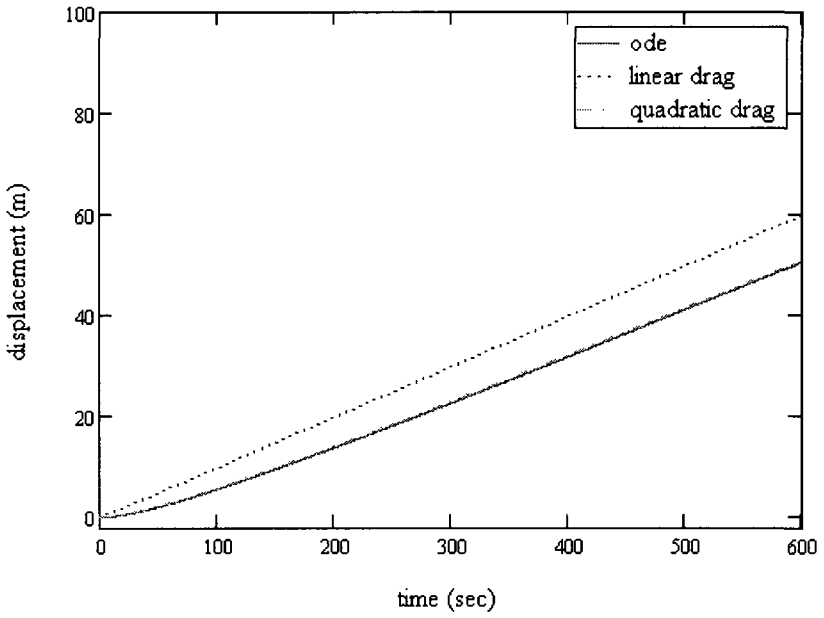

(a) Flow velocity 0.1 m/s

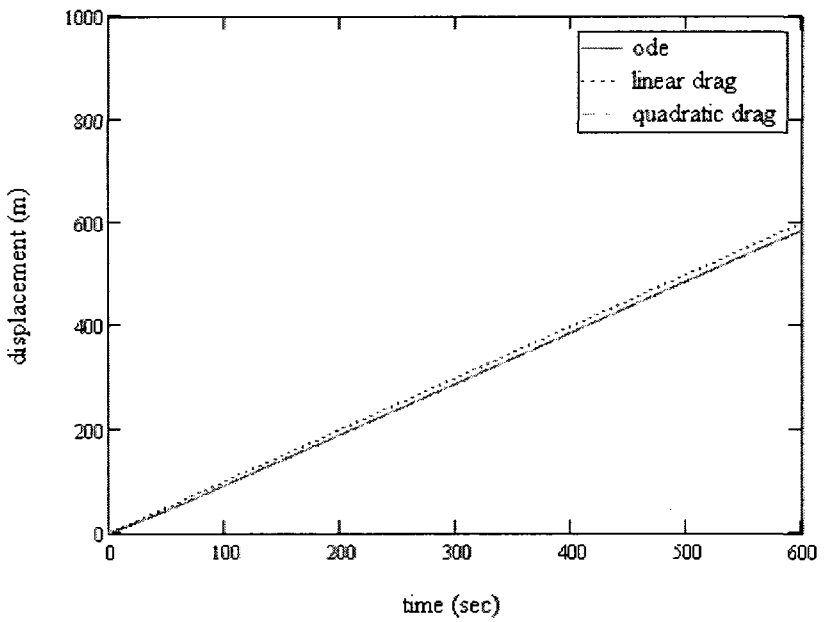

(b) Flow velocity 1 m/s

Figure 5.10: Comparison of the linearized and quadratic drag

in which Δt is previously defined as a time step. $\dot{z}$ is given by

$$\dot{z}_i = \dot{z}_{i-1} + \frac{d\dot{z}_{i-1}}{dt}\Delta t = \dot{z}_{i-1} + \ddot{z}_{i-1}\Delta t \tag{5.43}$$

By substituting equation (5.41) into equation (5.43),

$$\dot{z}_i = \dot{z}_{i-1} + \left[-\frac{B}{M}\left(\dot{z}_{i-1} - \dot{u}\right)\left|\dot{z}_{i-1} - \dot{u}\right|\right]\Delta t \tag{5.44}$$

Given the initial displacement and velocity of the ice, the displacement of the ice can be numerically solved by using equation (5.42) and (5.44) as simultaneous equations. The simulation results of equation (5.42) and (5.44) are also plotted in Figure 5.10. At the high flow velocity, Figure 5.10 (b), equation (5.42) and (5.44) predict the displacement of the ice close enough to the one evaluated with the built-in ordinary differential equation solver. In the algorithm of the numerical simulation, equation (5.42) and (5.44) replace equation (5.13) and (5.14).

Using the same parameters as those used in Figure 5.2 but with a different flow velocity, the responses of the impact IIV model with the quadratic drag force are compared with the one with the linearized drag force in Figure 5.11. At high flow velocities, over 1 $^{m}/_{s}$, the quadratic drag force model approaches steady-state vibration more quickly than the linearized drag force model because at high flow velocity the quadratic drag induces more damping while it transfers more forces than the linearized drag. In Figure 5.12 the quadratic drag force model exhibits the characteristic of the steady-state vibration while the linearized drag force model still displays quasi-static vibration. As ice velocities increase, which corresponds to flow velocities in the impact IIV model, increasing IIVs are closer to the steady-state vibrations. The linearized drag force model, however, does not show a steady-state vibration until 400 seconds in Figure 5.12. The linearization factor allows the linearized drag force model to follow the quadratic drag force model in the beginning, but when the system is in a series of low velocity impacts, the linearization factor causes a difference. The linearized drag force model, therefore, is inappropriate to simulate the impact IIV model at high flow velocities.

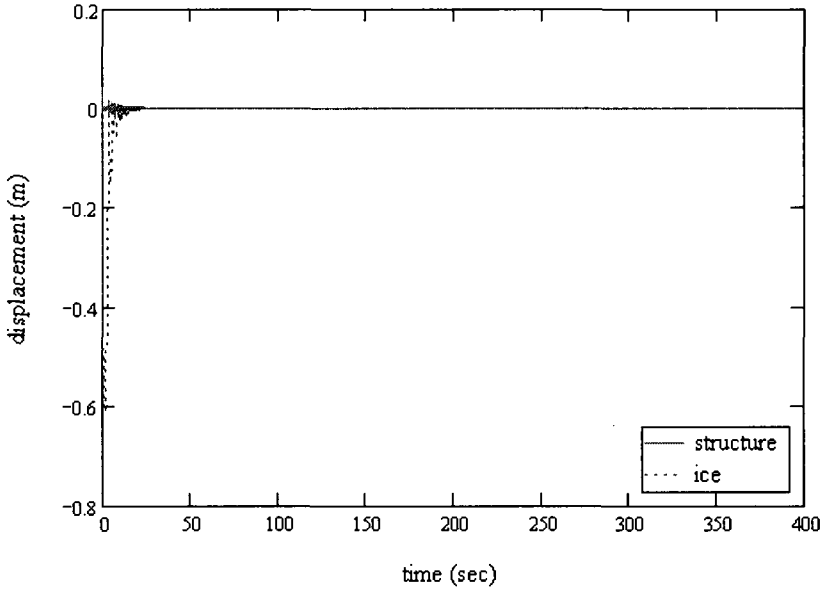

(a) Overall responses with the quadratic drag

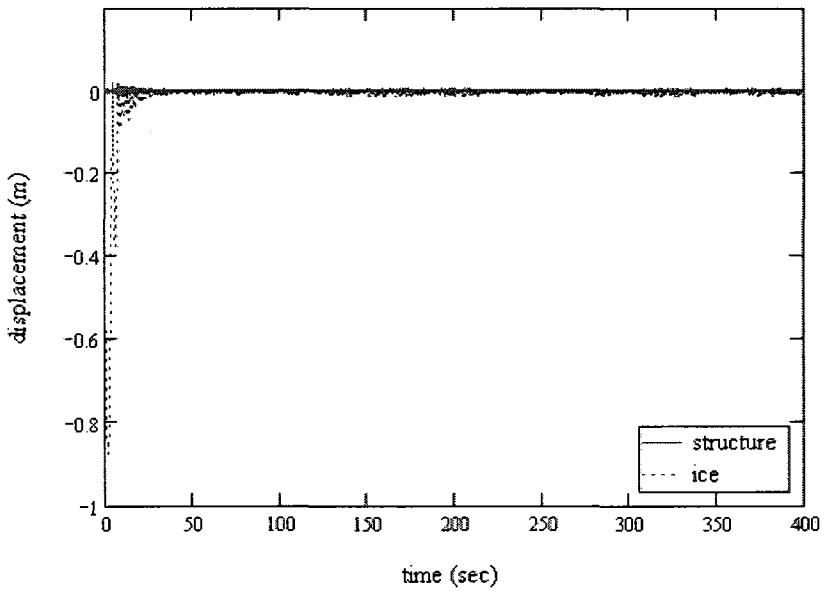

(b) Overall responses with the linear drag

Figure 5.11: Responses with the quadratic and linear drags 1

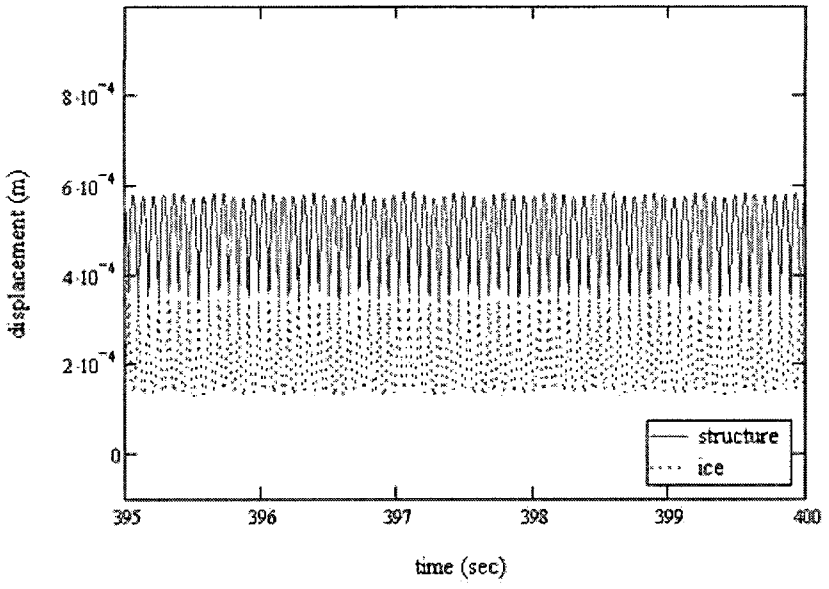

(a) Responses with the quadratic drag from 395 to 400 seconds

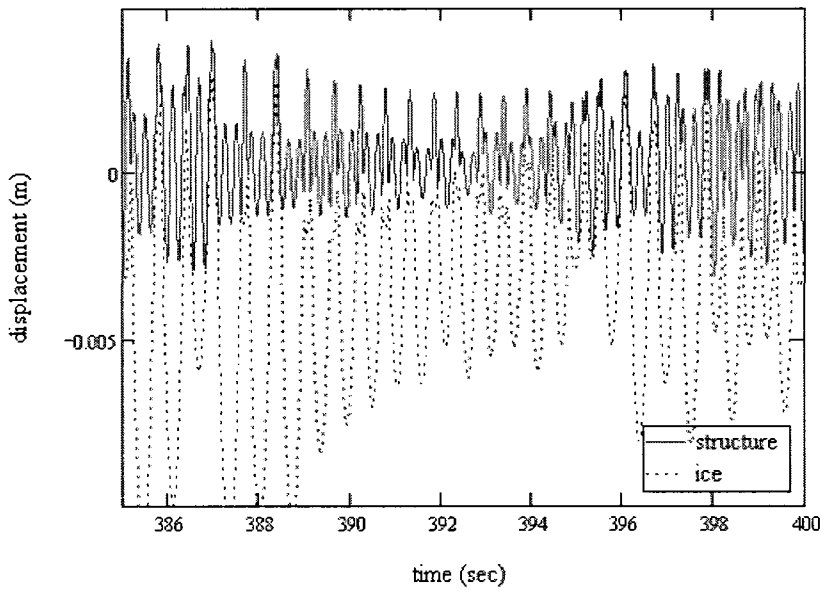

(b) Responses with the linear drag from 385 to 400 seconds

Figure 5.12: Responses with the quadratic and linear drags 2

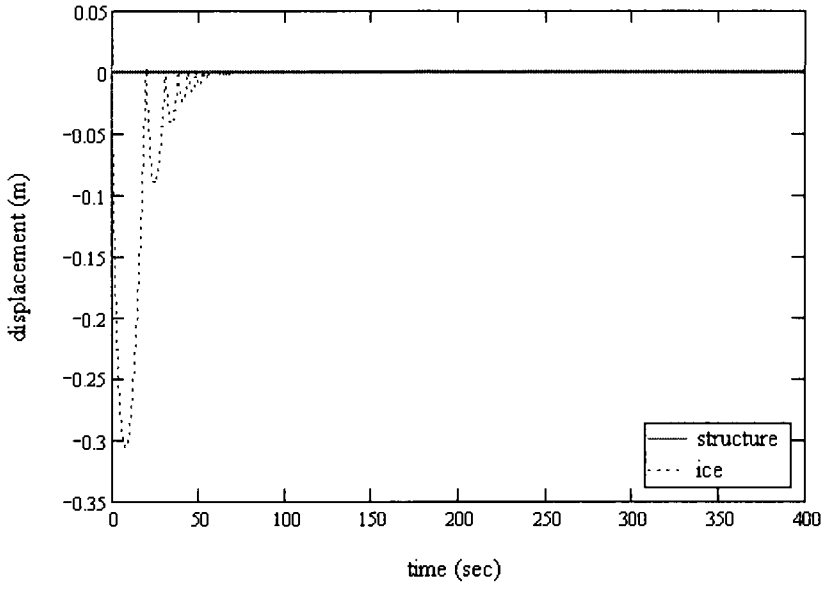

(a) Overall responses with $A = 2$ m^2

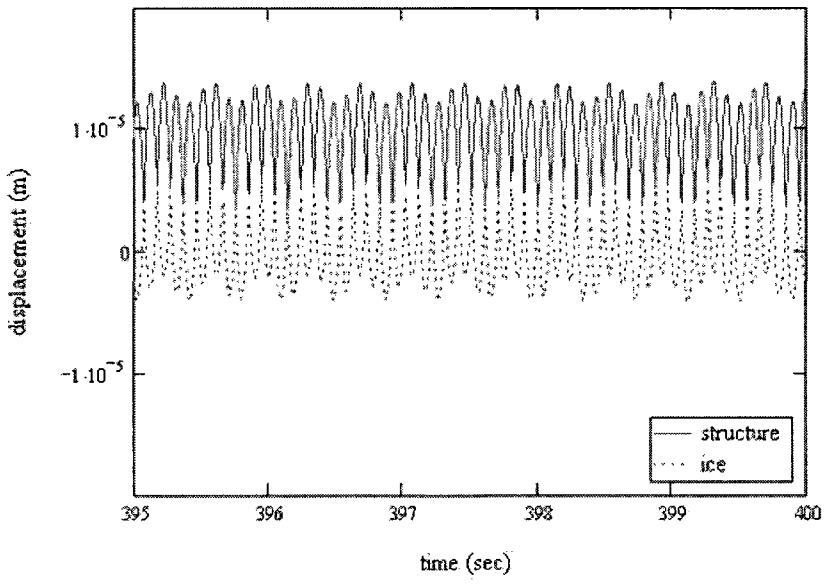

(b) Responses with $A = 2$ m^2 from 395 to 400 seconds

Figure 5.13: Responses with $A = 2$ m^2

Since the ice area, A, plays a similar role as the flow velocity in the impact IIV model, the model with wide ice area is also simulated with the quadratic drag force. The influence of the drag force on the response of the ice increases as the size of the ice area increases because the ice area is related to the drag force by equation (5.1), $f_D = -\frac{1}{2}\rho C_D A\,(\dot{z} - \dot{u})^2$. Figure 5.13 is plotted with the ice area $A = 2$ m, the flow velocity $\dot{u} = 0.1\ {}^{\mathrm{m}}/_{\mathrm{s}}$ and the rest of parameters are the same as the parameters used in Figure 5.11. The flow velocity of Figure 5.13 is identical to that of Figure 5.2 but the responses quickly approach the steady-state vibrations as if they are driven by high flow velocity. Figure 5.13 (b) also shows a similar vibration characteristic to Figure 5.12 (a) because both flow velocity and ice area influence the drag force in the impact IIV model. Therefore, the ice area can be another controlling factor of IIVs. The ice area shares a similar concept to that of a contact zone which was proposed by other IIV research [Dempsey, 1999]. Since the ice area is related to the size of the contacting area of a structure, reducing the contacting area has a similar effect to that of reducing the flow velocity.

In the previous section, the roles of the ice mass and the coefficient of restitution have been defined by changing relevant parameters. To verify if those definitions still hold with the quadratic drag force, the impact IIV model with the quadratic drag is plotted with change in ice mass and the coefficient of restitution. Figures 5.14, 5.15, and 5.16 are plotted on the same parameters used in Figures 5.2, 5.4 (a), and 5.4 (b), respectively except they are based on the quadratic drag force. The responses of Figure 5.14, 5.15, and 5.16 prove that the defined role of the ice mass holds with the quadratic drag force. The responses of the system with heavier ice mass, Figures 5.16 (b), is still unstable while the system with the ice mass $M = 800$ kg, Figure 5.15 (b), is in the steady-state vibration. The quadratic drag force, however, induces more drag force, thus the system responses tend to be stabilized faster than those with the linearized drag forces.

Figures 5.17 and 5.18 are plotted on the same conditions with Figures 5.7 (a) and (b), respectively but with the quadratic drag force. The coefficient of restitution also

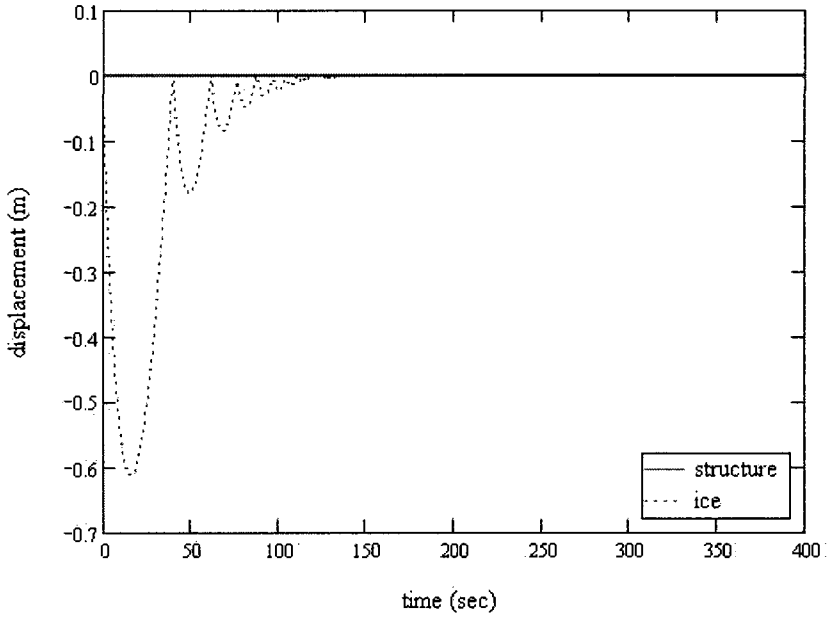

(a) Overall responses with $M = 1600$ kg

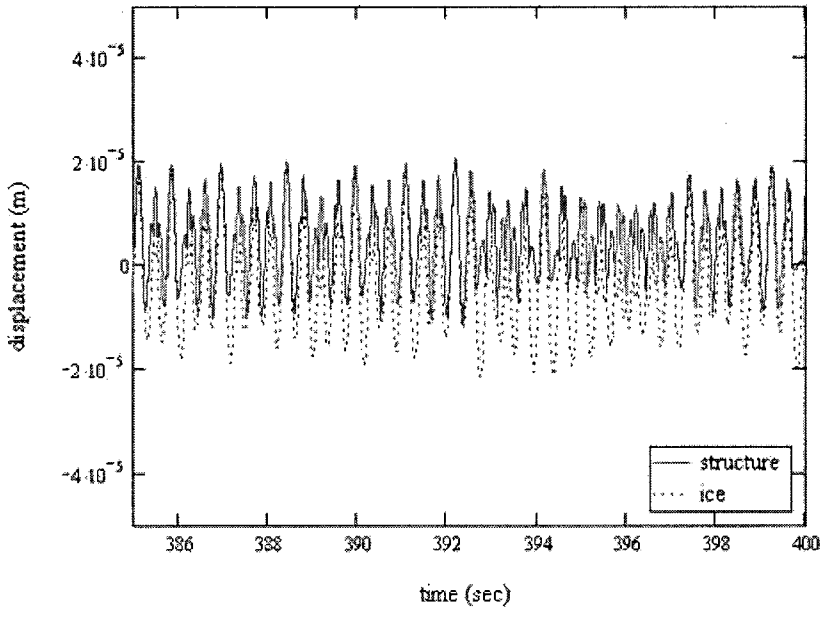

(b) Responses with $M = 1600$ kg from 385 to 400 seconds

Figure 5.14: Responses with $M = 1600$ kg

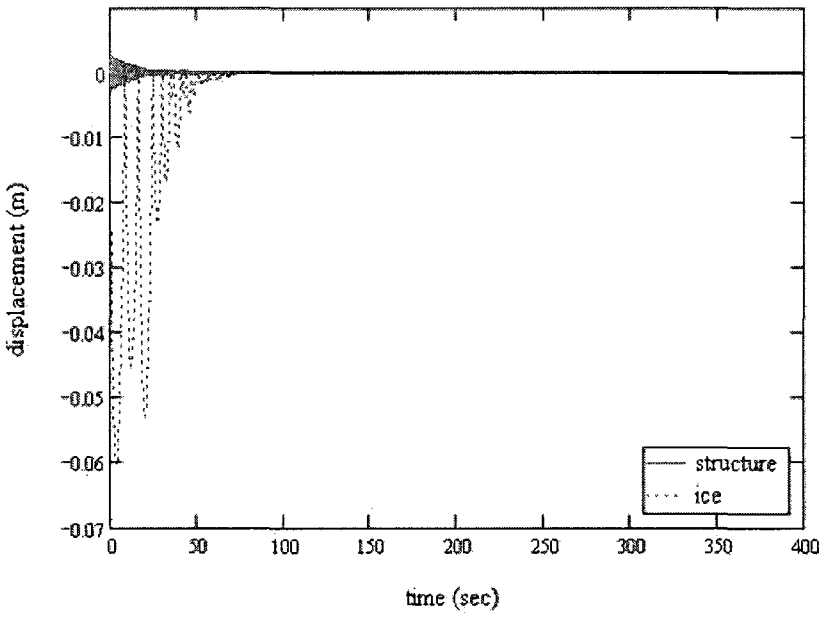

(a) Overall responses with $M = 800$ kg

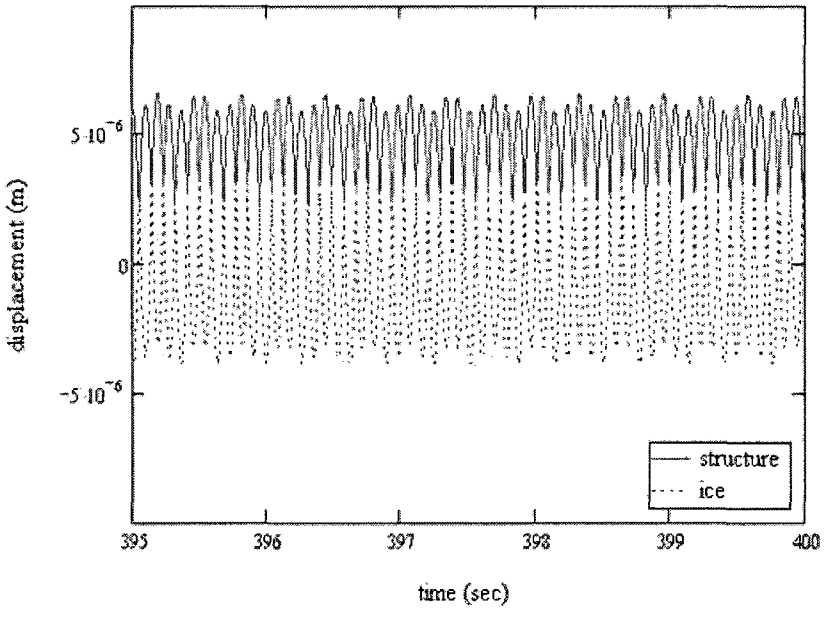

(b) Responses with $M = 800$ kg from 395 to 400 seconds

Figure 5.15: Responses with $M = 800$ kg

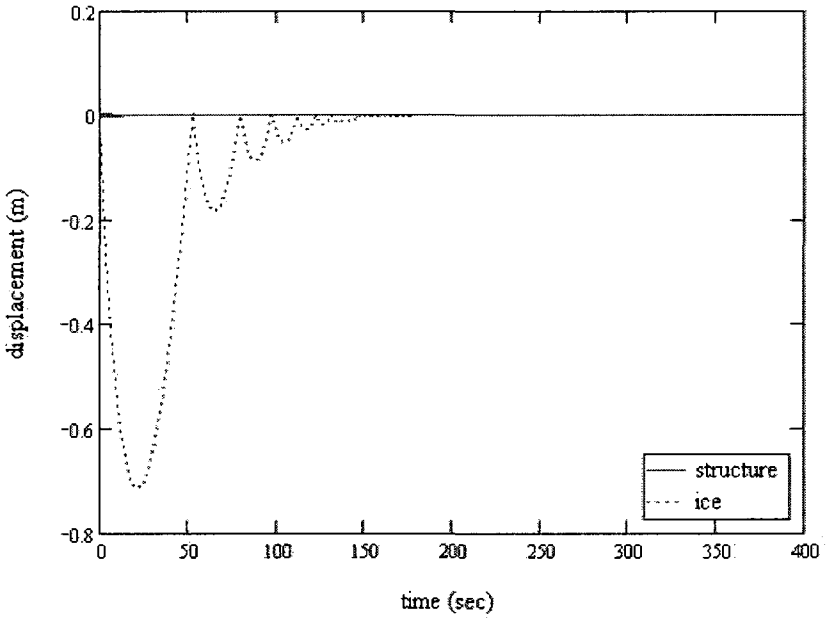

(a) Overall responses with $M = 2400$ kg

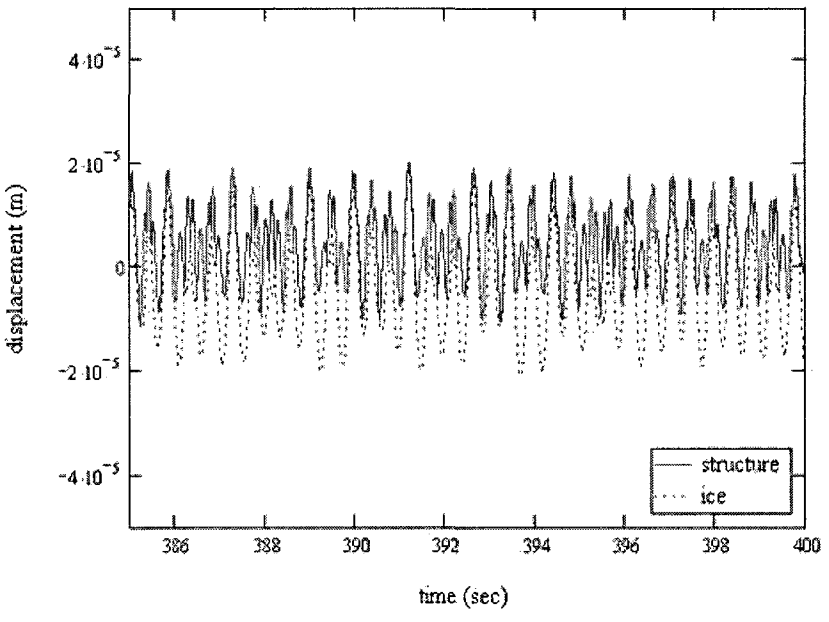

(b) Responses with $M = 2400$ kg from 385 to 400 seconds

Figure 5.16: Responses with $M = 2400$ kg

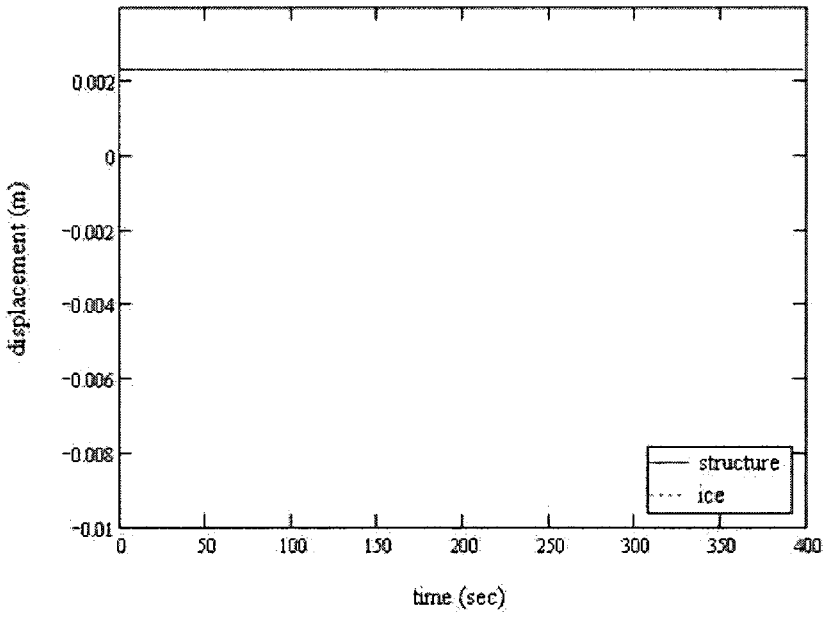

(a) Overall responses with $e = 0.1$

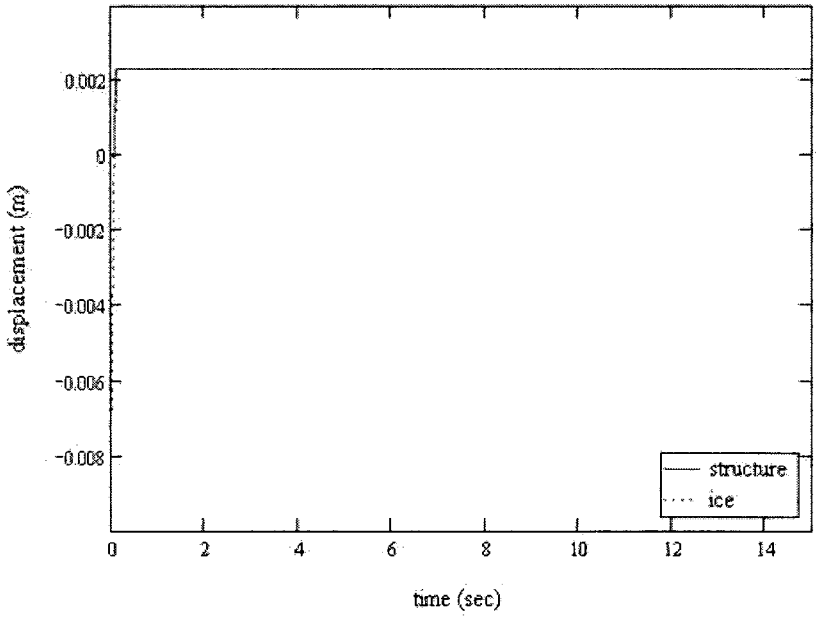

(b) Responses with $e = 0.1$ from 0 to 15 seconds

Figure 5.17: Responses with $e = 0.1$

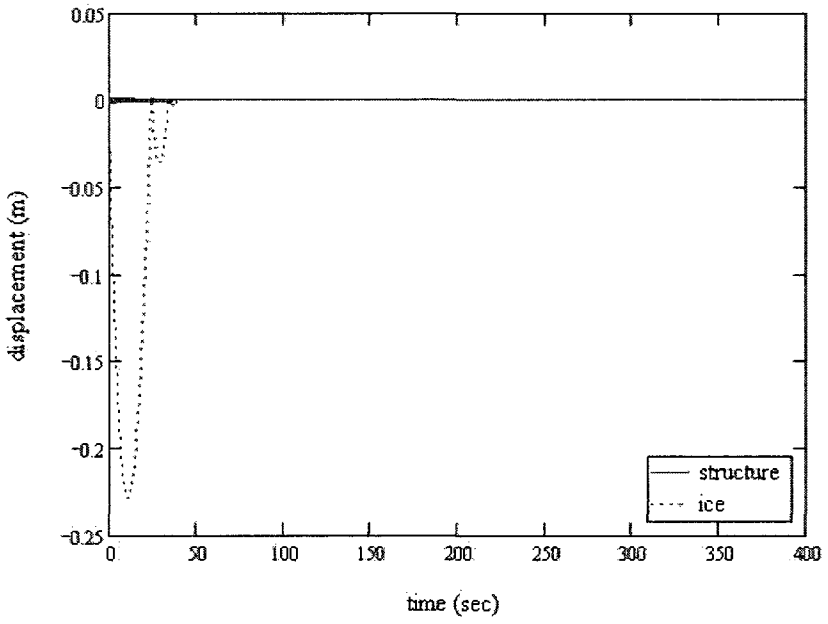

(a) Overall responses with $e = 0.5$

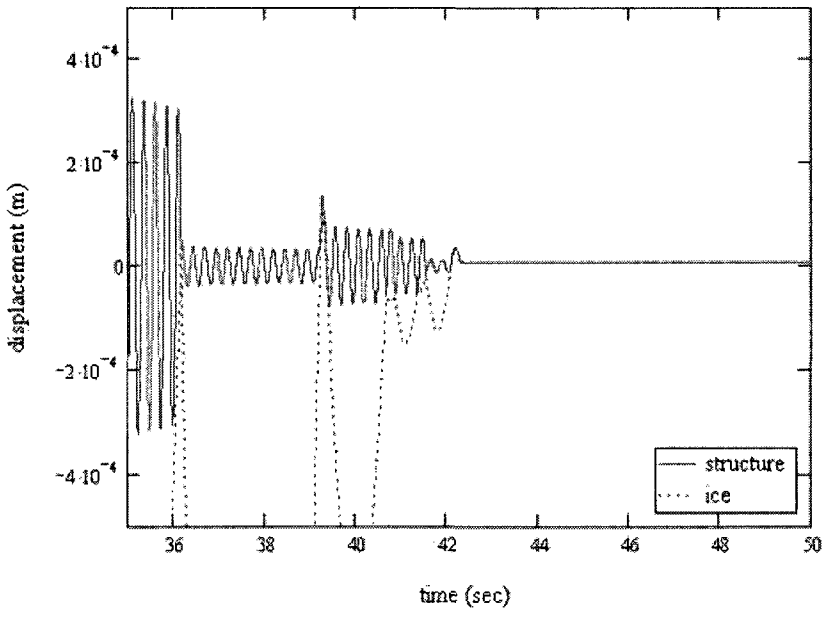

(b) Responses with $e = 0.5$ from 35 to 50 seconds

Figure 5.18: Responses with $e = 0.5$

governs the magnitudes of responses in the impact IIV model with the quadratic drag force, however, the system with the quadratic drag force is more sensitive to change in the coefficient of restitution than the one with the linearized drag force. The system with $e = 0.5$, Figure 5.18 (b), loses the momentum at approximately 43 seconds under the influence of the quadratic drag force while the system with the linearized drag force and $e = 0.5$, Figure 5.8 (b), loses the majority of its momentum at approximately 54 seconds. This is again because the quadratic drag force dissipates energy more quickly than the linearized drag force. However, it is sufficiently proven in Figure 5.17 and 5.18 that the coefficient of restitution plays the same role in both quadratic and linearized drag forces.

5.4 Resonance Conditions

One of the main objectives of IIV analysis aims to find a resonance condition which is often referred to as lock-in in IIV research. The structural vibration frequency increases as the ice velocity increases but when lock-in occurs, the structural frequency remains at the natural frequency even with increasing ice velocity [Sodhi, 1989]. In the impact IIV model, however, the velocities of the ice cannot be the primary lock-in condition because the velocities of the ice are not fixed. One possible interpretation of the impact IIV model is that it considers the ice forces to be a series of discrete impulses as shown in Figure 5.19 (a) while the other IIV models consider them as continuous periodic forces. The impact IIV model in fact proposes a way to calculate the strength of each impulse and the times between impulses and these depend on the momenta of the ice and structure as well as the coefficient of restitution for the collision. Under certain conditions, it is possible for the discrete impulses of Figure 5.19 (a) to approach the regular periodic series of impulses of Figure 5.19 (b) which is suspected to cause the lock-in condition.

This view of the impact IIV model can be analyzed by using a Fourier transform [De Silva, 1999] given by

$$\hat{F}(\omega) = \int_{-\infty}^{\infty} f(t)\, e^{-i\omega t} dt \tag{5.45}$$

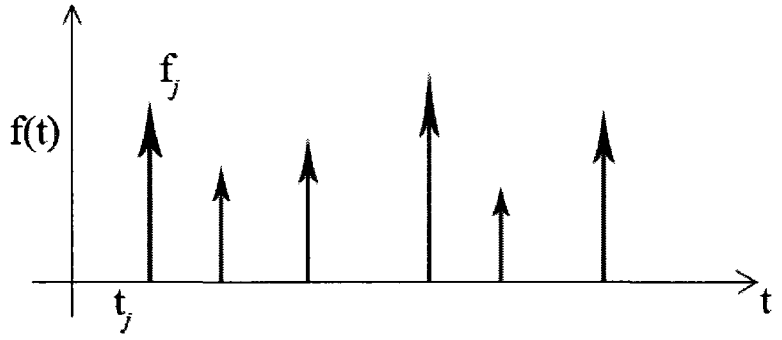

(a) Random impulses

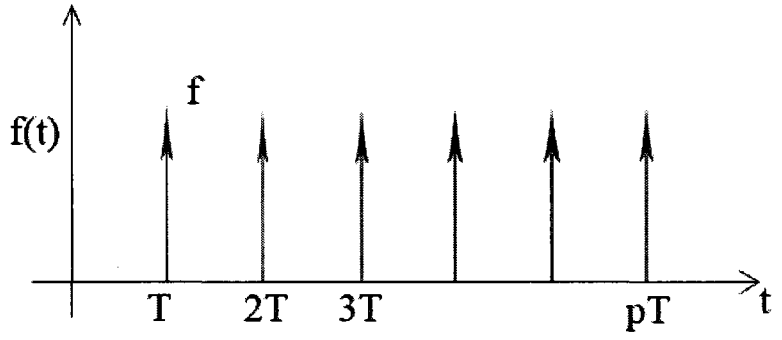

(b) Uniform impulses

Figure 5.19: Ice forces as a series of impulses

and the corresponding inverse Fourier transform given by

$$f(t) = \frac{1}{2\pi} \int_{-\infty}^{\infty} \hat{F}(\omega) e^{i\omega t} d\omega \tag{5.46}$$

The discrete ice forces of Figure 5.19 (a) can be expressed as a series of impulses as

$$f(t) = \sum_{j=1}^{\infty} f_j \delta_D (t - t_j) \tag{5.47}$$

where δ_D indicates the Dirac delta function and f_j indicates the strength of each impact. If the sizes and intervals of the impulses are uniform as shown in Figure 5.19 (b),

equation (5.47) is rewritten as

$$f(t) = \sum_{p=1}^{\infty} f\delta_D (t - pT) \tag{5.48}$$

In reality, the repeated ice impacts will not all have the same strength or occur at a fixed interval, however it is sufficient for the situation of Figure 5.19 (a) to approach that of Figure 5.19 (b) for this analysis to be relevant.

Equation (5.48) is often called a comb function. A Fourier transform of the comb function is given [Weaver, 1983] by

$$\hat{F}(\omega) = 2\pi \sum_{N=1}^{\infty} f\delta_D \left(\omega - \frac{2\pi N}{T}\right) \tag{5.49}$$

From equation (3.5)

$$\ddot{x} + 2\zeta\omega_n\dot{x} + \omega_n^2 x = \sum_{p=1}^{\infty} f\delta_D (t - pT) \tag{5.50}$$

Taking Fourier transforms on the both sides,

$$\left(-\omega^2 + 2\zeta\omega_n\omega i + \omega_n^2\right)\hat{X}(\omega) = 2\pi \sum_{N=1}^{\infty} f\delta_D \left(\omega - \frac{2\pi N}{T}\right) \tag{5.51}$$

or

$$\hat{X}(\omega) = 2\pi \frac{\sum_{N=1}^{\infty} f\delta_D \left(\omega - \frac{2\pi N}{T}\right)}{\left(-\omega^2 + 2\zeta\omega_n\omega i + \omega_n^2\right)} \tag{5.52}$$

Taking the inverse Fourier transforms to find the structure response in time gives

$$x(t) = 2\pi \sum_{N=1}^{\infty} \frac{1}{2\pi} \int_{-\infty}^{\infty} \frac{f\delta_D \left(\omega - \frac{2\pi N}{T}\right)}{\left(-\omega^2 + 2\zeta\omega_n\omega i + \omega_n^2\right)} e^{i\omega t} d\omega \tag{5.53}$$

or

$$x(t) = f \sum_{N=1}^{\infty} \frac{e^{i\frac{2\pi N}{T}t}}{\left(-\frac{4\pi^2 N^2}{T^2} + i\zeta\omega_n\frac{4\pi N}{T} + \omega_n^2\right)} \tag{5.54}$$

Equation (5.54) experiences a resonance when the denominator of any of the terms in the sum goes to zero. That is when

$$\omega_n = \frac{2\pi N}{T} \tag{5.55}$$

where N is an integer larger than 0. This says that the structures will experience a resonance when the natural frequency is an integral multiple of the forcing frequency, as would be expected. In the previous numerical simulations, this condition has been observed in several cases, Figures 5.12 (a) and 5.13 (b). For instance, the structural frequency of Figure 5.13 (b) is

$$\frac{2\pi}{T} = \frac{2\pi}{0.5} = 12.57 \ {}^{\text{rad}}/_{\text{sec}}$$

The natural frequency of the structure is

$$\sqrt{\frac{k}{m}} = \sqrt{\frac{1000000}{1600}} = 25 \ {}^{\text{rad}}/_{\text{sec}}$$

With $N = 2$ the structural frequency is close to the natural frequency. The result is what is seen in Figure 5.13 (b). The structure and ice vibrate at the same frequency of ${}^{2\pi}/_{T}$ which is half of the natural frequency. The structural frequency remains at that level, which is lock-in, and so does the frequency of the ice response.

Thus, the impact IIV model successfully predicts the existence of the lock-in condition and also predicts that it can happen when the frequency of the structure and ice impacts are synchronized together at a multiple of the natural frequency of the structure. The question of the precise conditions necessary for the frequency of ice and structure impacts to occur at a multiple of the natural frequency still remains open.

5.5 New Modeling Approach Combined with Flow Effect

The impact IIV model has neglected the influence of flow on the structure although the dynamics of the ice have been developed under the influence of flow. In Chapter 3, it was shown that the flow affects the dynamics of the structure, but the impact IIV model applies different points of view to the ice and structure. For the consistency of the impact IIV model, the structural dynamics should also include the influence of the flow. The

structural equation of motion including the flow effect is developed in equation (3.14). By assuming a small flow-induced force, equation (3.14) can be written as

$$\bar{M}_a\ddot{x} + \left(\bar{c} + C'_D\rho\frac{D}{2}\right)\dot{x} + \bar{k}x = 0 \tag{5.56}$$

where the bars indicate per-unit-length dimensions and $\bar{M}_a$ is given as equation (3.11), $\bar{M}_a = \left(\bar{m} + C_A\rho\pi\frac{D^2}{4}\right)$. The equation of the ice, equation (5.41), also needs to be rewritten to be in units of per unit length so that

$$\bar{M}\ddot{z} = -\bar{B}\left|\dot{z} - \dot{u}\right|(\dot{z} - \dot{u}) \tag{5.57}$$

where

$$\bar{B} = \frac{1}{2}\rho C_D\bar{A}$$

The rest of the procedure is the same as for the quadratic drag force model.

Figure 5.20 is plotted with the same parameters used in Figure 5.11 (a) where the structural response includes the flow effect. Comparing the structural responses with and without flow effect, the system loses momentum more quickly in the model with flow than in the one without the flow effect since the flow causes additional damping on the system, Figure 5.20 (a). Since the mass of the structure is also changed by the added mass term, the vibration frequencies, Figure 5.20 (b), are different from Figure 5.12 (a). It is obvious that the flow influences the impact IIV model as predicted in Chapter 3. By adding the flow effect to the structural dynamics, therefore, the impact IIV model achieves the consistency and completeness of the theory.

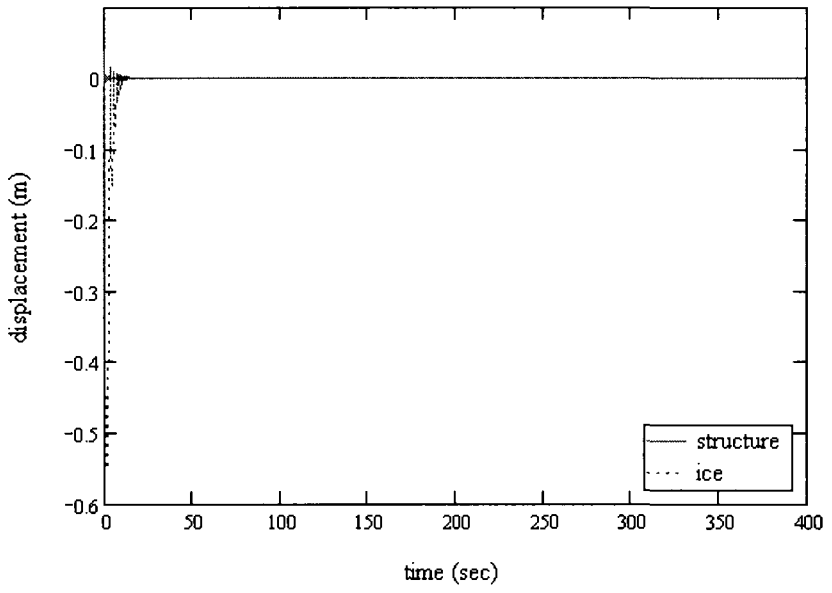

(a) Overall responses with the flow effect

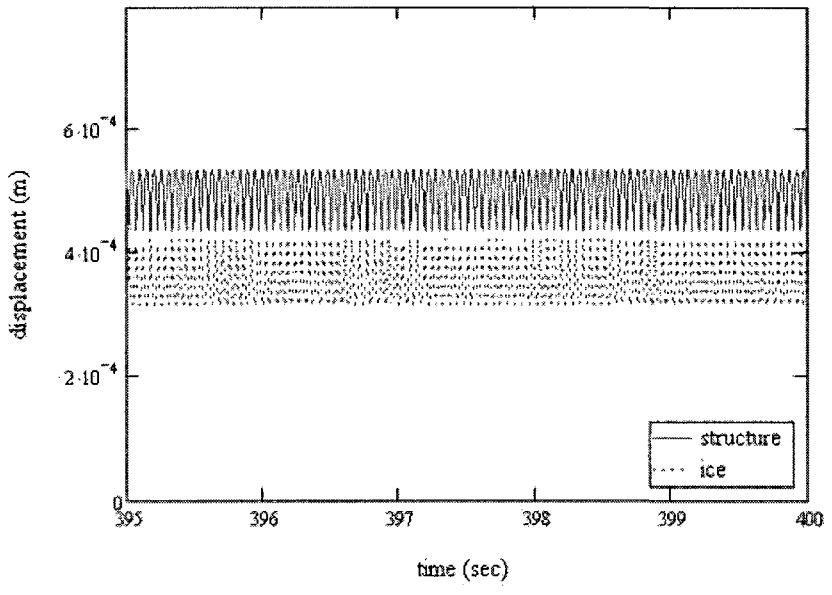

(b) Responses with the flow effect from 395 to 400 seconds

Figure 5.20: Responses of the impact IIV model with the flow effect

Chapter 6

Conclusions and Future Work

As the final chapter, this chapter highlights important results from the previous chapters. The main theme of this thesis is how ice-induced vibrations (IIVs) are developed by a moving fluid. A new IIV model has been proposed and numerical simulations have been conducted on the model. Several conclusions have been drawn from the numerical simulations. Future work for the impact ice-induced vibration model is also briefly discussed.

6.1 Summary and Conclusions

Chapter 2 presented a review of the current literature on IIVs. It was shown that there are two main models that are in current use. The first model presents IIVs as a continuous interaction due to a self-excited effect, while the other explains IIVs as a series of discrete events. The first theory is often called the self-excited model and the second one is called the characteristic failure frequency model. The characteristic failure frequency model is more widely accepted than the self-excited model. The structure does not play an active role in the characteristic failure frequency model. In this model, the frequencies of IIVs are determined by the ice failure mechanism which is governed by the properties and velocities of the ice in contact with the structure. It was also observed that although any

structure subject to IIV is usually located in a flowing fluid, the effect of the flow of that fluid has never been considered in the modeling of the IIVs.

Chapter 3 thus considered the effect of the fluid flow on the vibrations of the structure, and thus the effect of flow on IIVs. A simple model was presented using Morison's equation and a one degree-of-freedom spring-mass-damper system representing the structure. Numerical simulations were performed in order to predict the influence of the flow on the structure. It was noted that the flow makes the structure heavier and more damped as if the structure has an additional mass and damper. The flow effect is inversely proportional to the mass of the structure, therefore the concept of a density ratio was presented based on the structural density versus fluid density. This density ratio is to act as an indicator of the flow effect. The lower the density ratio, the higher the flow effect. Since the flow also influences the dynamics of the ice, the impact IIV model of Chapter 5 was also developed so that the dynamics of both structure and ice can respond to the flow.

Chapter 4 reproduced the two IIV models proposed in Toyama et al. (1983) and Huang and Liu (2006). Both models are based on the characteristic failure frequency model but with different expressions. The Tomaya model needed to be modified to be applicable to general cases of IIVs. With the improved Toyama model, the numerical simulations were conducted on the same parameters and ice force in order to enable a fair comparison. The numerical simulations of both models presented completely different responses although they were simulated using the same parameters and ice force. In addition, the model developed in Chapter 3, which is also another characteristic failure frequency model, was compared with the two models using the same parameters and ice force. All three models based on the same modeling approach predicted different vibration responses. This inconsistency of the IIV models gave motivation for a new IIV modeling approach.

Chapter 5 presented a new model for IIVs based on repeated impacts of the ice and structure, conservation of linear momentum and using the coefficient of restitution to characterize the nature of the impact between ice and structure. This model was referred to as the impact IIV model. The properties of the impact IIV model were investigated

through numerical simulations. The ice mass is one of the factors determining the vibration characteristics of IIVs rather than determining the magnitudes of IIVs at every impact since it is related to the momentum of each impact. The magnitudes of the vibrations are governed by the coefficient of restitution which encapsulates all ice properties mentioned in other IIV models. In addition to the ice properties, the coefficient of restitution is also related with the interaction between the structure and ice. The last ice property of the impact IIV model is that of the ice area which influences the dissipation of the system momenta through the drag force. An ice with a small ice area shows the same behavior of an ice driven by lower flow velocity. Through the impact IIV model, therefore, two factors which can control characteristics of IIVs have been proposed, the ice area and the coefficient of restitution. By changing the size of the contact area between the ice and structure, the driving force of the ice can be reduced as if the ice were driven by lower flow velocities. Furthermore, by changing factors related to the coefficient of restitution such as the surface roughness or shape of the structure, IIVs can be reduced to avoid the lock-in condition which occurs when the frequencies of the structure and ice are synchronized at a multiple of the natural frequency of the structure. In addition to the inclusion of the flow effect, the new approach to ice forces through the impact IIV model permits the answering of some existing IIV questions which originate from the weak theoretical points of existing IIV models.

6.2 Future Work

The primary work for reinforcing the impact IIV model will be extensive laboratory tests in order to find a way to define the relevant ice mass and area. The ice mass and area for the impact IIV model have been obscurely defined in this thesis inspite of their importance because there is no proven literature. The definitions of the ice mass and area, therefore, are conceptual. The contact zone which is suggested by other IIV researchers shares a similar idea, however, it is not proven that the contact zone is

directly proportional to the ice mass and area. The coefficient of restitution, another important factor of the impact IIV model, also requires experimental verification. The definition of the coefficient of restitution is the crucial idea of the impact IIV model which distinguishes itself from other existing IIV models. Numerical simulations can verify the roles of the ice properties and the coefficient of restitution, yet quantitative definitions are beyond the scope of numerical simulation. Therefore experimental research for the impact IIV model should be followed.

Another weak point of the impact IIV model is the approach to the dynamics of the ice. The impact IIV model considers the ice mass as an independent mass from the entire ice cover so that the ice mass can float on the water freely. The equation of motion of the ice mass, therefore, only consists of the inertia force and drag force. The actual ice mass, however, cannot be exclusively modeled without considering the boundary between the ice mass and entire ice cover. In other words, the equation of the ice needs to adopt damping and stiffness terms to model the interaction at the boundary. It also enables the impact IIV model to add a residual force from the previous impact. It is mathematically straightforward, but defining them in a quantitative manner will again require experimental research.

The investigated models in this thesis are one degree-of-freedom lumped parameter systems. A one degree-of-freedom model is effective for simulations and for quickly gaining insight into a problem. However, it is not adequate for representing the overall dynamics of structures, especially for relatively long structures. The top end of a long structure may experience different vibration characteristics from the part where the ice is in contact. Therefore, a multi degree-of-freedom or continuous model should be developed to further investigate the response of the whole structure. Additionally, as demonstrated in this thesis, the choice of a time step to use for the simulations is an important parameter. In this work, the time step was chosen in an ad-hoc manner. It is proposed for further work to develop a criterion or algorithm for the choice of a time step. In particular, it is suggested that the natural frequency of the structure can be used as a guideline in

choosing the time step.

Although the most important purpose of the proposed impact IIV model is to address the unsolved questions which could not be answered by the existing IIV models, the nature of the impact IIV model, which is a very adaptive and flexible, allows it to be easily applied to other vibration systems. In this thesis, the main driving force of the ice is assumed to be the drag from the moving fluid, however, the impact IIV model can be adapted to other external forces by modifying the forcing term. Furthermore, vibrations originated from repeated impacts are also applicable to the impact IIV model. Therefore, the applications for the impact IIV model are not restricted to IIV analysis.

Appendix A

Mathcad Codes

A.1 The Impact IIV model Based on Linear Drag

$L := 1 \quad F_0 := 8388 \quad m := 1600 \quad k := 1000000$

$\rho := 999 \quad u' := 0.1 \quad A := 1 \quad c := 200 \quad \omega_n := \sqrt{\frac{k}{m}} \quad \xi := \frac{c}{2m \cdot \omega_n} \quad \omega_d := \sqrt{1 - \xi^2} \cdot \omega_n$

$M := 1600$ ice mass $\quad e := 1$ coe. of restitution $\quad C_d := 1 \quad b := u' \frac{1}{2} \rho \cdot C_d \cdot A$

Equations of the ice

$z(t, c1, c2) := c1 + u' \cdot t + c2 \cdot e^{-\frac{b}{M} \cdot t} \quad z'(t, c2) := u' - c2 \cdot \frac{b}{M} \cdot e^{-\frac{b}{M} \cdot t} \quad z''(t, c2) := \frac{d}{dt} z'(t, c2)$

$$matZ(t) := \begin{pmatrix} 1 & e^{-\frac{b}{M} \cdot t} \\ 0 & -\frac{b}{M} \cdot e^{-\frac{b}{M} \cdot t} \end{pmatrix} \quad matI1(t, z_f, z'_f) := \begin{pmatrix} z_f - u' \cdot t \\ z'_f - u' \end{pmatrix}$$

Equations of the structure

$x(t, c3, c4) := c3 \cdot e^{-\xi \cdot \omega_n \cdot t} \cdot \cos(\omega_d \cdot t) + c4 \cdot e^{-\xi \cdot \omega_n \cdot t} \cdot \sin(\omega_d \cdot t)$

$x'(t, c3, c4) := \frac{d}{dt} x(t, c3, c4) \quad x''(t, c3, c4) := \frac{d}{dt} x'(t, c3, c4)$

$$matX(t) := \begin{bmatrix} e^{-\xi \cdot \omega_n \cdot t} \cdot \cos(\omega_d \cdot t) & e^{-\xi \cdot \omega_n \cdot t} \cdot \sin(\omega_d \cdot t) \\ -e^{-\xi \cdot \omega_n \cdot t} \cdot (\xi \cdot \omega_n \cdot \cos(\omega_d \cdot t) + \omega_d \cdot \sin(\omega_d \cdot t)) & e^{-\xi \cdot \omega_n \cdot t} \cdot (\omega_d \cdot \cos(\omega_d \cdot t) - \xi \cdot \omega_n \cdot \sin(\omega_d \cdot t)) \end{bmatrix}$$

$$matI2(x_f, x'_f) := \begin{pmatrix} x_f \\ x'_f \end{pmatrix}$$

Impact

$$matM := \begin{pmatrix} M & m \\ -1 & 1 \end{pmatrix} \quad matI3(t, c2, c3, c4) := \begin{pmatrix} M \cdot z'(t, c2) + m \cdot x'(t, c3, c4) \\ e \cdot z(t, c2) - e \cdot x'(t, c3, c4) \end{pmatrix}$$

```
X(N) := n ← 1
        t_0 ← 0
        step ← 0.01
        dx_0 ← 0
        dz_0 ← 0
        xf_0 ← 0
        x'f_0 ← 0
        dispStr_0 ← xf_0
        zf_0 ← -0.01
        z'f_0 ← u'
        displce_0 ← zf_0
        indicator_0 ← 0
        impactT_0 ← 0
        phaseT_0 ← 0
        (c1_0, c2_0)^T ← matZ(t_0)^-1 · matI1(t_0, zf_0, z'f_0)
        (c3_0, c4_0)^T ← matX(t_0)^-1 · matI2(xf_0, x'f_0)
        velox_0 ← x'f_0
        veloz_0 ← z'f_0
        while n ≤ N
            t_n ← t_(n-1) + step
            phaseT_n ← t_n - impactT_(n-1)
            if max(|veloz_(n-1)|, |velox_(n-1)|) < 0.0001 ∧ max(|z'(phaseT_n, c2_(n-1))|, |x'(phaseT_n, c3_(n-1), c4_(n-1))|) < 0.0001 ∧ max(|displce_(n-1)|, |dispStr_(n-1)|) < 0.0001
                indicator_n ← 2
                impactT_n ← impactT_(n-1)
                xf_n ← xf_(n-1)
                zf_n ← zf_(n-1)
                x'f_n ← x'f_(n-1)
                z'f_n ← z'f_(n-1)
                c1_n ← c1_(n-1)
                c2_n ← c2_(n-1)
                c3_n ← c3_(n-1)
                c4_n ← c4_(n-1)
                displce_n ← (b/k) u'
                dispStr_n ← (b/k) u'
                velox_n ← 0
                veloz_n ← 0
            otherwise
                impact_n ← x(phaseT_n, c3_(n-1), c4_(n-1)) - z(phaseT_n, c1_(n-1), c2_(n-1))
                dx_n ← velox_(n-1) step
```

$dz_n \leftarrow veloz_{n-1} \cdot step$

$impactcond_n \leftarrow 0.000001 \quad \text{if } min\left(\left|dx_n\right|, \left|dz_n\right|\right) = 0$

$impactcond_n \leftarrow \frac{1}{10} \cdot min\left(\left|dx_n\right|, \left|dz_n\right|\right) \quad \text{otherwise}$

if $impact_n \le impactcond_n$

$indicator_n \leftarrow 1$

$impactT_n \leftarrow t_n$

$\begin{pmatrix} z'f_n \\ x'f_n \end{pmatrix} \leftarrow matM^{-1} \cdot matI3\left(phaseT_n, c2_{n-1}, c3_{n-1}, c4_{n-1}\right)$

$xf_n \leftarrow dispStr_{n-1}$

$zf_n \leftarrow displce_{n-1}$

$veloz_n \leftarrow z'f_n$

$displce_n \leftarrow displce_{n-1}$

$dispStr_n \leftarrow dispStr_{n-1}$

$velox_n \leftarrow x'f_n$

$phaseT_n \leftarrow t_n - impactT_n$

$\begin{pmatrix} c1_n \\ c2_n \end{pmatrix} \leftarrow matZ\left(phaseT_n\right)^{-1} \cdot matI1\left(phaseT_n, zf_n, z'f_n\right)$

$\begin{pmatrix} c3_n \\ c4_n \end{pmatrix} \leftarrow matX\left(phaseT_n\right)^{-1} \cdot matI2\left(xf_n, x'f_n\right)$

otherwise

$indicator_n \leftarrow 0$

$impactT_n \leftarrow impactT_{n-1}$

$xf_n \leftarrow xf_{n-1}$

$zf_n \leftarrow zf_{n-1}$

$x'f_n \leftarrow x'f_{n-1}$

$z'f_n \leftarrow z'f_{n-1}$

$c1_n \leftarrow c1_{n-1}$

$c2_n \leftarrow c2_{n-1}$

$c3_n \leftarrow c3_{n-1}$

$c4_n \leftarrow c4_{n-1}$

$veloz_n \leftarrow z\left(phaseT_n, c2_n\right)$

$displce_n \leftarrow z\left(phaseT_n, c1_n, c2_n\right)$

$dispStr_n \leftarrow x\left(phaseT_n, c3_n, c4_n\right)$

$velox_n \leftarrow x'\left(phaseT_n, c3_n, c4_n\right)$

$time_n \leftarrow t_n$

$n \leftarrow n + 1$

return (time phaseT c2 velox veloz dispStr displce indicator)

A.2 The Impact IIV model Based on Quadratic Drag and Flow Effect

$L := 44.93$ $F_0 := 8388$ $C_M := 2$ $C_A := C_M - 1$ $D := 0.076$

$\rho := 999$ $u' := 1$ $A := 1$ $C_d := 1$ $b := \frac{1}{2}\rho \cdot C_d \cdot \frac{A}{L}$

$m := \frac{1600}{L} + C_A \cdot \rho \cdot \pi \cdot \frac{D^2}{4}$ $k := \frac{1000000}{L}$

$c := \frac{200}{L} + C_d \cdot \rho \cdot \frac{D}{2}$ $\omega_n := \sqrt{\frac{k}{m}}$ $\xi := \frac{c}{2m \cdot \omega_n}$ $\omega_d := \sqrt{1 - \xi^2} \cdot \omega_n$

$M := \frac{1600}{L}$ ice mass $e := 1$ coe. of restitution

Equations of the ice $bM := \frac{b}{M}$

$z(dt, z_{old}, z'_{old}) := z_{old} + z'_{old} \cdot dt$ $z'(dt, z'_{old}) := z'_{old} - bM \left|z'_{old} - u'\right| (z'_{old} - u') \, dt$

$z''(z'_{old}) := -bM \left|z'_{old} - u'\right| (z'_{old} - u')$

Equations of the structure

$x(t, c3, c4) := c3 \cdot e^{-\xi \cdot \omega_n \cdot t} \cdot \cos(\omega_d \cdot t) + c4 \cdot e^{-\xi \cdot \omega_n \cdot t} \cdot \sin(\omega_d \cdot t)$

$x'(t, c3, c4) := \frac{d}{dt} x(t, c3, c4)$ $x''(t, c3, c4) := \frac{d}{dt} x'(t, c3, c4)$

$$matX(t) := \begin{bmatrix} e^{-\xi \cdot \omega_n \cdot t} \cdot \cos(\omega_d \cdot t) & e^{-\xi \cdot \omega_n \cdot t} \cdot \sin(\omega_d \cdot t) \\ -e^{-\xi \cdot \omega_n \cdot t} \cdot (\xi \cdot \omega_n \cdot \cos(\omega_d \cdot t) + \omega_d \cdot \sin(\omega_d \cdot t)) & e^{-\xi \cdot \omega_n \cdot t} \cdot (\omega_d \cdot \cos(\omega_d \cdot t) - \xi \cdot \omega_n \cdot \sin(\omega_d \cdot t)) \end{bmatrix}$$

$$matI2(x_f, x'_f) := \begin{pmatrix} x_f \\ x'_f \end{pmatrix}$$

Impact

$$matM := \begin{pmatrix} M & m \\ -1 & 1 \end{pmatrix}$$

$$matI3(t, dt, z'_{old}, c3, c4) := \begin{pmatrix} M \cdot z'(dt, z'_{old}) + m \cdot x'(t, c3, c4) \\ e \cdot z'(dt, z'_{old}) - e \cdot x'(t, c3, c4) \end{pmatrix}$$

$X(N) :=$

$n \leftarrow 1$

$t_0 \leftarrow 0$

$step \leftarrow 0.001$

$dx_0 \leftarrow 0$

$dz_0 \leftarrow 0$

$x_{f_0} \leftarrow 0$

$x'_{f_0} \leftarrow 0$

$dispStr_0 \leftarrow x_{f_0}$

$z_{f_0} \leftarrow -0.01$

$z'_{f_0} \leftarrow u'$

$displce_0 \leftarrow z_{f_0}$

$indicator_0 \leftarrow 0$

$impactT_0 \leftarrow 0$

$phaseT_0 \leftarrow 0$

$$\begin{pmatrix} c3_0 \\ c4_0 \end{pmatrix} \leftarrow matX(t_0)^{-1} \cdot matI2(xf_0, x'f_0)$$

$velox_0 \leftarrow x'f_0$

$veloz_0 \leftarrow z'f_0$

while $n \le N$

$t_n \leftarrow t_{n-1} + step$

$phaseT_n \leftarrow t_n - impactT_{n-1}$

if $\max(|veloz_{n-1}|, |velox_{n-1}|) < 0.0001 \wedge \max(|z''(veloz_{n-1})|, |x''(phaseT_n, c3_{n-1}, c4_{n-1})|) < 0.0001 \wedge \max(|displce_{n-1}|, |dispStr_{n-1}|) < 0.0001$

$indicator_n \leftarrow 2$

$impactT_n \leftarrow impactT_{n-1}$

$xf_n \leftarrow xf_{n-1}$

$zf_n \leftarrow zf_{n-1}$

$x'f_n \leftarrow x'f_{n-1}$

$z'f_n \leftarrow z'f_{n-1}$

$c3_n \leftarrow c3_{n-1}$

$c4_n \leftarrow c4_{n-1}$

$displce_n \leftarrow \frac{b}{k} \cdot u'$

$dispStr_n \leftarrow \frac{b}{k} \cdot u'$

$velox_n \leftarrow 0$

$veloz_n \leftarrow 0$

otherwise

$impact_n \leftarrow x(phaseT_n, c3_{n-1}, c4_{n-1}) - z(step, displce_{n-1}, veloz_{n-1})$

$dx_n \leftarrow velox_{n-1} \cdot step$

$dz_n \leftarrow veloz_{n-1} \cdot step$

$impactcond_n \leftarrow 0.000001$ if $\min(|dx_n|, |dz_n|) = 0$

$impactcond_n \leftarrow \frac{1}{10} \cdot \min(|dx_n|, |dz_n|)$ otherwise

if $impact_n \le impactcond_n$

$indicator_n \leftarrow 1$

$impactT_n \leftarrow t_n$

$$\begin{pmatrix} z'f_n \\ x'f_n \end{pmatrix} \leftarrow matM^{-1} \cdot matI3(phaseT_n, step, veloz_{n-1}, c3_{n-1}, c4_{n-1})$$

$xf_n \leftarrow dispStr_{n-1}$

$zf_n \leftarrow displce_{n-1}$

$veloz_n \leftarrow z'f_n$

$displce_n \leftarrow displce_{n-1}$

$dispStr_n \leftarrow dispStr_{n-1}$

$velox_n \leftarrow x'f_n$

$phaseT_n \leftarrow t_n - impactT_n$

```
      (c3_n)
      (c4_n) ← matX(phaseT_n)^-1 · matJ2(x_f_n, x'_f_n)
   otherwise
      indicator_n ← 0
      impactT_n ← impactT_n-1
      x_f_n ← x_f_n-1
      z_f_n ← z_f_n-1
      x'_f_n ← x'_f_n-1
      z'_f_n ← z'_f_n-1
      veloz_n ← z'(step, veloz_n-1)
      dispIce_n ← z(step, dispIce_n-1, veloz_n)
      c3_n ← c3_n-1
      c4_n ← c4_n-1
      dispStr_n ← x(phaseT_n, c3_n, c4_n)
      velox_n ← x'(phaseT_n, c3_n, c4_n)
  time_n ← t_n
  n ← n + 1
return (time  x'_f  z'_f  velox  veloz  dispStr  dispIce  indicator)
```

Bibliography

[Barker et al., 2005] Barker, A., Timco, G., Gravesen, H., and Vølund, P. (2005). Ice loading on danish wind turbines, part1: Dynamic model tests. In *Proceedings of Cold Regions Science and Technology*, 41, pages 1–23.

[Bedford and Fowler, 1999] Bedford, A. and Fowler, W. (1999). *Engineering Mechanics: Dynamics.* Addison Wesley Longman, Inc., CA, USA, second edition.

[Blenkarn, 1970] Blenkarn, K. A. (1970). Measurement and analysis of ice forces on cook inlet structures. In *Proceedings of Offshore Technology Conference*, OTC 1261, pages 365–378.

[De Silva, 1999] De Silva, C. W. (1999). *Vibration: fundamentals and practice.* CRC Press LLC, Florida, USA, first edition.

[Dempsey, 1999] Dempsey, J. P. (1999). Reserch trends in ice mechanics. *International journal of Solids and Structures*, (37):131–153.

[Eranti et al., 1981] Eranti, E., Hayes, F. D., Määttänen, M., and Soong, T. T. (1981). Dynamic ice-structure interaction analysis for narrow vertical structures. In *Proceedings of 6th International Conference on Port and Ocean Engineering under Arctic Conditions*, volume 1, pages 472–479.

[Huang and Liu, 2006] Huang, G. and Liu, P. (2006). A dynamic model for ice-induced vibration of structures. In *Proceedings 25th Inthernational Conference on Offshore Mechanics and Arctic Engineering*, OMAE2006-92077.

[Kärnä, 1994] Kärnä, T. (1994). Steady-state vibrations of offshore structures. In *Hydrotechnical Construction*, vol. 28 No. 9, pages 446–453.

[Kärnä and Turunen, 1989] Kärnä, T. and Turunen, R. (1989). Dynamic response of narrow structures to ice crushing. In *Proceedings of Cold Regions Science and Technology*, 17, pages 173–187.

[Kreyszig, 1999] Kreyszig, E. (1999). *Advanced Engineering Mathematics.* John Wiley and Sons, Inc., Ames, Iowa, USA, eighth edition.

[Määttänen, 1989] Määttänen, M. (1989). Ice-induced vibrations of structures self-exciation. Special Report 89-5, International Association for Hydraulic Research Working Group on Ice Forces.

[Määttänen, 2001] Määttänen, M. (2001). Numerical simulation of ice-induced vibrations in offshore structures. Keynote lecture, Proc. 14th Nordic Seminar on Computational Mechanics.

[Munson et al., 2002] Munson, B., Young, D., and Okiishi, T. (2002). *Fundamentals of Fluid Mechanics.* John Wiley and Sons, Inc., Ames, Iowa, USA, fourth edition.

[Qu et al., 2006] Qu, Y., Yue, Q., Bi, X., and Kärnä, T. (2006). A random ice force model for narrow conical structures. In *Proceedings of Cold Regions Science and Technology*, 45, pages 148–157.

[Salapaka et al., 1998] Salapaka, S., Salapaka, M., Dahleh, M., and Mezic, I. (1998). Complex dynamics in repeated impact oscillators. In *Proceedings of the 37the IEEE*, TA16 10:20, pages 2053–2057.

[Shih, 1991] Shih, L. Y. (1991). Analysis of ice-induced vibrations on a flexible structure. In *Proceedings of Applied mathematical Modelling*, 15, pages 632–638.

[Sodhi, 1989] Sodhi, D. S. (1989). Ice-induced vibrations of structures. Special Report 89-5, International Association for Hydraulic Research Working Group on Ice Forces.

[Sodhi and Morris, 1986] Sodhi, D. S. and Morris, C. E. (1986). Characteristic frequency of force variations in continuous crushing of sheet ice against rigid cylindrical structures. In *Proceedings of Cold Regions Science and Technology*, 12, pages 1–12.

[Thomson, 1998] Thomson, W. (1998). *Theory of Vibration with Applications.* Prentice-Hall, Inc., Upper Saddle River, New Jersey, USA, fifth edition.

[Toyama et al., 1983] Toyama, Y., Sensu, T., Minami, M., and Yashima, N. (1983). Model tests on ice-iceduced self-excited vibration of cylindrical structures. In *Proceedings of 7th Internationsl Conference on Port and ocean Engineering under Arctic Conditions*, volume 2, pages 834–844.

[Weaver, 1983] Weaver, H. J. (1983). *Applications of Discrete and Continuous Fourier Analysis.* John Wiley and Sons, Inc., USA, first edition.

[Wilson et al., 2003] Wilson, J., Muga, B., and Reese, L. (2003). *Dynamics of Offshore Structures.* john Wiley and Sons, Inc., Hoboken, New Jersey, second edition.

[Wolfram, 1999] Wolfram, J. (1999). On alternative approaches to linearization and morison's equation for wave forces. In *Proceedings of The Royal Society*, 455, pages 2957–2974.